2011

Study of magnetorheology and sensing capabilities of graphite based MR elastomers

Tongfei Tian
University of Wollongong

Study of Magnetorheology and Sensing Capabilities of graphite based MR Elastomers

A thesis submitted in fulfillment of the requirements for the award of the degree of Master of Engineering – Research

Tongfei TIAN

Faculty of Engineering, University of Wollongong

January 2011

Wollongong, New South Wales, Australia

CERTIFICATION

I, Tongfei TIAN, declare that this thesis, submitted in partial fulfillment of the requirements for the award of Master of Engineering – research, in the School of Mechanical, Materials & Mechatronic Engineering, Faculty of Engineering, University of Wollongong, is wholly my own work unless otherwise referenced or acknowledged.

The document has not been submitted for qualifications at any other academic institution.

Tongfei TIAN

14 January 2011

ACKNOWLEDGEMENTS

I wish to thank my supervisor, Assoc. Prof. Weihua Li for his enthusiastic support, professional direction and constant encouragement that inspired me to overcome the challenges on my road of life and study.

Particular thanks are extended to Xianzhou Zhang and Yang Zhou for their help on theoretical discussion for this project. Without the assistance of my lab mates I could not complete this dissertation. I thank all who helped me during my graduate studies.

Thanks are also extended to Mario Solitro, Keith Maywald, Doug Henness, Greg Tillman, Nick Mackie, Wayne Ireland and Ron Marshall for their kind assistance and discussions.

Finally, I specially would like to thank my parents for their understanding, patience and unwavering support throughout the course of my graduate studies.

ABSTRACT

This study focuses on the magnetorheology and sensing capabilities of graphite based MR Elastomers (Gr MREs). By introducing graphite to conventional MREs, the Gr MREs with various graphite weight fraction are derived.

Both steady state tests and dynamic tests such as strain amplitude sweep and angular frequency sweep were used to test the magnetorheology of Gr MREs. With the help of graphite in MREs, the storage and loss moduli are both changed. The samples with higher graphite weight fraction show higher initial storage and loss moduli and lower MR effects.

Also the microstructures of isotropic and anisotropic Gr MREs are observed. We can see that the carbonyl iron particles array in chains in the anisotropic MREs and the graphite powders disperse in matrix randomly. Graphite powders contribute to the magnetorheology of MREs such as increasing the initial mechanical properties and diminishing the MR effect. Also the graphite powders connect different carbonyl iron chains parallelly, which helps to reduce the total resistance of MREs.

The conductivity of Gr MREs is affected by three factors. The first is the weight fraction of graphite in the Gr MRE samples; the more weight fraction of graphite is, the more conductive Gr MRE sample is. The external force applied on the samples is another factor. Increasing external force can cause the electrical resistance decrease. The other cause affecting sample conductivity is the intensity of magnetic field. When the intensity rises, the resistance of samples goes down. This paper introduces the Gr MREs' fabrication process, analyzes the relationship between the resistance of Gr MREs, the external force and the intensity of magnetic field and shows the data gotten from the experiments.

TABLE OF CONTENTS

LIST OF FIGURES

LIST OF TABLES

LIST OF SYMBOL

V_s	volume of the two carbonyl iron hemispheres
r_p	radius of carbonyl iron particle
h	thickness of the film between two adjacent iron particles
h_r	thickness of RVU
V_s	volume of RVU
ϕ	carbonyl iron particle volume fraction in RVU
Sr	area of cross section in RVU
E	intensity of current flowing through the polymer
E	intensity of local electric field
j_t	sum of the tunnel density
j_c	conduction density
α	constant in Fowler-Nordheim equation
β	constant in Fowler-Nordheim equation
Φ_0	potential barrier height
σ_f	conductivity of the polymer film
j	total current density
j_r	density of RVU
r_i	the radius of the area between the two adjacent iron particles
σ_r	conductivity of typical MRE
σ	compressive stress
F_p	compressive force
v	Poisson's ratio
E_p	Young's Modulus
σ_o	initial compressed stress
r_{i0}	initial contact area radius
σ_1	stress from external force
σ_2	stress from the magnetic attraction
k_g	the ratio of magnetic field strength to stress from the magnetic attraction

B	magnetic field strength
σ_m	conductivity of MREs
ρ	electrical resistivity
A	section area of samples
R	resistance of MREs
ϕ_g	graphite weight fraction
ϕ_i	carbonyl iron weight fraction
λ_g	effective parameter for graphite
λ_i	effective parameter for carbonyl iron

CHAPTER 1
INTRODUCTION

The dissertation aims to study the magnetorheology and sensing capabilities of graphite based Magnetorheological Elastomers (Gr MREs).

The major tasks include: (1) fabrication of Gr MREs with various graphite weight fraction (Gr %); (2) microstructure observation; (3) magnetorheology under both steady & dynamic conditions; (4) modeling & experimental studies of sensing capabilities of Gr MREs

1.1 BACKGROUND AND MOTIVATION

A sensor is a device that measures a physical quantity and converts it into a signal which can be read by an observer or by an instrument.

Sensors are used in everyday objects such as the Three-axis gyro, Accelerometer, Proximity sensor and Ambient light sensor which are all used in iphone 4. There are also innumerable applications for sensors which include cars, machines, aerospace, medicine, manufacturing and robotics. Force sensor is one kind of sensor to convert force to other readable signal, which has been widely used in various industries. In force sensors, there are many typical techniques of using a force collector such as diaphragm, piston, bourdon tube, piezoresistive strain gauge, capacitive, electromagnetic, piezoelectric and etc. to measure strain or deflection due to applied force over an area [1, 2]. Also, some smart materials such as PZT，SMA and etc. are used as key components in force sensors [3-5].

Magnetorheological elastomers (MREs) are smart materials where polarized particles are suspended in a non-magnetic solid or gel-like matrix. There are two kinds of MREs which are anisotropic and isotropic MREs. In anisotropic samples, polarized particles can be arranged as chains in polymer media such as silicone rubbers and natural rubbers. The

modulus of MRE can be controlled by the external magnetic field. Meanwhile, the Gr MREs show resistance changing when an external load is applied on MRE samples. By this feature of MREs, the external stress signal can be converted to a resistance signal, which can be used potentially in a force sensor.

1.2 AIMS AND OBJECTIVES

The objectives of this thesis study consist of the study of magnetorheology and sensing capabilities of graphite based MREs.

1) To fabricate both isotropic and anisotropic Gr MREs with various graphite weight fraction
2) To measure the magnetorheology of Gr MREs
3) To observe microstructure of Gr MREs and study their relationship with mechanical properties
4) To theoretically and experimentally study sensing properties of Gr MREs

1.3 THESIS OUTLINE

This thesis begins with a literature review on MRE material, MRE fabrication, MRE properties, Model study of MREs, MRE applications and MRE snesing in *Chapter 2*, which gives a comprehensive overview of the achievements of previous research and the aim of this project. *Chapter 3* shows the fabrication of graphite based MREs and the microstructures of various MREs. Also in *Chapter 3*, the effect of graphite in MREs are presented and analyzed. *Chapter 4* explains the experimental setup and the development and study of the conductive model of MREs. Meanwhile, the theoretical result and experimental are shown and compared. *Chapter 5* concludes with a review and summary of the project and suggestions for further research work.

CHAPTER 2
LITERATURE REVIEW

2.1 INTRODUCTION

The literature review deals with the combined technologies of MRE material, MRE fabrication, MRE property, applications of MRE and MRE resistance.

MRE material consists of suspensions of polarized particles in a non-magnetic solid or gel-like matrix. These polarized particles can be dispersed or arranged in chains in polymer media such as silicone rubber and natural rubber [6, 7].

2.2 MRE MATERIALS

Conventional MREs consist of three components namely polarized particles, matrix and additives [8].

2.2.1 Polarized particles

In MREs, spherical carbonyl iron particles are usually used as the polarized particles whose particle size is a few microns. Iron has one of the highest saturation magnetization values of metallic elements. High permeability, low remnant magnetization and high saturation magnetization are also the features of carbonyl iron particles. High inter-particle attraction is thought to be provided by high permeability and saturation magnetization, thereby the particles can have a high MR effect. A low remnant magnetization is also recommended because the highly remnant particles will stick together when the magnetic field is turned off [9]. The magnetostriction of iron particles is also low [10]. Kchit and Bossis [11] used two kinds of magnetic particles: nickel and nickel coated with silver, dispersed in a silicone

polymer to fabricate MREs. Their study showed that the sensitivity to pressure of a field structured composites was about ten times larger than the one of a usual composite.

2.2.2 Matrix

For MREs, the conventional matrixes are usually natural rubber or silicone rubber. Natural rubber is an elastomer, an elastic hydrocarbon polymer that originally derived from a milky colloidal suspension or latex, found in the sap of some plants. The purified form of natural rubber is the chemical polyisoprene which can also be produced synthetically. Silicone rubber is a rubber-like material composed of silicone containing silicone together with carbon, hydrogen, and oxygen. During manufacture heat is required to vulcanize the silicone into its rubber-like form [12]. The silicone rubber and a vulcanizing silicone sealant (at room temperature), is mixed with silicone oil to changing its ductility. The silicone oil is selected on the basis of preliminary studies with different elastomers. Silicone rubber offers good resistance to extreme temperatures, being able to operate normally from -55°C to +300°C. At the extreme temperatures, the tensile strength, elongation, tear strength and compression set can be far superior to conventional rubbers although still low relative to other materials [13]. Nitrile rubber was also used as matrix in MREs [9, 14].

2.2.3 Additives

Additives are used to adjust the mechanism properties or electrical performance of MREs. In MREs, silicone oil is usually used as an additive. When the molecules of silicone oil enter into the matrix, the gaps between the matrix molecules are increased and the conglutination of molecules is decreased. Apart from increasing the plasticity and fluidity of the matrix, the additives can average the distribution of internal stress in the materials, which makes them ideal for fabricating MRE materials [15]. Graphite powder is a kind of additive which can adjust the conductivity of MREs [16-19]. By introducing graphite microparticles into the elastic matrix, MREs become electroconductive. This property of MREs can be used for achieving magnetoresistors, magnetic field sensors, transductors of

mechanical distortions, strains, etc [17]. Chen et al. demonstrates that carbon black has significant effects in improving the mechanical performance and reducing the damping ratio of MR elastomers [20].

2.3 MRE FABRICATION

There are two categories of MREs: isotropic MREs and anisotropic MREs. Fig. 2.1 shows the major steps of fabrication of these two MREs [6, 9, 19, 21].

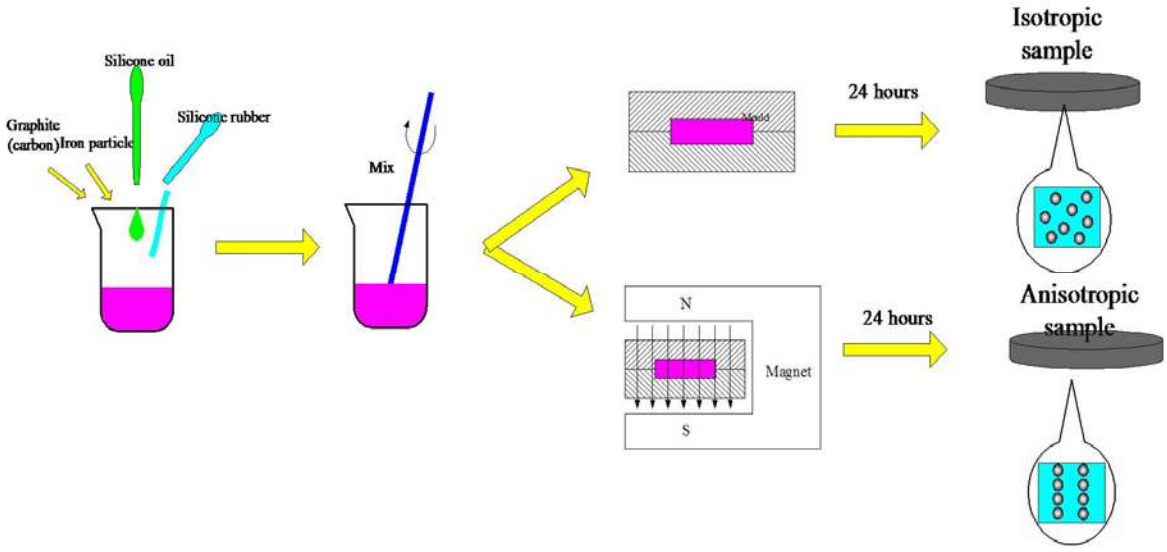

Fig. 2.1 Procedures of conventional anisotropic and isotropic MRE fabrication

The difference between the fabrication procedures of isotropic and anisotropic MREs is that if the mixture of polarized particles, matrix and additives is curing under a magnetic field.

The general procedure for fabricating an anisotropic MR elastomer with natural rubber is similar to conventional rubber. Normally, the ingredients are natural rubber, zinc oxide, stearic acid, sulfur, and iron particles. After all the ingredients are evenly mixed in a mixing machine at a high temperature such as 120º, the mixture is packed in a mould and then cured under an electric-magnetic field for a certain time. The samples are then left at the room temperature for more than 24 hours prior to testing. The chain formation results from the anisotropic magnetic forces among the particles. The MREs fabricated with this method

are called anisotropic MREs [21]. For isotropic MREs, carbonyl iron particles firstly immerse in silicone oil then were mixed with silicone rubber. All the ingredients in the beaker were mixed by using a stirrer bar for about 5 min at room temperature. After all ingredients were evenly mixed, the mixture was put under a vacuum to remove air bubbles, and then cured for 24 h at room temperature in an open sheet mould without a magnetic field [6]. According to current research, the anisotropic MREs have a much larger MR effect than that of isotropic MREs [22].

2.4 MAGNETORHEOLOGY OF MREs

2.4.1 Steady-state and dynamic properties of MRE

MREs contain viscoelastic properties and magnetorheology [23]. The magnetorheology of MREs is described as a reversible change in modulus in an applied magnetic field. Aligned MREs have mostly been characterized at relatively low frequencies (1 to 20 Hz) to measure the changes in the dynamic shear modulus induced by the external magnetic field [23, 24]. Ginder et al. found a substantial magnetorheology over the entire frequency range studied. The increase in the shear modulus varied initially with the strength of the magnetic field but saturated at higher strength fields. When the magnetic field was increased from 0 to 0.56 Tesla the consequent increase in shear modulus was nearly 2 MPa and the frequency of the resonance was shifted upward by over 20% [24]. Zhou et al. [23] started that the changes of dynamic shear storage modulus can be over 50%, while Gong et al. [6] said it can be over 100%. Lokander et al. studied the dynamic shear modulus for isotropic MR elastomers with different filler particles and matrix materials. They measured the magnetorheology as a function of the amplitude of strain and found that the magnetorheology decreases rapidly with increasing strain within the measured range, and is not dependent on the frequency of testing. The fact that the absolute magnetorheology is independent of the matrix material means that softer matrix materials will show a greater relative magnetorheology [9, 14].

2.4.2 Influence factors of MRE

2.4.2.1 Influence of magnetic field

The magnetic field is a key parameter in influencing magnetorheology. The origin of the field dependence of these properties is the existence of field-induced dipole type magnetic forces between the separate particles. The behavior of MR elastomers is thought to be a combination of the properties of the matrix and the internal network of magnetized particles. Because these magnetic particles interact the elastomers exhibit a field dependent modulus at low strains. A field-induced increase in shear modulus reaching over 60% has been reported for applied magnetic field strength values of about 0.8 Tesla [8, 25].

2.4.2.2 Influence of the matrix material and additives

When the material in the matrix is magnetic, the polarization of the particles will be less effective and the magnetorheology therefore smaller. The addition of magnetically active additives (other than MR particles) decreases the magnetorheology [9, 25].

The overall properties of the elastomer composite are also influenced by the additives, as the filler material causes the volume to increase, so the previous effect also increases. Lokander et al. [9, 14] have shown that the absolute effect of MR (the difference between the zero-field modulus and modulus measured under an external magnetic field) is independent on the matrix material. However, the zero-field modulus can be much higher for hard matrix material, where materials with high volume fraction of iron already have a high zero-field modulus, which means that the relative magnetorheology is quite low.

2.4.2.3 Influence of particle size, shape and volume fraction

In conventional MREs the size of the particle varies typically from 0.1 to 10 μm and is from one to three orders of magnitude larger than typical particles of colloidal ferrofluid.

Typical micron-sized MR filler particles will support hundreds of magnetic domains. Larger particles allow for obtaining stable, highly magnetic materials and reversible particle aggregation. Thus the particles should be large enough to support at least several magnetic domains in order to have a substantial magnetorheology.

Lokander et al. [9, 14] have shown experimentally that the shape and size of the particle has an influence on the properties of MREs. They measured the MR effect for isotropic nitrile rubber MRE with varying sizes and content of iron particles. The Magnetorheology was larger for materials with ASC300 iron (particle size < 60 μm) than for materials with carbonyl iron (particle size 3.9-5.0 μm). For particles larger than 60 μm, the magnetorheology appeared to be slightly smaller.

The optimal particle volume fraction for the largest relative change in modulus at saturation was predicted to be 27% [26]. Shiga et al. measured the increase in shear modulus as a function of the particle volume fraction. For aligned MREs the change in shear modulus increases with an increasing particle volume fraction. When the concentration of filler is higher than 30 vol. %, the mechanical properties of the composite deteriorate rapidly and the stiffening of the material is larger than the increase of the Magnetorheology [27].

2.4.2.4 Influence of working modes on the MREs properties

Borcea and Bruno[28] and Dorfmann and Ogden [29] have shown theoretically that the existence of a magnetic field stiffens the shear response of an isotropic MRE. Farshad and Benine [30] characterized isotropic and aligned MREs in tension and compression. The aligned MREs were either longitudinally or transversely oriented to the applied load. They found that the direction of alignment influences the tensile properties of the MRE. Samples aligned longitudinally to the direction of the tensile load exhibited the highest tensile strength. In shear static compression the applied magnetic field increased the stiffness of both isotropic and aligned MREs. Bellan and Bossis [31] also considered aligned MREs to be analogous to fibre-reinforced composites. In MREs, the fibres consist of chains of particle whose stiffness is sensitive to the amount of polymer in the gaps between the

particles. The stiffness of the fibres formed by particles is increased when a magnetic field was applied while the stiffness of the composite depends on the cross section of the number of chains per unit.

According to Yalcintas and Dai [32], the external magnetic field will affect the strain amplitude, loss factor, and natural frequency of the vibrating MRE system when dynamically testing in the pre-yield regime. When the strength of the magnetic field increases, the strain amplitude decreases and natural frequencies shift to higher values. The loss factors (tan δ) were found to increase with the strength of the magnetic field in every vibration mode. When an external magnetic field but no mechanical load was applied the MREs deformed slightly. Borcea and Bruno [28] showed theoretically that an isotropic MRE would expand in the direction of the applied magnetic field while an aligned MRE will compress if the field is parallel to the oriented structure. Zhou and Jiang [33] proved this experimentally and also stated that the deformations are related to the strength of the field applied. The magnetically induced deformation of an aligned MRE in the direction of the chain only changes slightly with different volumes of filler. The deformation of an aligned MRE driven by an external magnetic field is smaller than an isotropic MRE of the same volume. This means that aligned MREs are stiffer than isotropic MREs in the direction of the chain. Wang et al. [34] reported that the resistance and impedance of MREs can be changed considerably by mechanical force and applied magnetic fields. This means that the structures of the magnetic particles within elastomers are very sensitive to the external stimulus of either mechanical force or magnetic field, which results in multiresponse behaviors in a MRE.

2.5 MRE SENSING CAPABILITIES

Bossis et al. [35] reported the relationship from resistance of MREs and magnetic field intensity which is shown in Fig. 2.2.

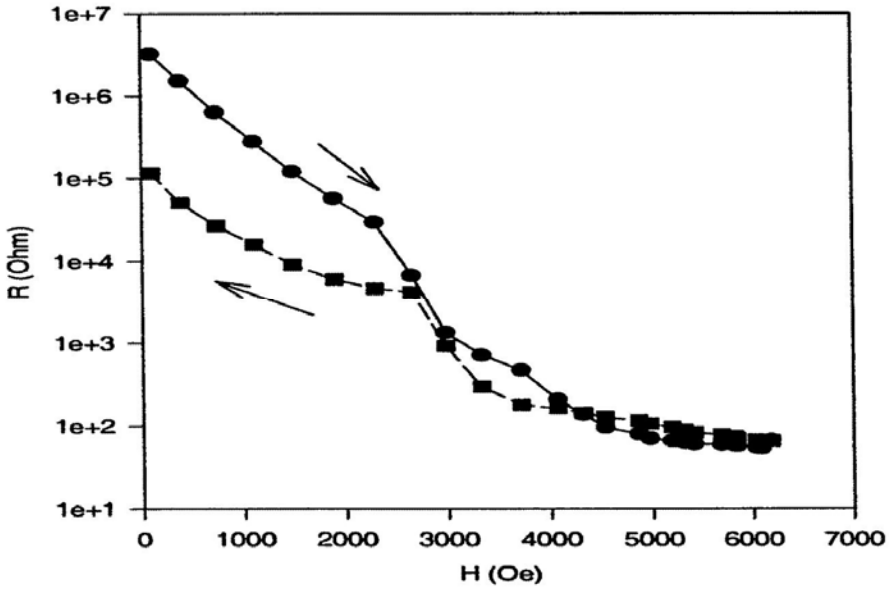

Fig. 2.2 resistance vs. magnetic field [35]

Kchit and Bossis [11] found that the initial resistivity of metal powder at zero pressure is about 108 Ωcm for pure nickel powder and 106 Ωcm for silver coated nickel particles. The change in resistance with pressure was found to be an order of magnitude larger for a MRE composite than for the same volume fraction of fillers dispersed randomly in the polymer. Wang et al. [34] proposes a phenomenological model to understand the impedance response of MREs under mechanical loads and magnetic fields. Their results showed that MRE samples exhibit significant changes in measured values of impedance and resistance in response to compressive deformation, as well as applied magnetic field. Bica [16] found that MRE with graphite micro particles (~14%) is electroconductive. The magnetoresistance has the electric resistance, whose value diminishes with both the increase of the intensity of the magnetic field and compression force. The variation of resistance with magnetic field intensity is due to the compression of MRE with graphite microparticles. In the approximation of the perfect elastic body, the sums of the main deformations and the compressibility module of MRE with graphite microparticles, depend on the magnetic field intensity. Li et al. [19] introduced graphite into conventional MREs and found a MRE sample with 55% carbonyl iron, 20% silicone rubber and 25% graphite powder which has the best performance. The test result showed that at a normal force of 5N, the resistance decreases from 4.62 kΩ without a magnetic field to 1.78 kΩ at the magnetic field of 600 mT. The decreasing rate is more than 60%. This result also demonstrated the

possibility of using MREs to develop a sensor for measuring magnetic fields. This result indicated that the detection is very sensitive to the normal force. When the normal force is 15N, the field-induced resistance only has less than 28% change from 0.65 kΩ at 0 mT to 0.47 kΩ at 600 mT. The repeatability of MRE is a big issue in developing MRE devices.

2.6 MODEL STUDIES OF MREs

A number of models were developed to investigate mechanical properties and the sensing capabilities of MREs. These include Dipole model, universal equivalent circuit model and etc.

2.6.1 Dipole model

Most models of MR material behavior are based on the magnetic dipole interaction between two adjacent particles in the chain. These inter-particle interactions are then averaged over the entire sample to yield a model of the bulk Magnetorheological behavior. Jolly et al. [8] proposed a quasi-static, one-dimensional model that assumed that a magnetic interaction only occurs between the adjacent particles within a chain. On the basis of this point-dipole model, the Magnetorheology was studied as a function of particle magnetization. According to the model the ferrous particles are magnetized linearly and it was assumed that in MR materials the strength was related to particle magnetization quadratically. Fig. 2.3 shows the chart of a dipole model.

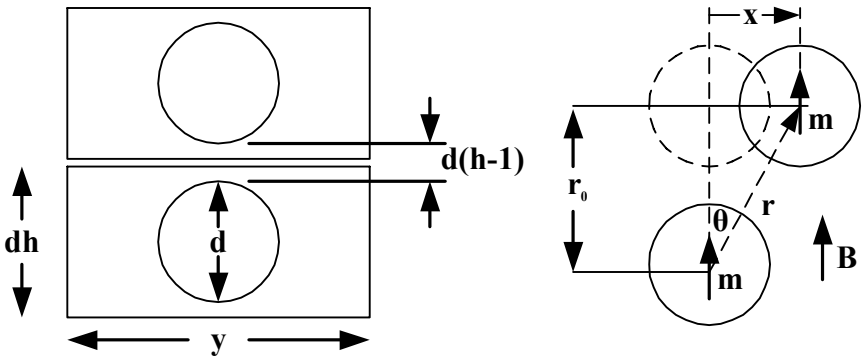

Fig. 2.3 Dipole model [8]

(a) Geometry of two particles of diameter d within a particle chain. Adjacent chains are a distance y apart and $h = r_0/d$. (b) Magnetic interaction of the two particles modeled as dipole moments m and sheared with respect to one another.

In this model the average particle polarisation *Jp* is the dipole moment magnitude per unit particle volume, $|M| = JpVi$, where *Vi* is the volume of the particle. The pre-yield modulus *G* of the particle network is stress divided by strain and can be expressed as

$$G \cong \frac{\varphi J_p^2}{2\mu_1\mu_0 h^3} \qquad \varepsilon < 0.1 \tag{2.1}$$

where $\mu 1$ is the relative permeability of the medium, $\varepsilon = x/r0$ is defined as the scalar shear strain of the particle chain. ϕ is the volume of particles in the composite and *h* is an indication of the gap between the particles in a chain.

The point-dipole model is basically quasi-static and one-dimensional and it concentrates on the magnetomechanical properties of parallel chains of magnetically permeable spherical particles. A magnetic field was applied parallel to the chains and the shear strength caused by inter-particle forces was conducted. Since the model was quasi-static the particles were assumed to be uniformly distributed, homogenous spheres that can be magnetically modeled as identically induced dipole moments. It was also assumed that the particles were aligned in perfect chains and that quasi-static shear strains and associated stresses were distributed uniformly over the length of each particle chain [8].

It was stated that the stress-strain relationship in the point-dipole model was independent of the size of the particle but the length of the gap between the particles in a chain was a very important parameter and the magnetic field- induced stress σ was inversely proportional to the third power of this gap h which is shown in Equation 2.2. Therefore it is useful to select filler materials with high saturation magnetization [8, 9].

$$\sigma = \frac{\phi\varepsilon\left(4-\varepsilon^2\right)J_p{}^2}{8\mu_1\mu_0 h^3\left(1+\varepsilon^2\right)^{7/2}} \tag{2.2}$$

where ϕ is the volume fraction of particles in the composite and J_p is the average particle polarization. ε is the scalar shear strain of the particle chain. μ_1 is the relative permeability of the medium.

The model by Jolly et al. [8] included a theory developed on the basis that saturation begins in the particle's polar regions at very low applied field strengths and increases towards total particle saturation as the strength of this field increases. Average particle polarisation is then calculated as a function of average composite flux density [8]. In reality however, the magnetic interaction between adjacent particle chains and packing arrangements is more complex than that occurring in simple linear chains. If the particles are spherical with the same size particles they will probably form face-centred cubic (FCC) and hexagonal close packed (HCP) microstructures [8]. Furthermore, a common weakness in modelling MR materials is still a lack of understanding of how magnetic flux density distributes itself within the particle network.

2.6.2 Model based on tunnel resistance of microcontacts between the asperities

Depending on elastic-plastic asperity microcontact model for contact between two nominally flat surfaces [36], Kchit and Bossis developed a model to analyze the contact of two rough surfaces. They used two kinds of magnetic particles: nickel and nickel coated with silver, dispersed in a silicone polymer as the polarized particles [11]. Fig. 2.4 shows the contact of a rough surface with a flat surface.

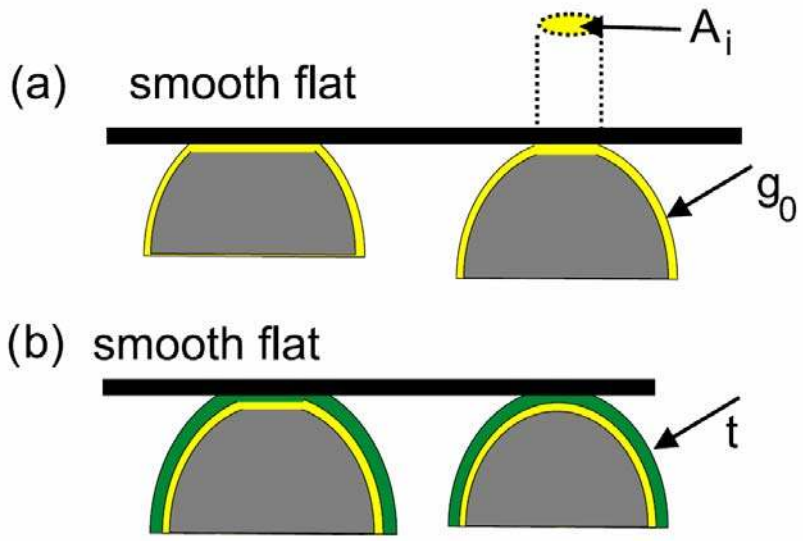

Fig. 2.4 Contact of a rough surface with a flat one [11]

By introducing the volume fraction φ, the total resistivity of composite ρ_c is

$$\rho_c = \frac{\pi}{6}\frac{d}{\phi}\frac{\rho_t}{A_c} \tag{2.3}$$

in which d is the mean diameter of particles. A_c and ρ_c are shown below.

$$A_c(\varepsilon) = 2\pi r_a N_a \int_0^{\infty} x \exp[-\frac{(x + h_0(1-(d/h_0)\varepsilon) - h_m)^2}{2\sigma^2}]dx \tag{2.4}$$

$$\rho_t(\varepsilon) = \rho_t(g_0)\frac{g_0 + t_0[1-\lambda(1-(d/h_0)\varepsilon)\varepsilon]}{g_0} \times \exp\left[\gamma t_0\left(1-\lambda\left(1-\frac{d}{h_0}\varepsilon\right)\varepsilon\right)\right] \tag{2.5}$$

in which, r_a, N_a, σ and h_m are the parameters of roughness given by AFM technique (see table 2.1). The initial separation h_0 between the two average planes is simply equal to $2h_m$ in the case of particles slightly in contact. Nevertheless if initially the particles were pressed against each other then h_0 would be a parameter [11].

2.6.3 Equivalent circuit model

To understand the complex conductivity of particle embedded composites, quantitative or semiquantitative models can be used. The Maxwell–Wagner and the Bruggeman symmetric and asymmetric media equations were introduced by McLachlan [37] to model the electrical behavior of conductor-insulator composites. The microstructures for which these effective media equations apply are considered in simulating the measured impedance and modular spectra of these composites. Woo et al. [38] developed a universal equivalent circuit model in modeling the impedance response of composites with insulating or conductive particles or fibers. Based on the microstructure of MREs, Wang et al. proposed an equivalent circuit model to interpret the impedance measurement results [34]. The model is shown in Fig. 2.5.

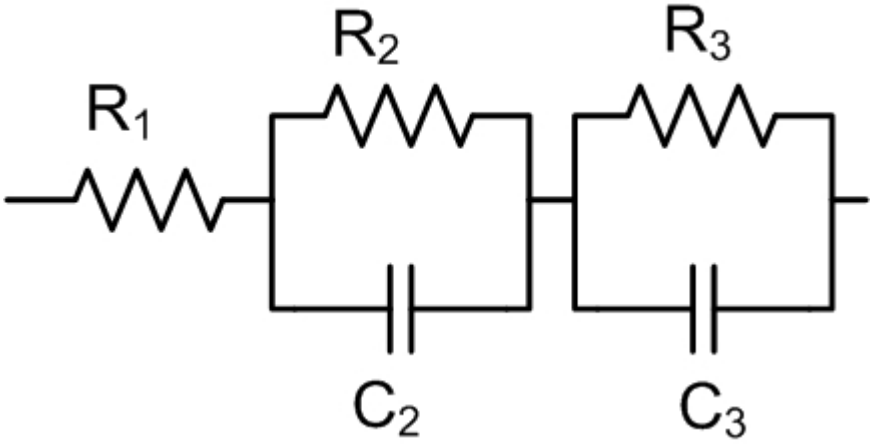

Fig. 2.5 Equivalent circuit model [34]

The resistance R_1 represents the particle resistance; R_2 and C_2 represent the electrode-sample interface resistance and capacitance, respectively. In addition, R_3 and C_3, which are arranged in parallel, correspond to the particles and the insulating particle boundaries. The real and imaginary parts of the impedance $\left(Z = Z' - jZ''\right)$ can be obtained as

$$Z' = R_1 + \frac{R_2}{1+\left(\omega R_2 C_2\right)^2} + \frac{R_3}{1+\left(\omega R_3 C_3\right)^2} \tag{2.6}$$

$$Z'' = \frac{\omega {R_2}^2 C_2}{1+\left(\omega R_2 C_2\right)^2} + \frac{\omega {R_3}^2 C_3}{1+\left(\omega R_3 C_3\right)^2} \tag{2.7}$$

where $\omega = 2\pi f$, and f is the applied electrical frequency [34].

By using the Impedance Spectroscopy technique, Wang et al. investigated the electrical response of MREs under combination effects of deformations and applied magnetic fields. Their result showed that the resistance and impedance of MREs can be changed considerably by mechanical force and applied magnetic fields. This finding was significant because it suggests that MREs are potentially capable of being used for tunable vibration absorbers and for sensing mechanical, as well as magnetic signals, simultaneously [34].

2.7 APPLICATIONS OF MRE

Until now there are many applications of MRE. Some applications are in the vibration absorber, and some are for the adaptive structure such as sandwich beam. Also there are applications are in the sensing field.

2.7.1 MRE ATVA

Deng et al. [39] developed an adaptive tuned vibration absorber (ATVA) based on the unique characteristics of MREs. The ATVA works in shear mode and consists of an oscillator, smart spring elements with MREs, a magnet conductor and two coils. The experimental results demonstrated that the natural frequency of the ATVA can be tuned from 55 to 82 Hz. The relative frequency change is as high as 147%. Hoang et al. [40] presented a conceptual ATVA with soft MREs for vibration reduction of vehicle powertrain systems. Numerical results show that with the MRE material the ATVA can effectively work in a wide frequency range from around 7 to 70 Hz (ten times increase in relative frequency change). In addition, this device can be properly tuned to shift the powertrain natural frequencies when the gear box is set to the first, second, third and fourth gear. It is found that the MR effect in this MRE is significant so that the ATVA effectiveness is very sensitive to the input current, which is used to control the magnetic field intensity. Lerner and Cunefare [41] used MREs as field-dependent springs within three vibration absorber

config.urations, and to determine their vibration absorption characteristics. Each vibration absorber config.uration exploits different magneto-mechanical properties, achieving very different results. The MRE iron concentration is varied to find the largest natural frequency shift for the squeeze-mode absorber due to an applied magnetic field.

2.7.2 MRE adaptive structure

Additionally, MREs have also been used to construct new devices such as sandwich beams. Zhou [42] indicated that the sandwich config.uration is an alternative to developing smart structures because it takes advantage of the field-controllable shear modulus of MRE and enhances the bulk flexural rigidity through the skins.

2.7.3 MRE sensors

Li et al. [19] presented the development of a new force sensor with MR elastomer as a sensing element. MREs with different composition were manufactured and measured with a modified Rheometer. The effects of additives on the sensing capabilities were systematically investigated and an optimal MR elastomer sample was selected for design and manufacturing of a force sensor prototype. The mechanical unit includes the MRE sample and the interface to the electronic circuit. Bica [17] reported that the electrical conductivity of MR elastomer can be used for achieving magnetoresistors, magnetic field sensors, transductors of mechanical distorsions, strains, etc. The electrical conductivity of MRE can be modified in magnetic field.

2.8 CONCLUSION

In this chapter the recent advances in various aspects of MR elastomers were described and reviewed. They include MRE materials, MRE properties, modeling of MREs, applications of MRE and resistance of MREs. MR elastomers are now classified as smart materials

particularly well suited to provide effective performance as an absorber or in the field of structural control. By the change of resistance under the different external force and magnetic field, MREs are also suitable to work as a force sensor. The MR properties of MRE materials relate directly to practical applications of MRE. Therefore, on going research based on previous researches of MREs will investigate a suitable model to represent the MR properties of MRE materials and devices, and evaluate its performance as a force sensor.

CHAPTER 3
FABRICATION, MICROSTRUCTURE & MR EFFECT OF MREs

3.1 INTRODUCTION

To test the MREs' reaction for the external force and external magnetic field, the resistance of MREs is an appropriate factor. Conventional MREs contain iron particles as the magnetical particles, silicone rubber as the matrix and silicone oil as an additive. Because of the nonconductive silicone rubber, the resistance of conventional MRE is too high (more than 20 MΩ) to be detected by a common multimeter. In this study, graphite powders, as an additive, are added to conventional MREs to decrease the resistance to a detectable level.

The outline of this chapter is materials, MREs fabrication, structure observation, MR effects and conclusion.

3.2 MRE FABRICATION

In this part, MRE material components, fabrication procedures and the compositions of MRE samples will be presented.

3.2.1 Material components

The materials used for the Graphite Magnetorheological Elastomers (Gr MREs) are: silicone rubber (Selleys Pty. LTD), silicone oil, type 378364 (Sigma-Aldrich Pty. LTD), carbonyl iron particles, type C3518 (Sigma-Aldrich Pty. LTD) and graphite powder, type

282863 (Sigma-Aldrich Pty. LTD). The particle sizes of graphite powder are less than 20 μm, the iron particles' diameter is between 3 μm and 5 μm.

3.2.2 MRE samples compositions and fabrication

The MREs with various graphite weight fractions (Gr %) were fabricated to compare the effect of graphite on to MREs. Table 3.1 shows the compositions of all Gr MRE samples.

Table 3.1 Components of Gr MRE samples

	Graphite based MREs							
Sample No.	1	2	3	4	5	6	7	8
Carbonyl iron	10g	10g	10g	10g	10g	10g	10g	10g
Silicone oil	3g	3g	3g	3g	3g	3g	3g	3g
Silicone rubber	3g	3g	3g	3g	3g	3g	3g	3g
Graphite	0g	1g	2g	3g	3.5g	4g	4.5g	5g
Graphite weight fraction (Gr %)	0%	5.88%	11.11%	15.79%	17.95%	20%	21.95%	23.81%

As shown in Table 3.1, all samples contain 10g carbonyl iron particles, 3g silicone rubber and 3g silicone oil. The only difference is the graphite weight fraction, which is from 0% to 23.81%. For each composition, there are two samples namely isotropic and anisotropic samples.

Fig. 2.1 shows the major steps of fabrication of isotropic and anisotropic conventional MREs. The difference of the fabrication procedures between conventional MREs and Gr MREs is not only adding graphite powders as an additive, but also in the mixing process.

To fabricate Gr MREs, the carbonyl iron particles are mixed and stirred with silicone rubber first, and then the other ingredients are added in. This helps the carbonyl iron to disperse in to the silicone rubber sufficiently. Otherwise the graphite powder, whose particle sizes are bigger than that of carbonyl iron, would affect the carbonyl iron particles' distribution in the matrix. The curing procedures are the same as conventional MREs in Fig. 2.2

MRE mixture are poured between two piece of plastic papers, Australian five cents coins whose thickness is around 1.36 mm and some 0.1 mm pieces of papers are used to control the MRE samples thickness to around 1mm. After curing the samples, all the Gr MREs are membranes with 1 mm thickness. Circle samples whose diameters are approximate 21 mm, shown in Fig. 3.1, were obtained by punching these membranes, and these samples were used for the following tests.

Fig. 3.1 MRE samples

3.3 MICROSTRUCTURE OBSERVATION

To see microstructure of Gr MREs, LV-SEM (JSM 6490LV SEM) is used. The following pictures gotten by SEM show the carbonyl iron particles, graphite powders and the Surface imaging for MRE microstructures.

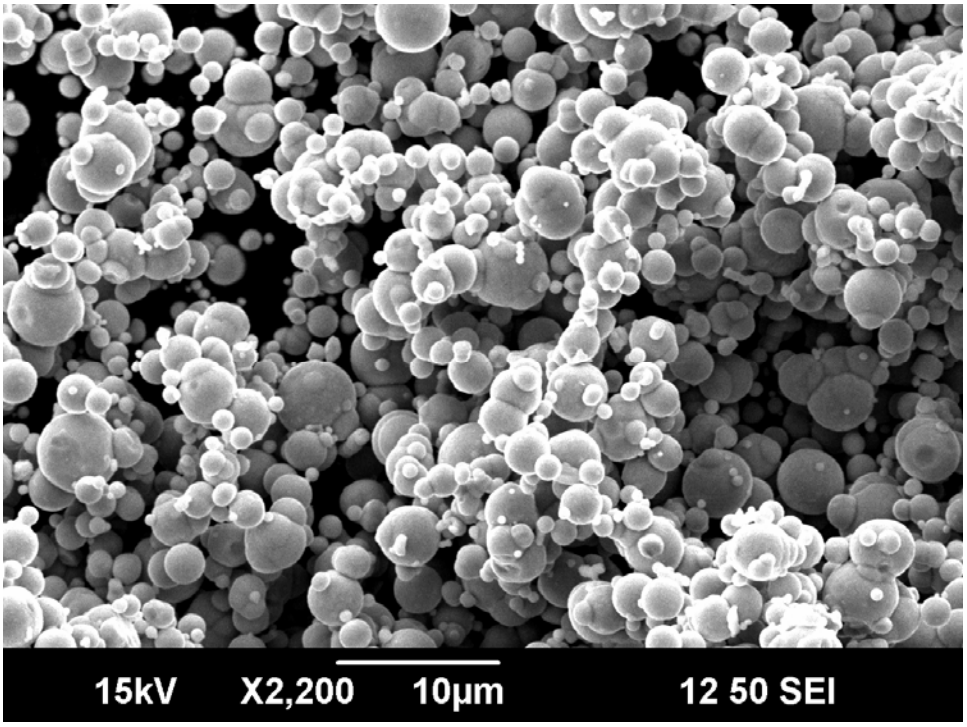

Fig. 3.2 Carbonyl iron particles

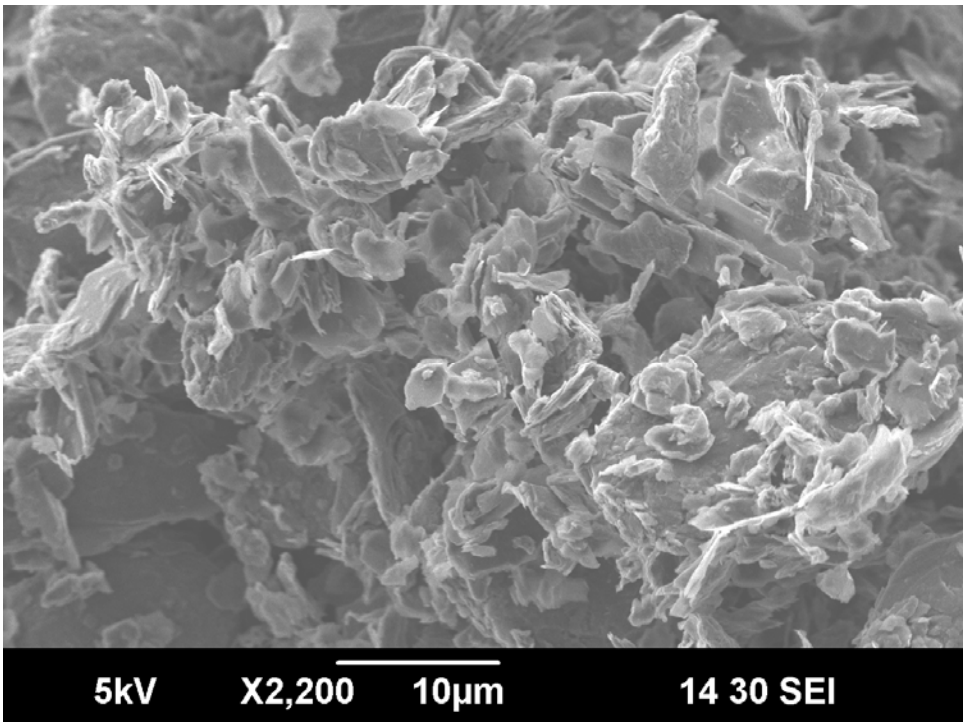

Fig. 3.3 Graphite powders

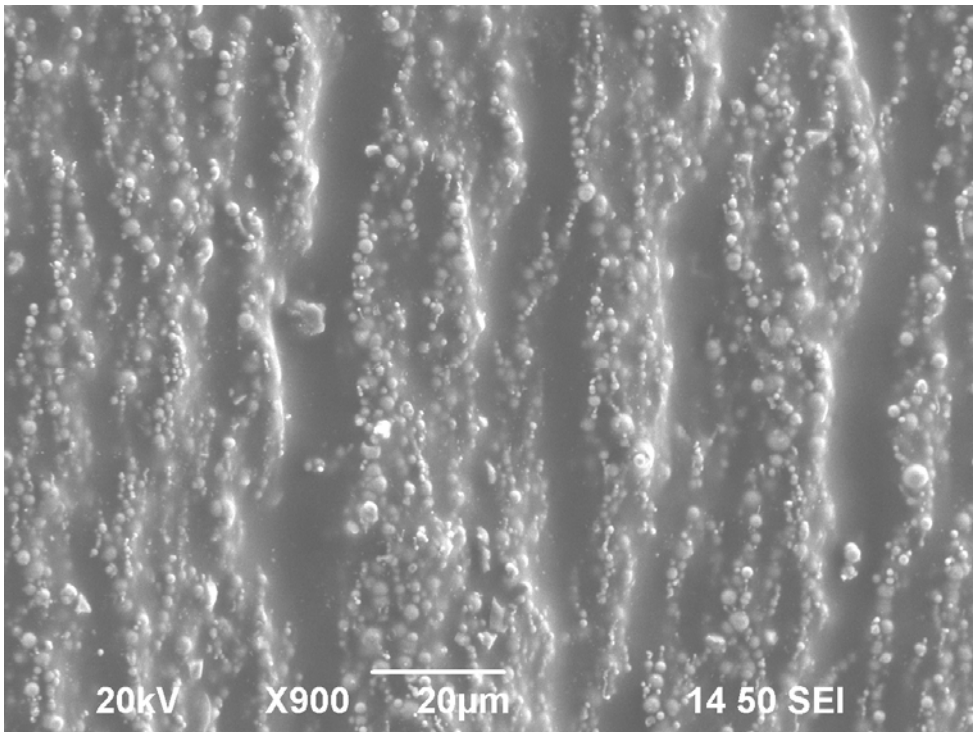

Fig. 3.4 Microstructure of anisotropic Gr MREs (Gr 0%)

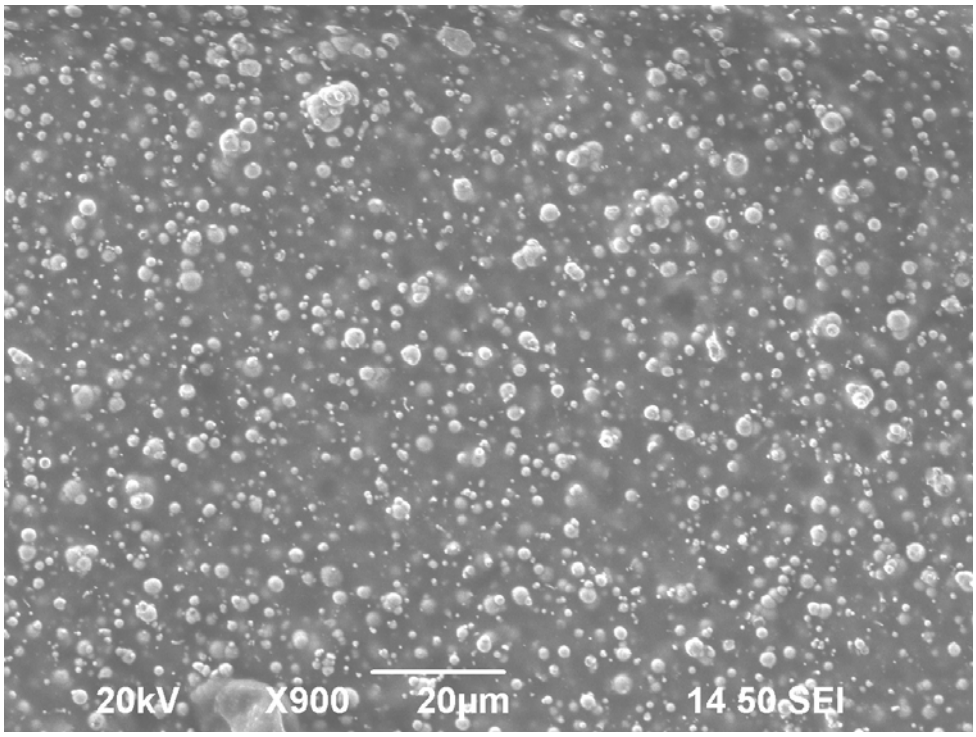

Fig. 3.5 Microstructure of isotropic Gr MREs (Gr 0%)

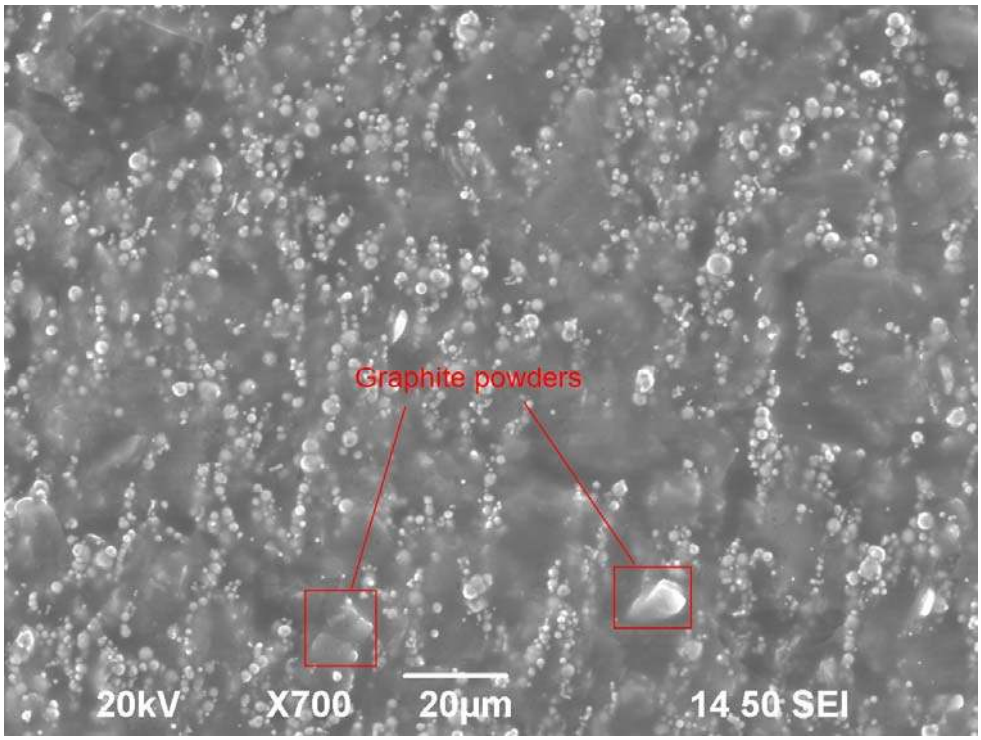

Fig. 3.6 Microstructure of anisotropic Gr MREs (Gr 11.11%)

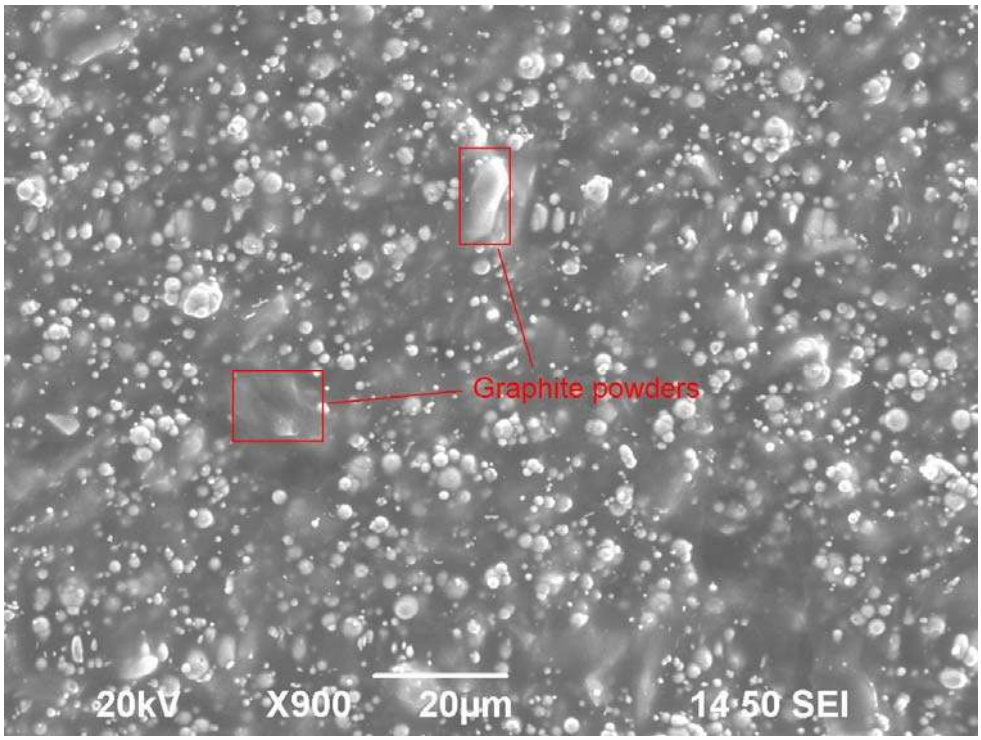

Fig. 3.7 Microstructure of isotropic Gr MREs (Gr 11.11%)

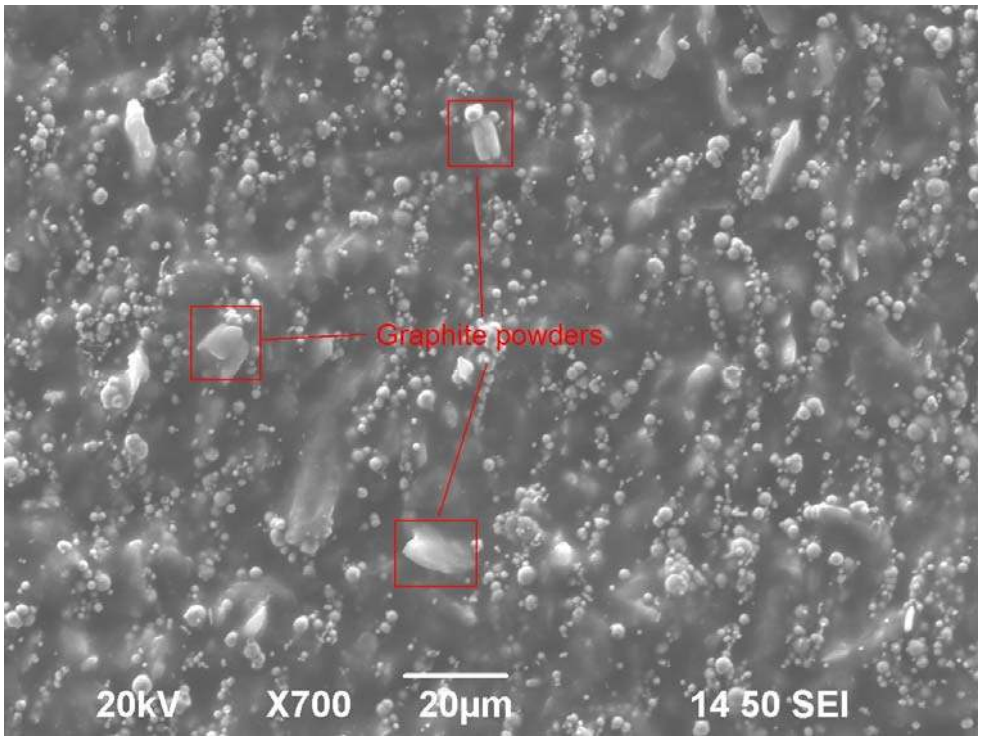

Fig. 3.8 Microstructure of anisotropic Gr MREs (Gr 20%)

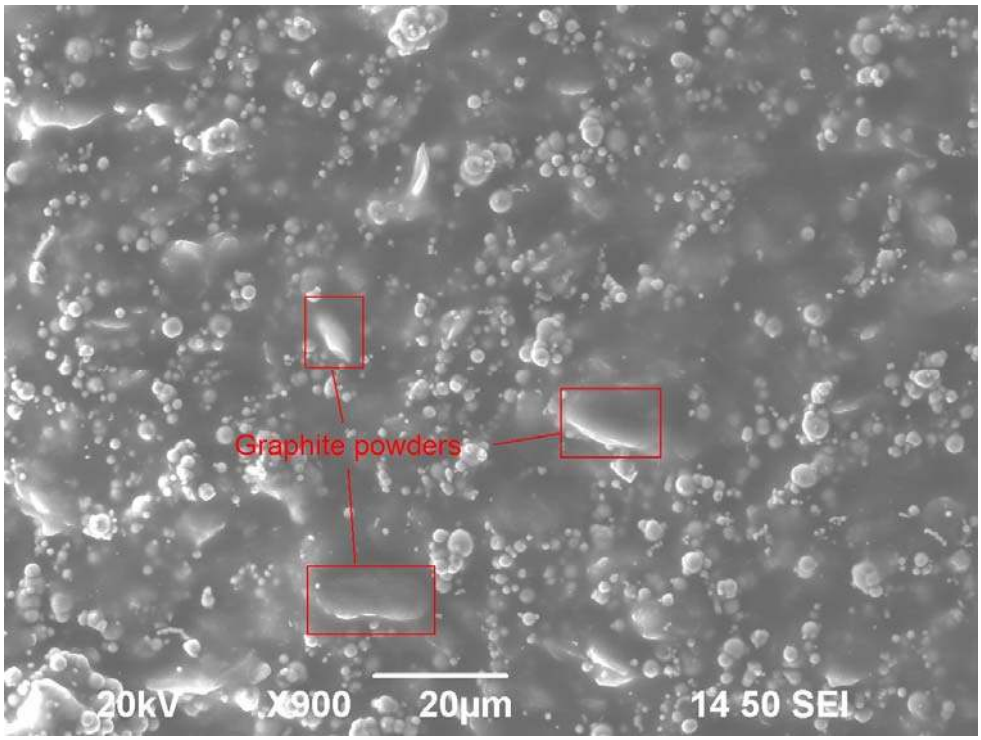

Fig. 3.9 Microstructure of isotropic Gr MREs (Gr 20%)

From Fig. 3.2 & 3.3, we can see that the particle sizes of neither carbonyl iron particles nor graphite powders are equal. Fig. 3.3 & 3.5 show the microstructure of isotropic and anisotropic Gr MREs without graphite. The carbonyl iron particles array in chains in the anisotropic sample and disperse randomly in the isotropic sample. According to Fig. 3.6 & Fig. 3.8, in the anisotropic Gr MREs, the carbonyl iron particles array in chains and the graphite powders disperse in the matrix randomly. The reason of this phenomenon is that the magnetic field only affects the carbonyl iron particles, but not the graphite. So by the magnetism, the carbonyl iron particles move to chains along the same direction as the magnetic field in the matrix.

By comparing Fig. 3.4, Fig. 3.6 & Fig. 3.8, we can see that the carbonyl iron chains in the sample without graphite have the best lines performance. Further, the carbonyl iron chains in Fig. 3.6 are alined better than those in Fig. 3.8. The reason is that when the mixture of carbonyl iron, silicone rubber, silicone oil and graphite is curing under the magnetic field, the graphite powders in Gr MREs affect the carbonyl iron particles' movement. The more graphite in the mixture, the more effects are applied on to the carbonyl iron chains.

Also, by SEM observation, we can see that although some chains of carbonyl iron particles are disconnected at some parts, some graphite powder connects the two disconnected parts of a chain. In section 3.4, this will be discussed with the mechanical properties.

3.4 STEADY STATE & DYNAMIC PROPERTIES OF MREs

3.4.1 Experimental device

A rotational Rheometer (MCR 301, Anton Paar Companies, Germany) and a Magneto Rheolgical Device (MRD 180, Anton Paar Companies, Germany) were used to measure the MREs' mechanical properties. The Magneto Rheolgical Device is equipped with an electromagnetic kit which can generate a magnetic field perpendicular to the direction of the shear flow. A 20mm diameter parallel-plate measuring system with 1 mm gap was used.

The samples were sandwiched between a rotary disk and a base parallelly. In this study a steady-state rotary shear and oscillatory shear were both used for the experiments.

The schematic of the experimental setup is shown in Fig. 3.10. The stress and stain signals were output from two ports which were detected through a Data Acquisition (DAQ) board (Type: LABVIEW PCI-6221, National Instruments Corporation. U.S.A) and transferred to a computer by which the data was processed.

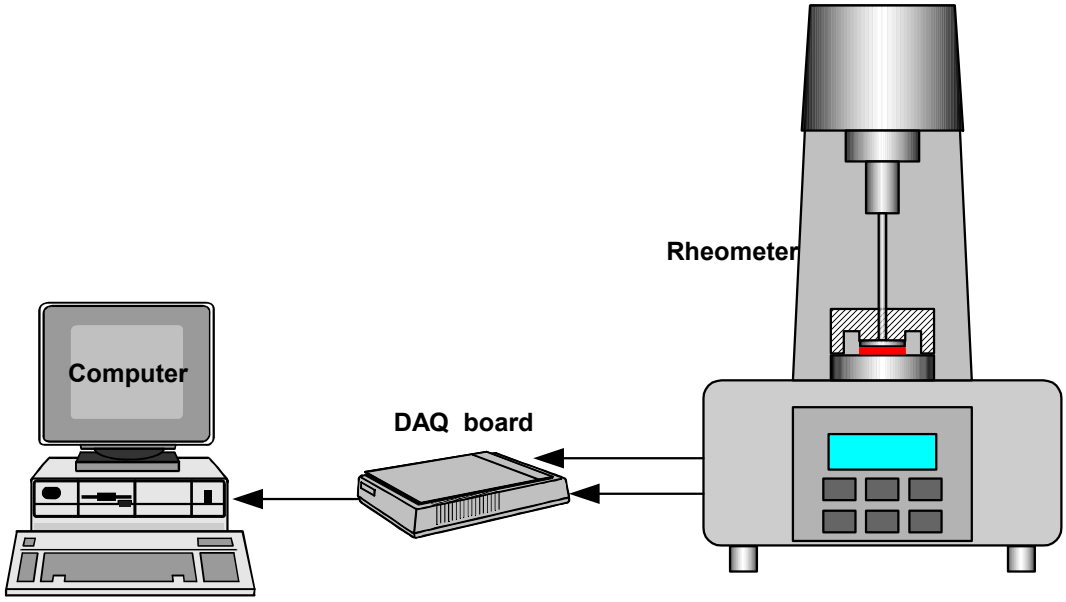

Fig. 3.10: A diagram of the experimental setup

In this experiment the magnetic flux density of the sample of MRE (B_{MRE}) in the measuring gap depends not only on the current (I) applied to the samples, but also on the magnetic properties of MRE materials. The relationship between B_{MRE} versus I is found to be:

$B_{MRE} = 220\ I$

where the units of B_{MRE} and I are in mT and amp (A), respectively.

In the following test, the test current varies from 0A to 2A with the increment 0.5A, whose intensity of magnetic field is 0 mT to 440 mT with the increment 110 mT.

3.4.2 Steady state

Under rotary shear the shear stress and shear strain of MREs under fields varying from 0~2A were measured. The MR effect was evaluated by measuring the shear strain-stress curve of the sample with and without a magnetic field applied.

Fig. 3.11-3.16 show the strain-stress curve of different samples at 5 different magnetic field intensities ranging from 0 to 440mT.

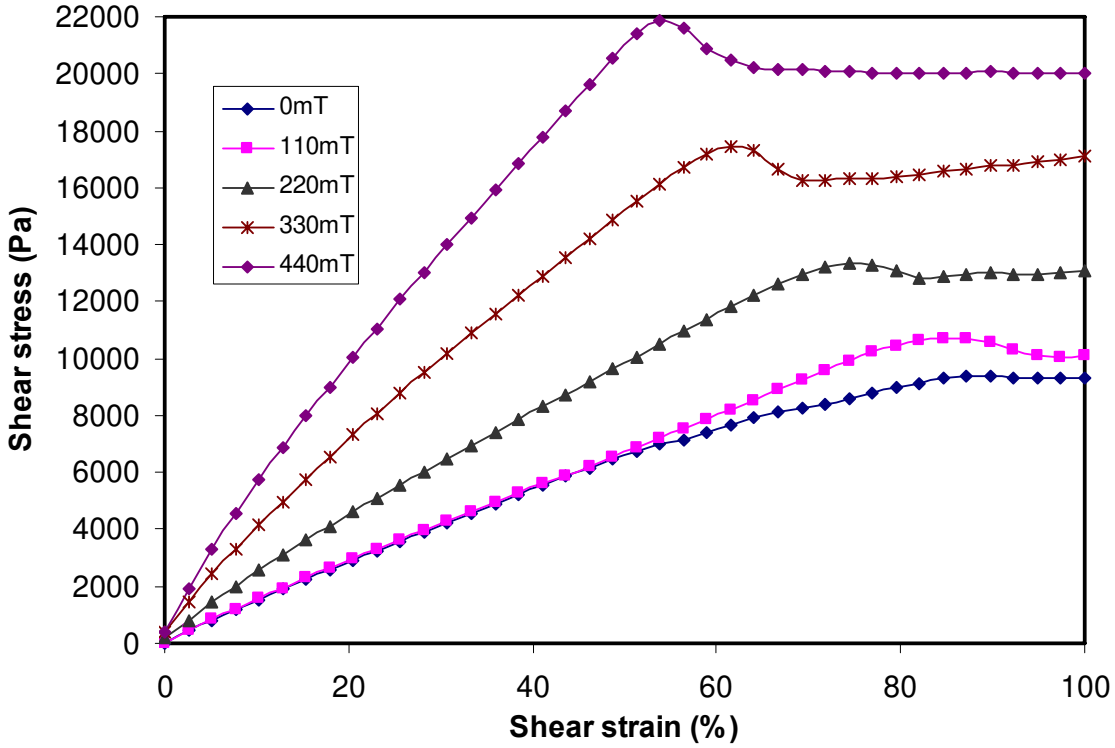

Fig. 3.11 Strain-stress curve versus magnetic field (isotropic MRE Gr 0%)

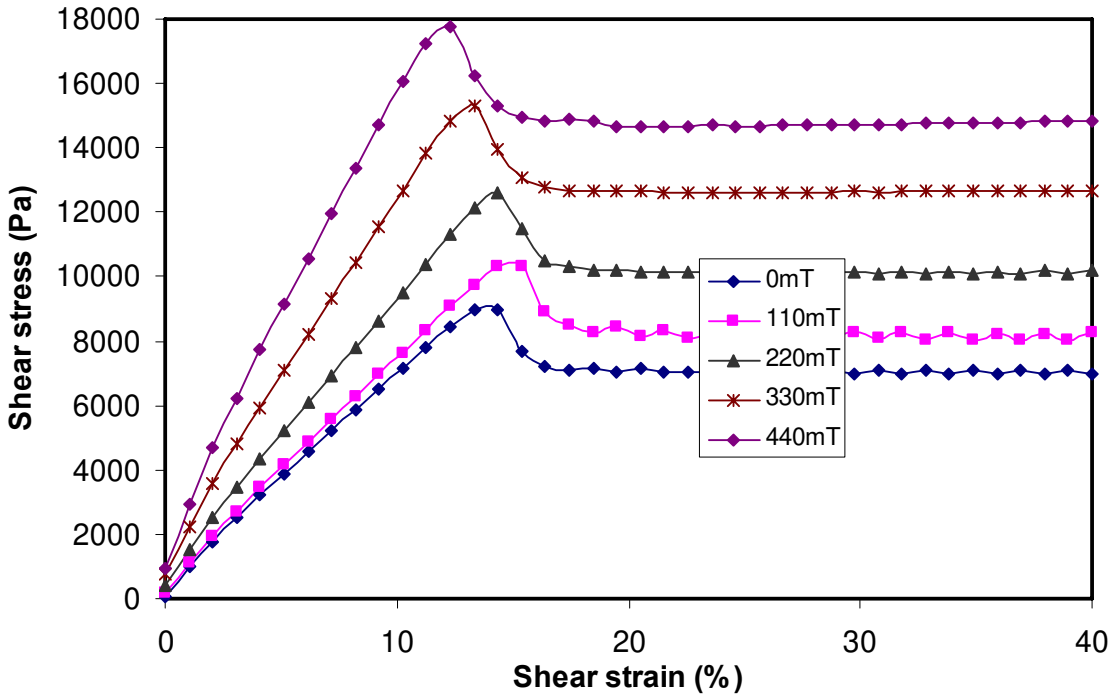

Fig. 3.12 Strain-stress curve versus magnetic field (isotropic MRE Gr 15.79%)

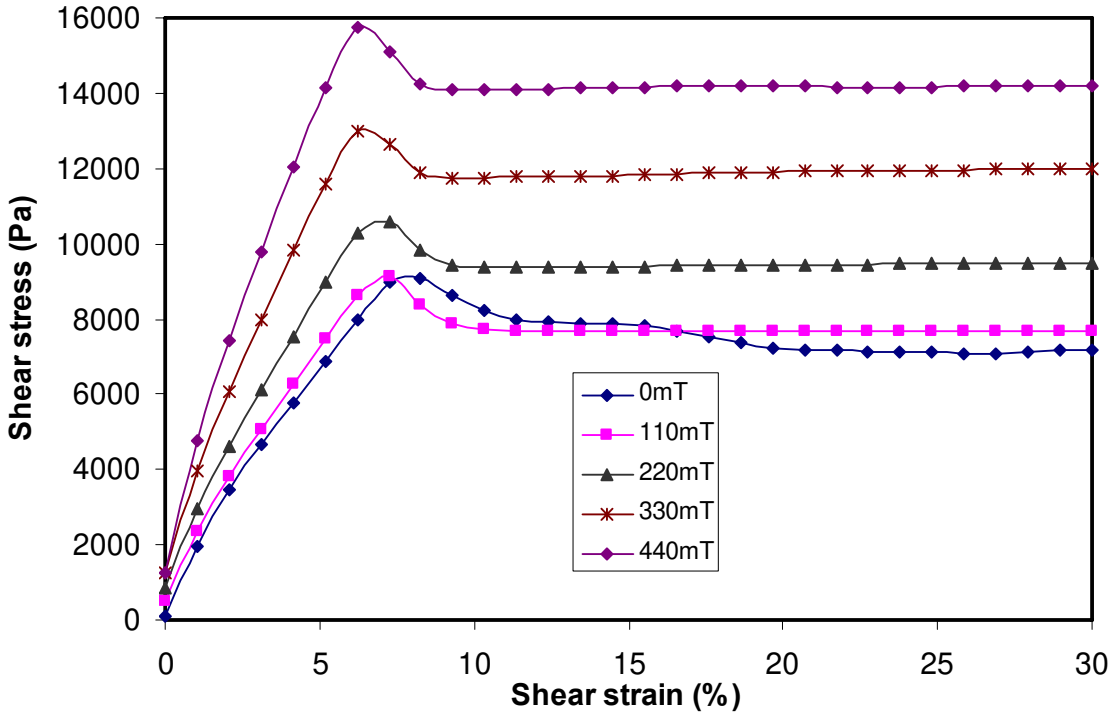

Fig. 3.13 Strain-stress curve versus magnetic field (isotropic MRE Gr 23.81%)

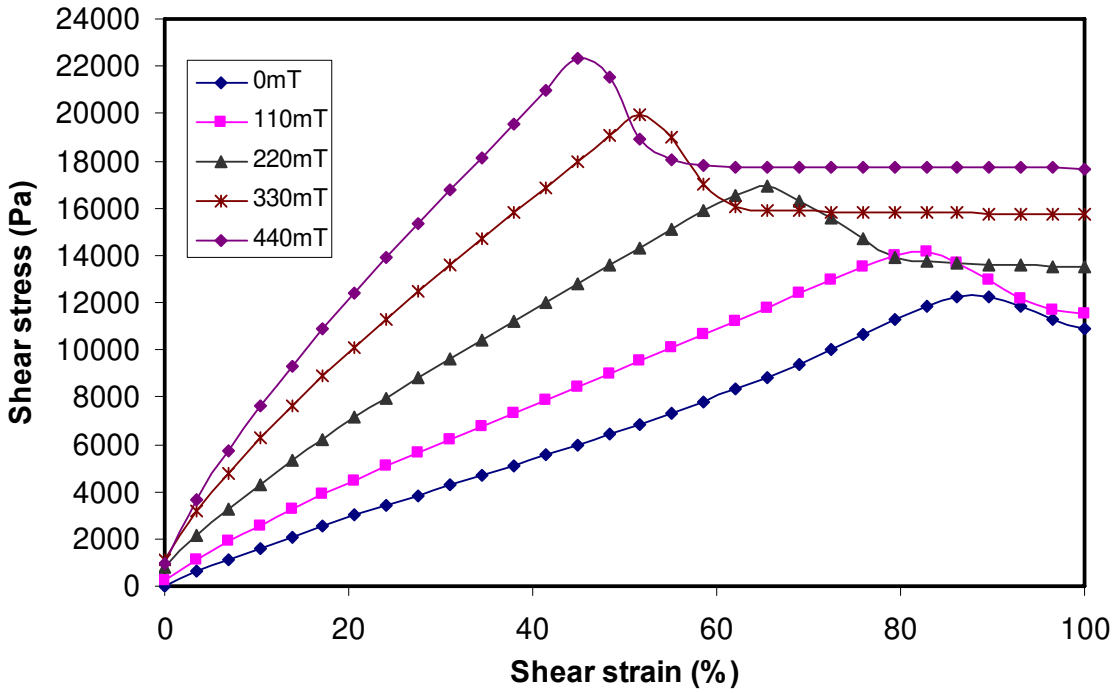

Fig. 3.14 Strain-stress curve versus magnetic field (anisotropic MRE Gr 0%)

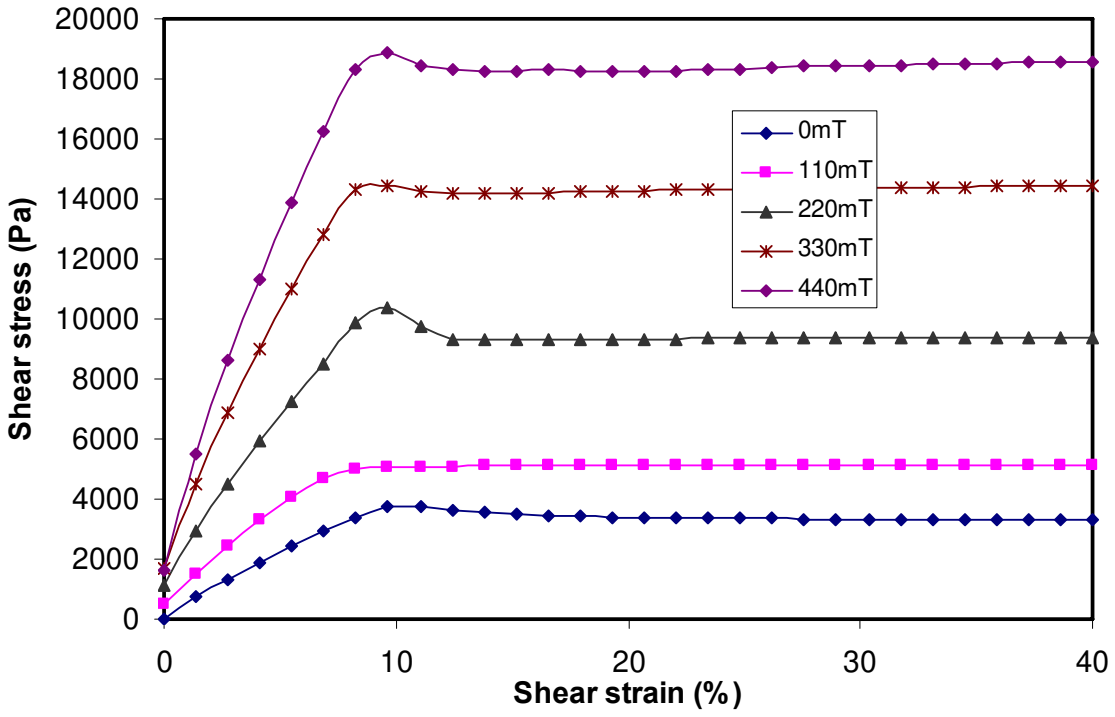

Fig. 3.15 Strain-stress curve versus magnetic field (anisotropic MRE Gr 15.79%)

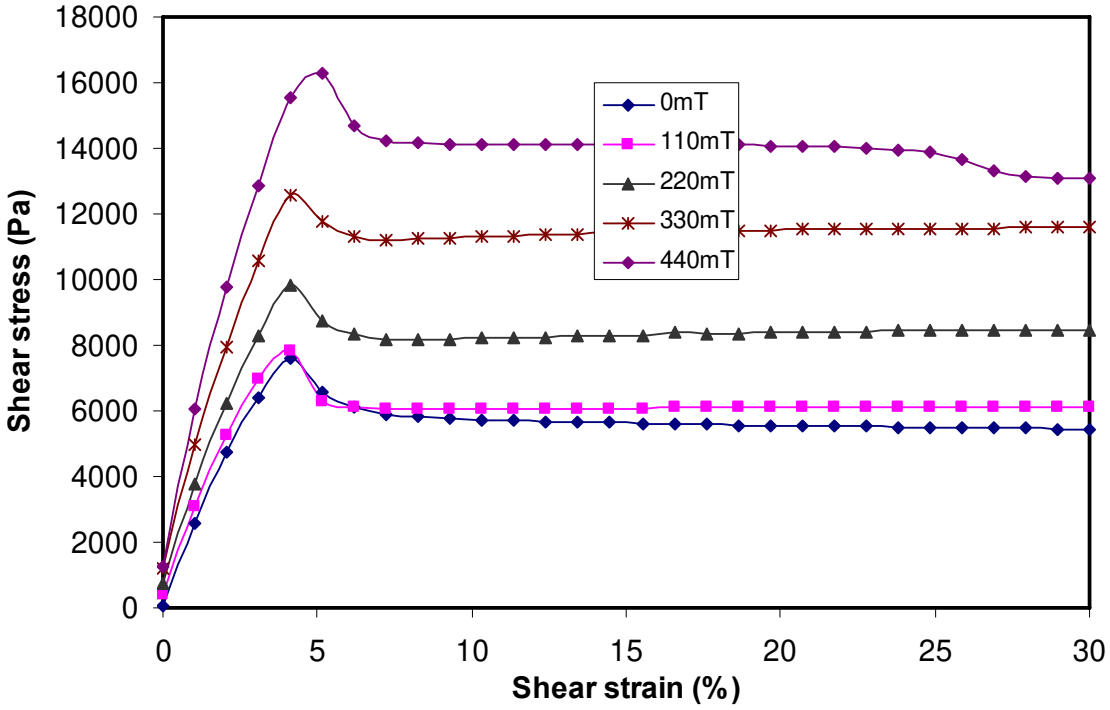

Fig. 3.16 Strain-stress curve versus magnetic field (anisotropic MRE Gr 23.81%)

The slope of the strain-stress curve is the shear modulus of the material. As can be seen in the figures, all the samples' shear modulus show an increasing trend with magnetic field before they reach magnetic saturation at high field strength, which proves that all the MRE samples exhibit obvious MR effects.

From above figures, the shear stress shows a linear relationship with the shear strain when the strain is within a range. This means the MRE acts with linear viscoelastic properties when the strain is below a limitation. For conventional MREs, the limitation is around 50% shear strain. When the graphite weight fraction increases from 0 to 15.79%, the range of linearity decreases from 50% to around 10%. For the samples with higher graphite weight fraction as 23.81%, the linearity ranges are only 6% and 4% for isotropic and anisotropic samples, respectively. When the strain is above the limitation, the shear modulus reaches a saturation (maximum value) and decrease steadily. This could be due to sliding effect. The higher magnetic field intensity leads to higher steady shear stress. Fig. 3.17 shows the linear ranges of different samples at various magnetic field intensities.

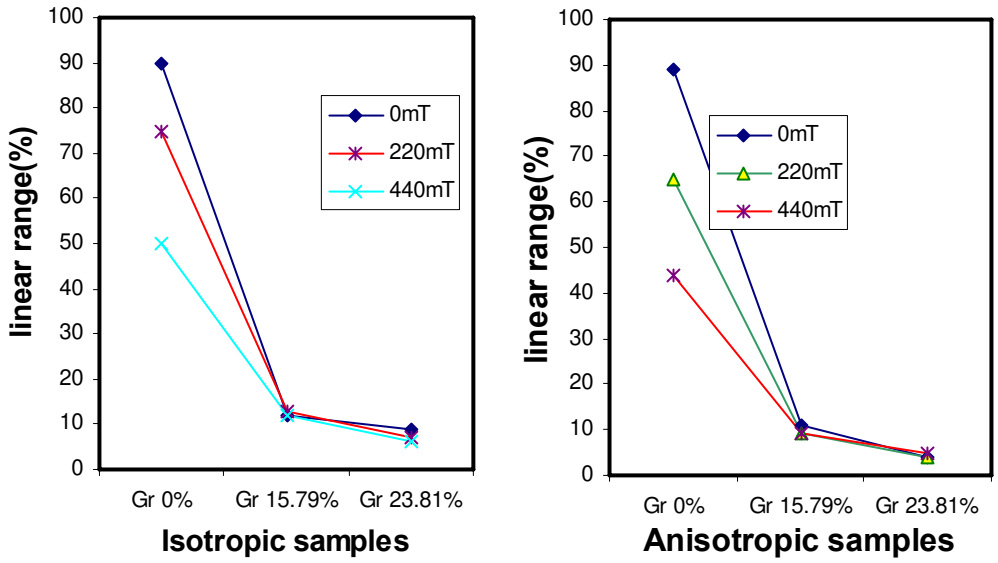

(a) (b)

Fig. 3.17 linear ranges versus different samples (a) isotropic samples (b) anisotropic samples

For the isotropic and anisotropic samples with same compositions, the isotropic samples always have the bigger linearity ranges and steady shear stress than chose of anisotropic samples.

For each curve, the slope equals to the ratio of peak yield shear stress to the relevant shear strain.

By analyzing the slope and of the curves, it is easy to see that the more graphite in the material, the less growth of slopes when the magnetic field increase from 0 to 440mT. This is because of the contributions of graphite powders to the stiffness of the samples. The graphite increases the initial stiffness of Gr MREs, thus the stiffness changing from the MR effect can not be as the same as the conventional MREs. Fig. 3.18 shows the peak yield stresses of different samples at 220mT, 330mT and 440mT magnetic field.

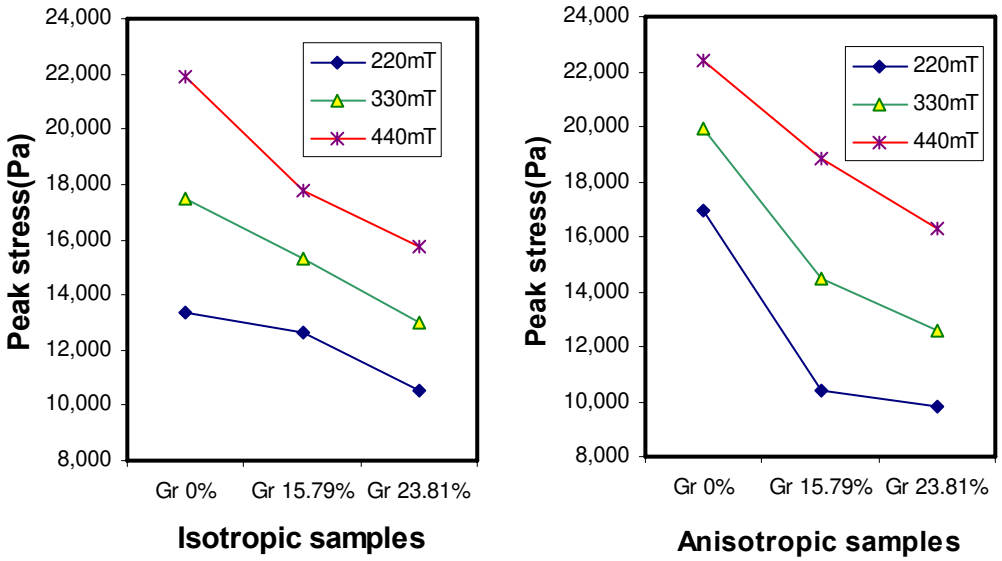

(a) (b)

Fig. 3.18 Peak yield stresses versus different samples (a) isotropic samples (b) anisotropic samples

The relative MR effect ($\Delta G_{max}/G_0$) of several samples is shown in Fig. 3.19. G_0 denotes the MRE samples' zero-field modulus, ΔG_{max} denotes the saturated field-induced modulus, and $\Delta G_{max}/G_0$ denotes the relative MR effect.

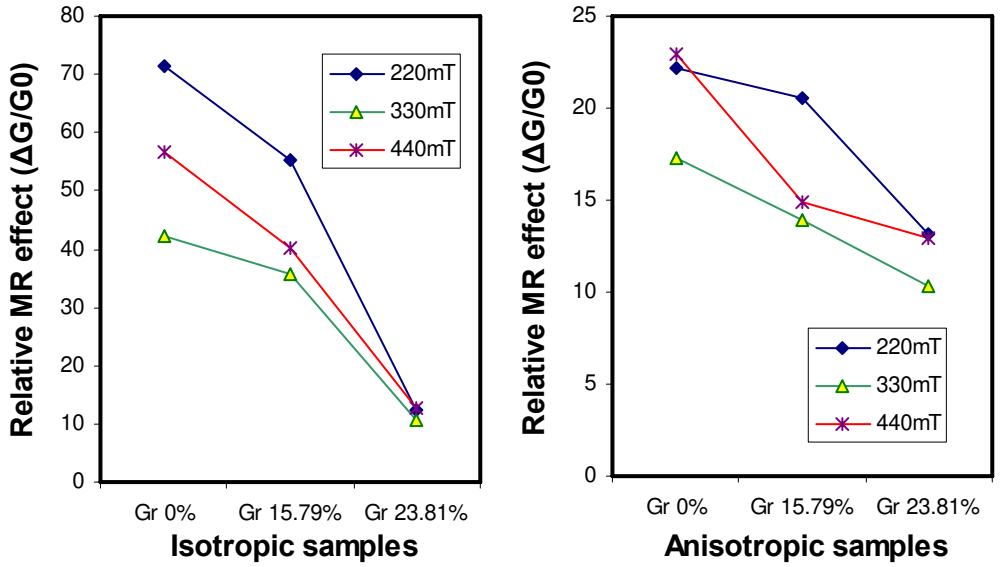

(a) (b)

Fig. 3.19 relative MR effects versus different samples (a) isotropic samples (b) anisotropic samples

It can be seen from Fig. 3.19 that G_0 is enhanced with the increase in graphite powders content. This result indicates that graphite powders can modify particle properties and, consequently, influenced the MR effect. The MR effects correspond well with the microstructures of Gr MREs.

3.4.3 Dynamic tests result

In order to obtain the dynamic mechanical behavior of MRE, both angular frequency sweep tests and strain amplitude sweep tests were used. Five sets of data were collected for different amplitudes of oscillation, according to the various magnetic fields input to the samples of MR elastomers. Same as the steady state tests, five different magnetic field intensities, 0, 110, 220, 330 and 440mT, were used in this experiment. The current intensities in the coil are ranged from 0 to 2A. The amplitude of shear strain in angular frequency sweep tests is set at 1% and the input frequency was 5Hz in the strain amplitude sweep tests.

3.4.3.1 Strain amplitude sweep

In the strain sweep test, the storage and loss moduli were tested by varying strain from 0.01% to 100% at different magnetic fields. The intensities of the magnetic field used in this test were still 0, 110, 220, 330 and 440mT. Fig. 3.20-3.23 show the changing of storage modulus and loss moduli at the strain amplitude sweep.

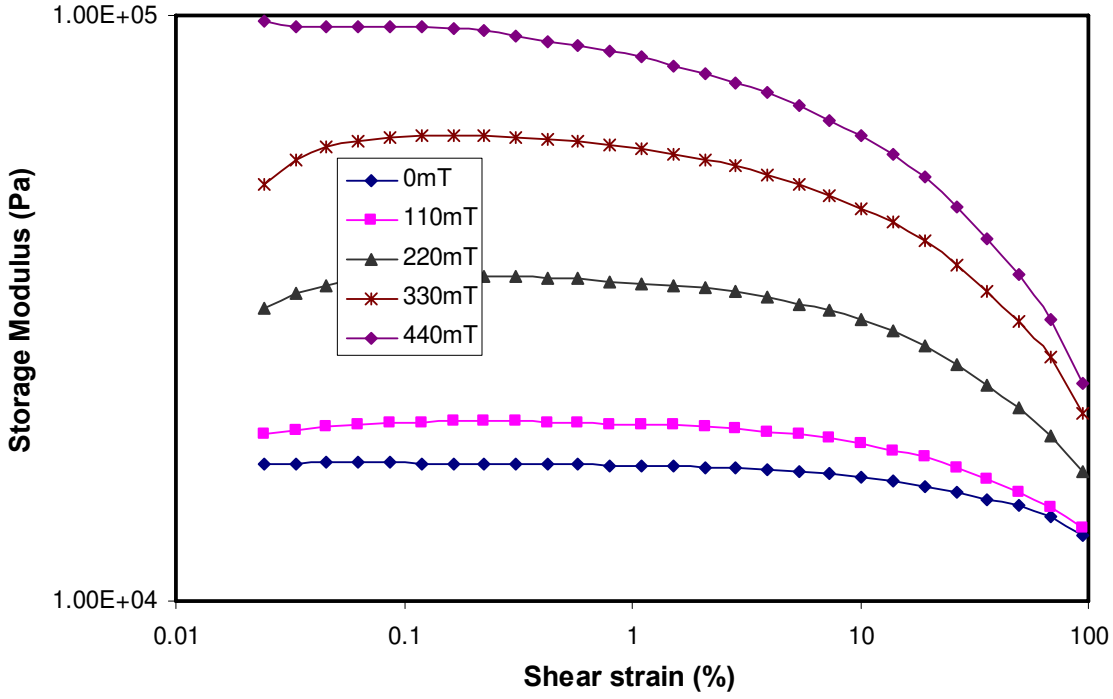

(a)

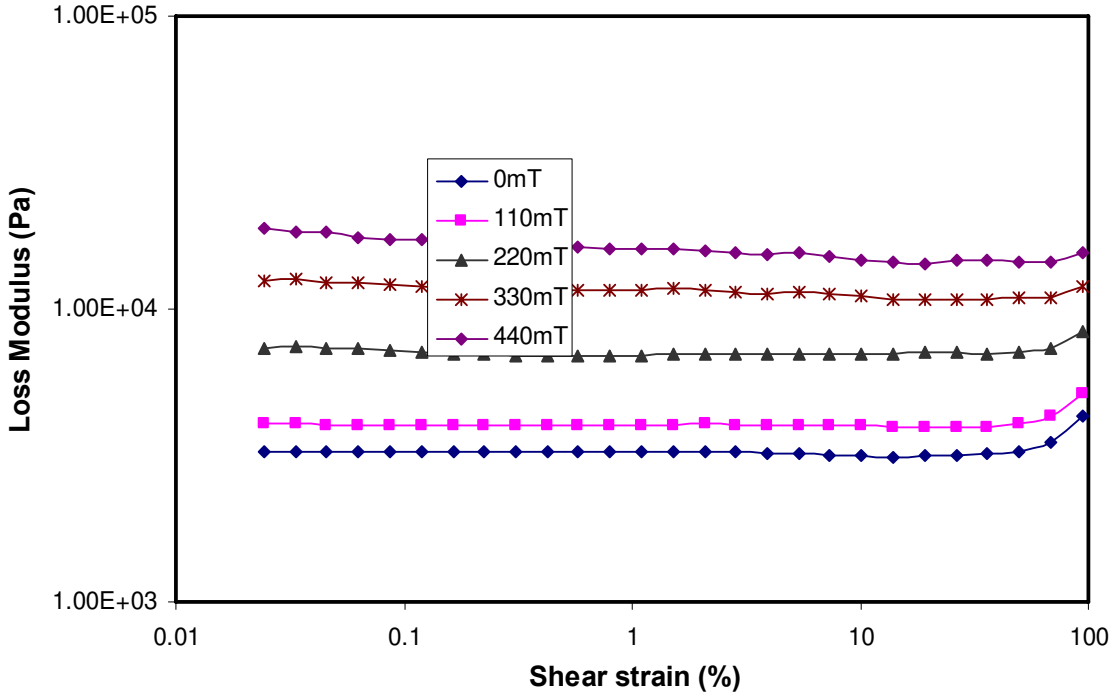

(b)

Fig. 3.20 Storage and Loss Modulus versus strain amplitude sweep (isotropic MRE Gr 0%) (a) Storage modulus vs. shear strain (b) Loss modulus vs. shear strain

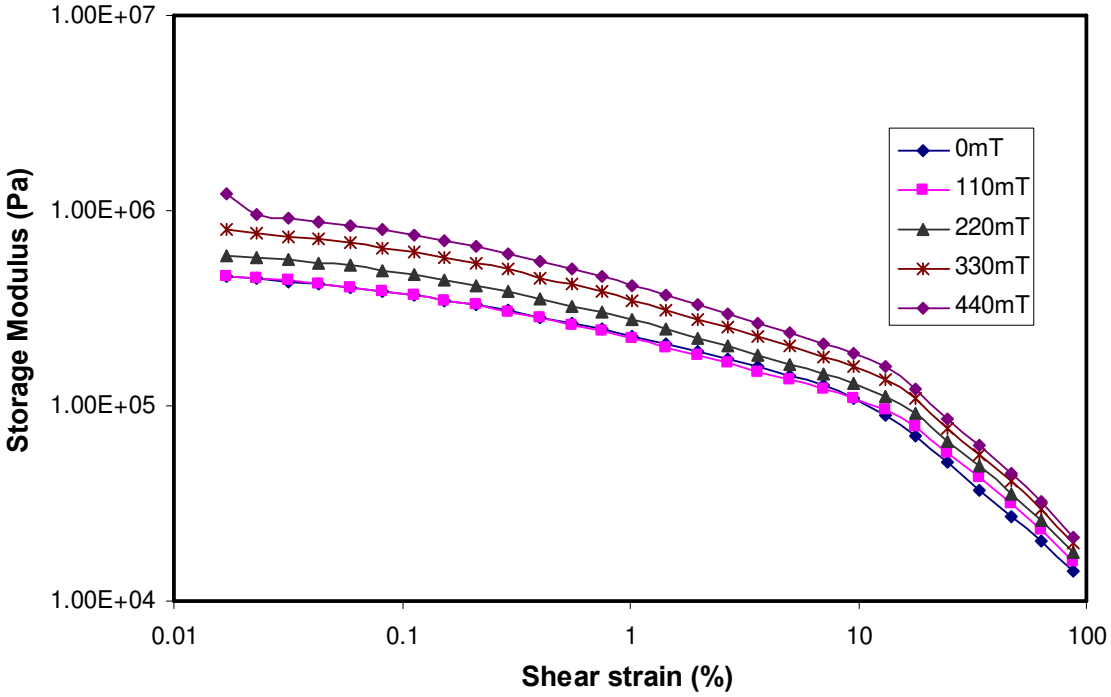

(a)

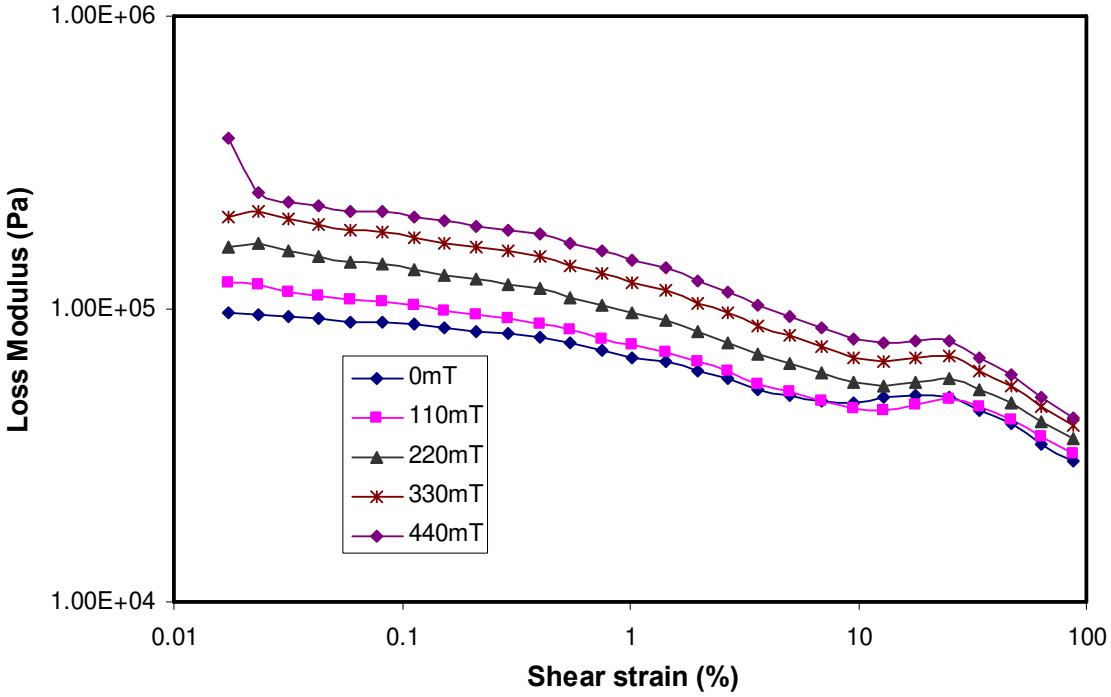

(b)

Fig. 3.21 Storage and Loss Modulus versus strain amplitude sweep (isotropic MRE Gr 20%) (a) Storage modulus vs. shear strain (b) Loss modulus vs. shear strain

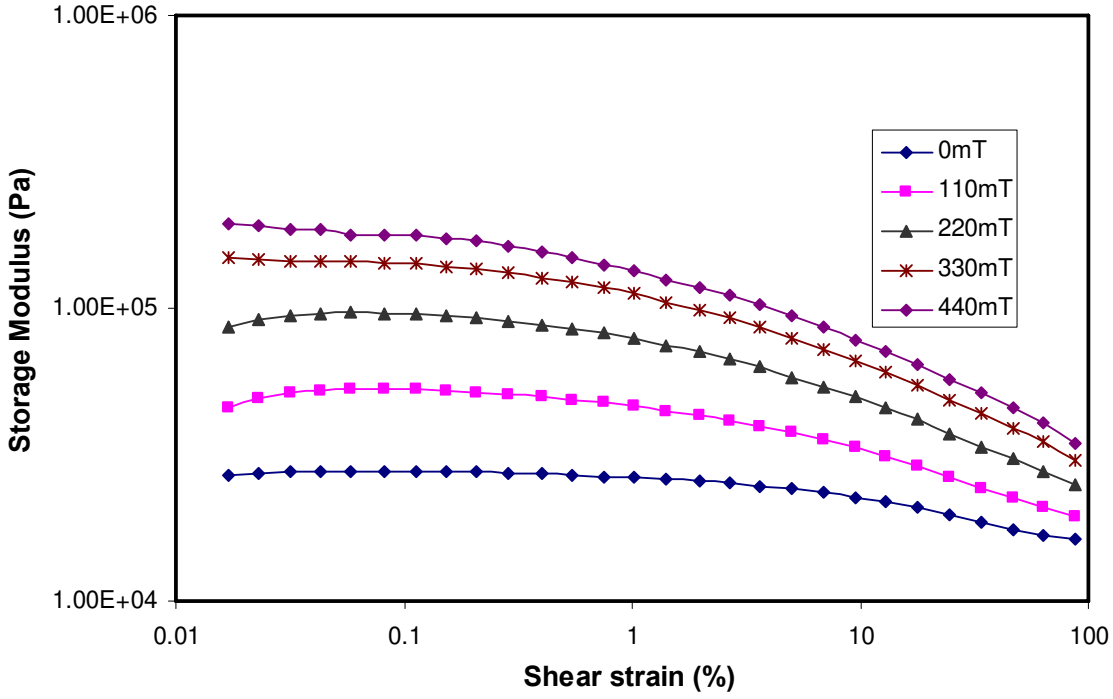

(a)

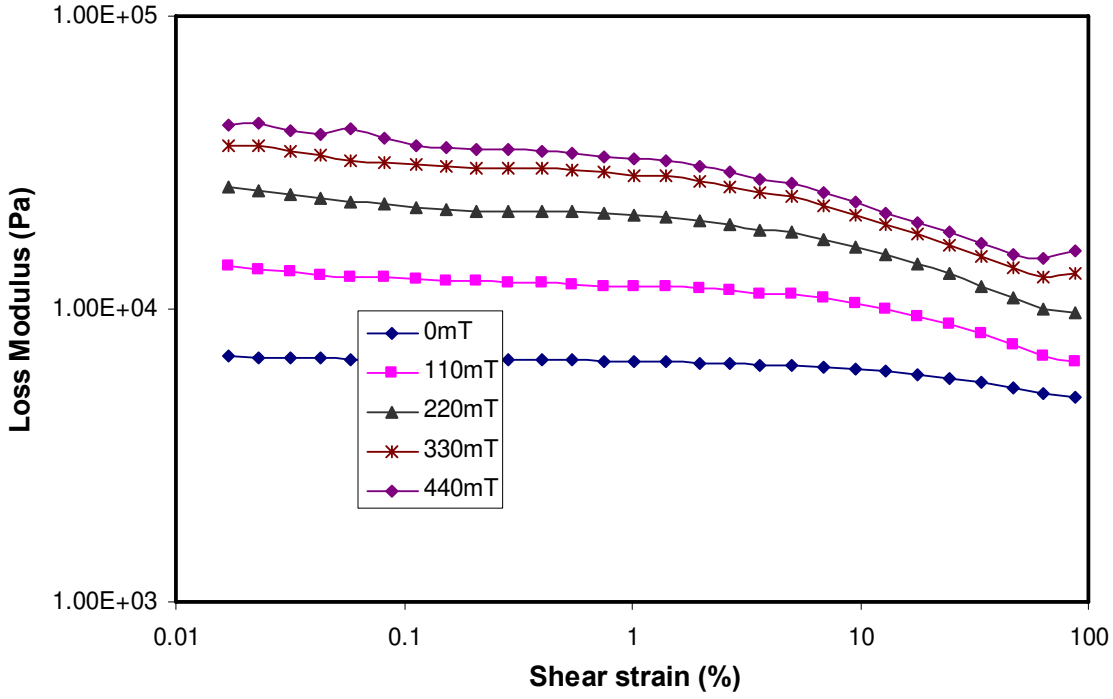

(b)

Fig. 3.22 Storage and Loss Modulus versus strain amplitude sweep (anisotropic MRE Gr 0%) (a) Storage modulus vs. shear strain (b) Loss modulus vs. shear strain

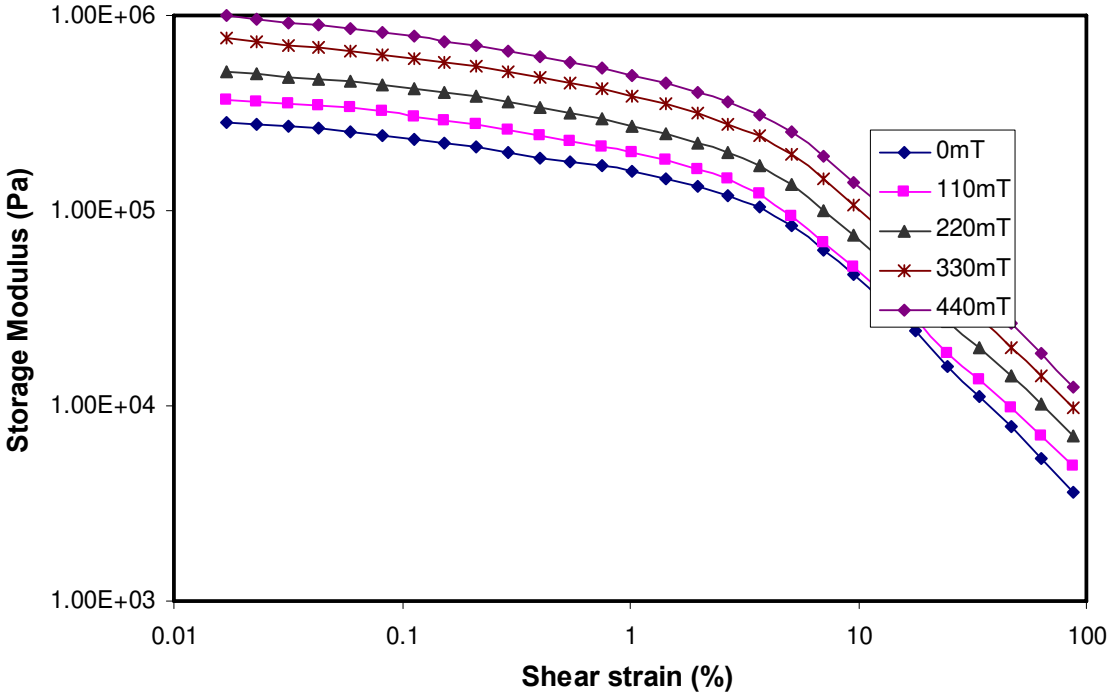

(a)

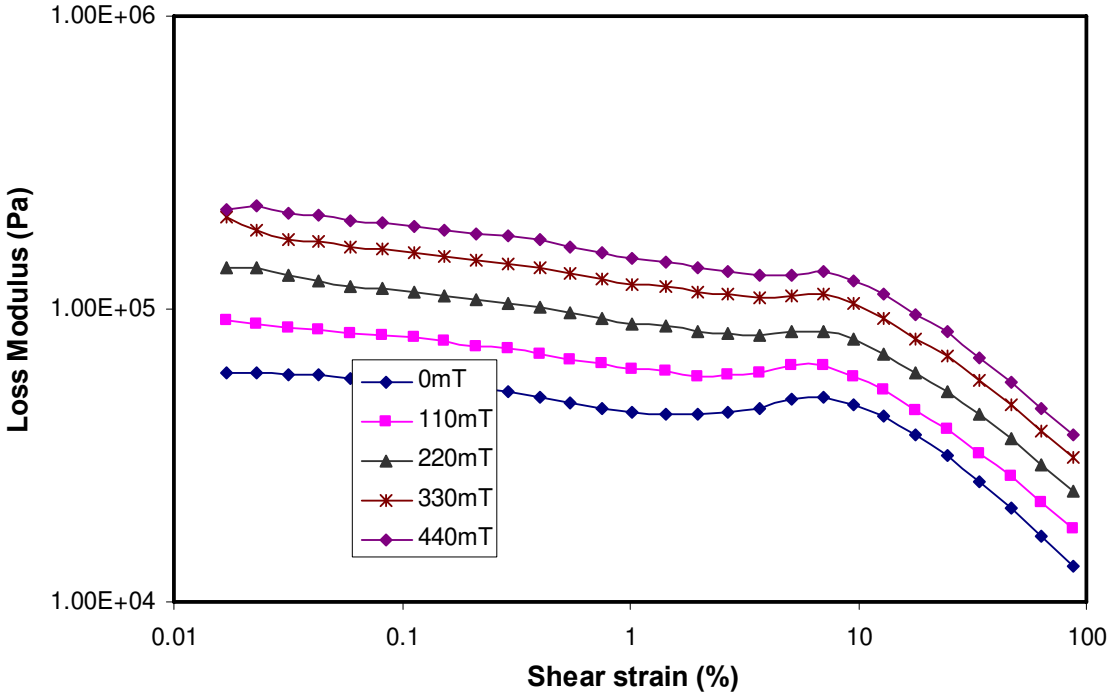

(b)

Fig. 3.23 Storage and Loss Modulus versus strain amplitude sweep (anisotropic MRE Gr 20%) (a) Storage modulus vs. shear strain (b) Loss modulus vs. shear strain

In Fig. 3.20 to 3.23, the overall trend of storage modulus is decreasing with the strain amplitude. It goes down smoothly within 10% shear strain and begins to drop significantly over 10% shear strain. Except of isotropic MREs without graphite, the Loss modulus has almost the same trends of storage modulus. This means at the high shear strain, the storage and loss moduli are much smaller than that at low shear strain.

Fig. 3.24 & 3.25 shows the storage modulus of different samples at 0mT, 220mT and 440mT magnetic field. The data are collected at 10% and 87.5% shear strain, respectively.

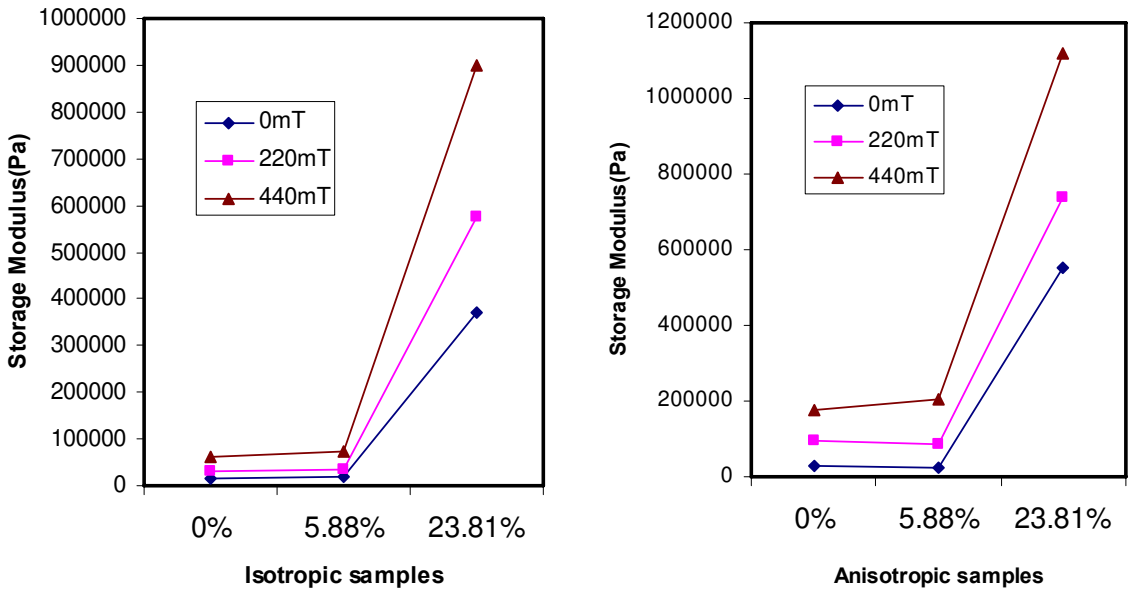

(a) (b)

Fig. 3.24 Storage Modulus of different samples at 10% shear strain (a) isotropic samples (b) anisotropic samples

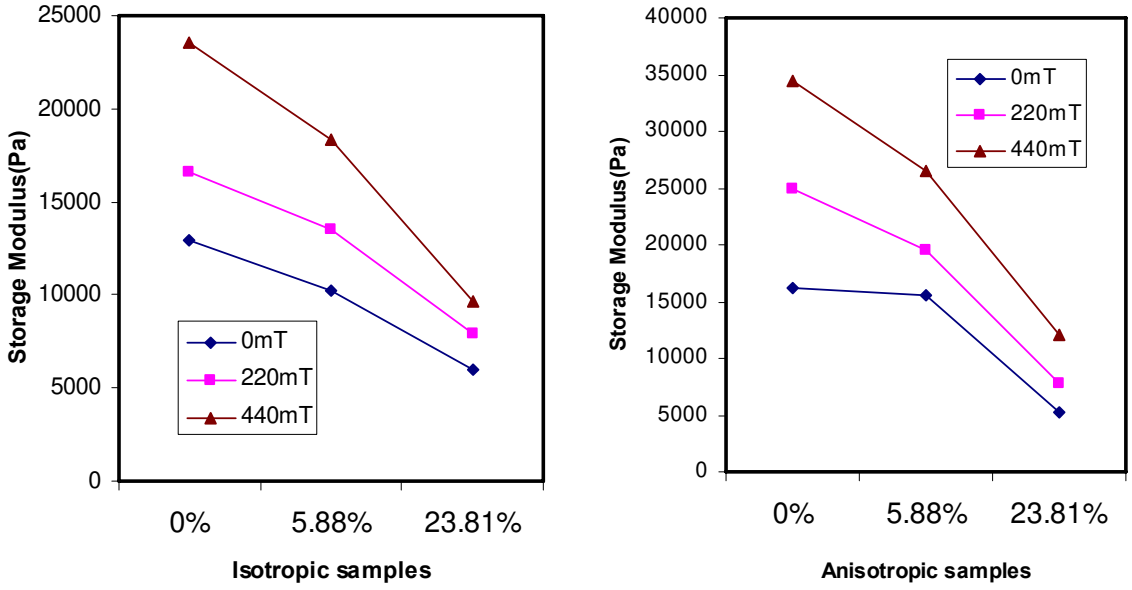

(a) (b)

Fig. 3.24 Storage Modulus of different samples at 87.5% shear strain (a) isotropic samples (b) anisotropic samples

As can be seen in Fig. 3.24, the storage modulus of all samples shows an increasing trend with graphite weight fraction at 10% shear strain which is in the linear range for most of samples. In Fig. 3.25, it turns to a diminishing trend with graphite weight fraction at 87.5% shear strain which is out of the linear range. This means in the linear range of shear strain, the samples with higher graphite weight faction have the bigger storage modulus.

Fig. 3.26 & 3.27 shows the storage modulus vs. magnetic field at 0.1% and 10% shear strain, respectively. The two shear strains are the beginning and end of linear range.

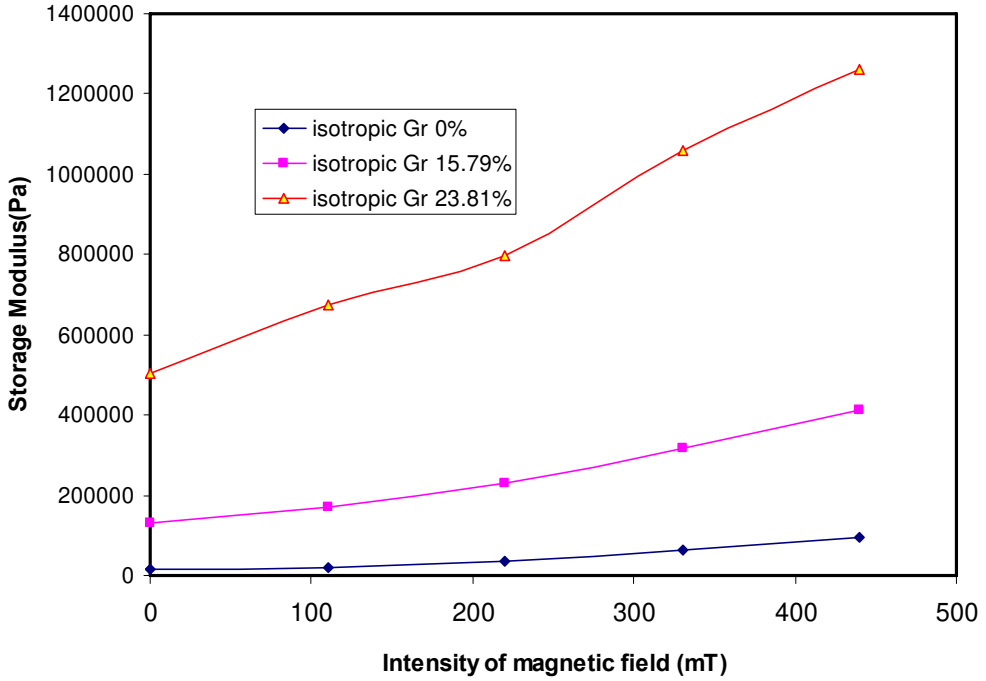

(a)

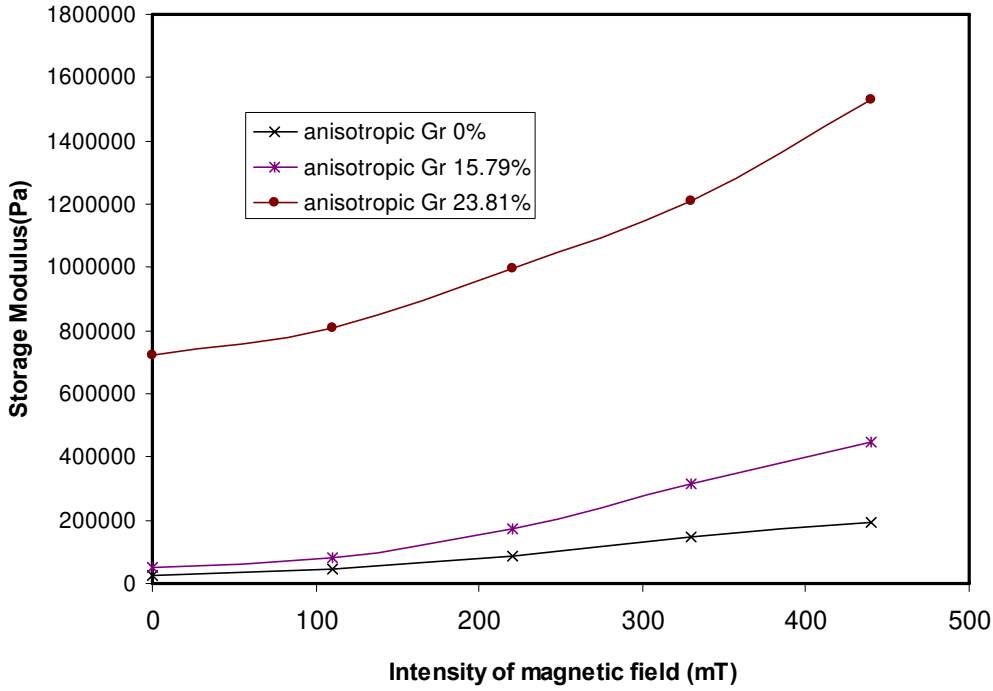

(b)

Fig. 3.26 Storage Modulus versus magnetic field at 0.1% shear strain (a) isotropic samples (b) anisotropic samples

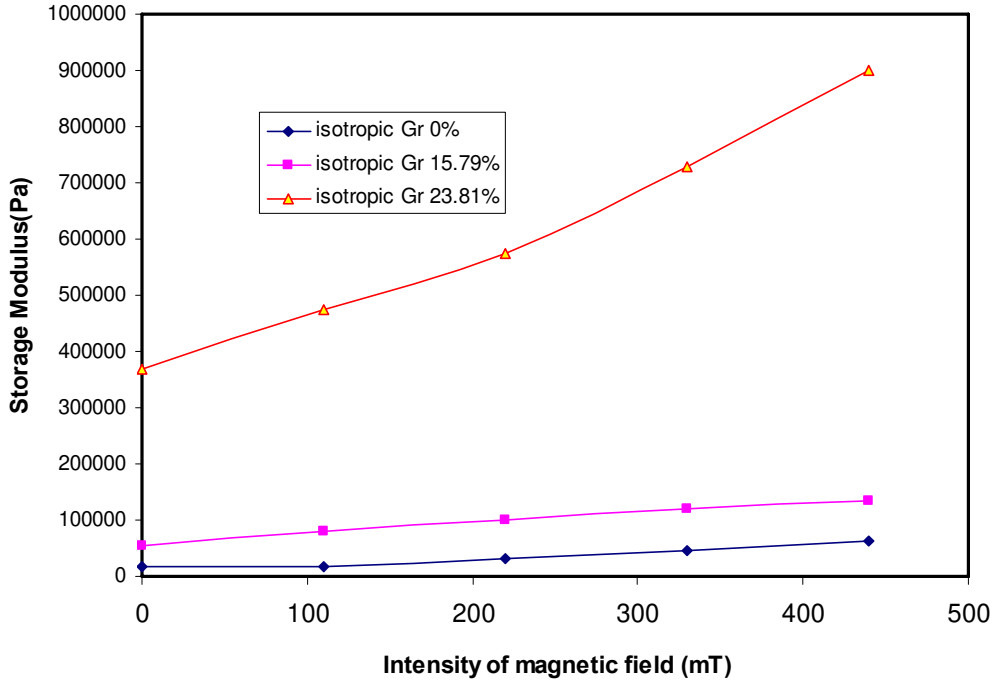

(a)

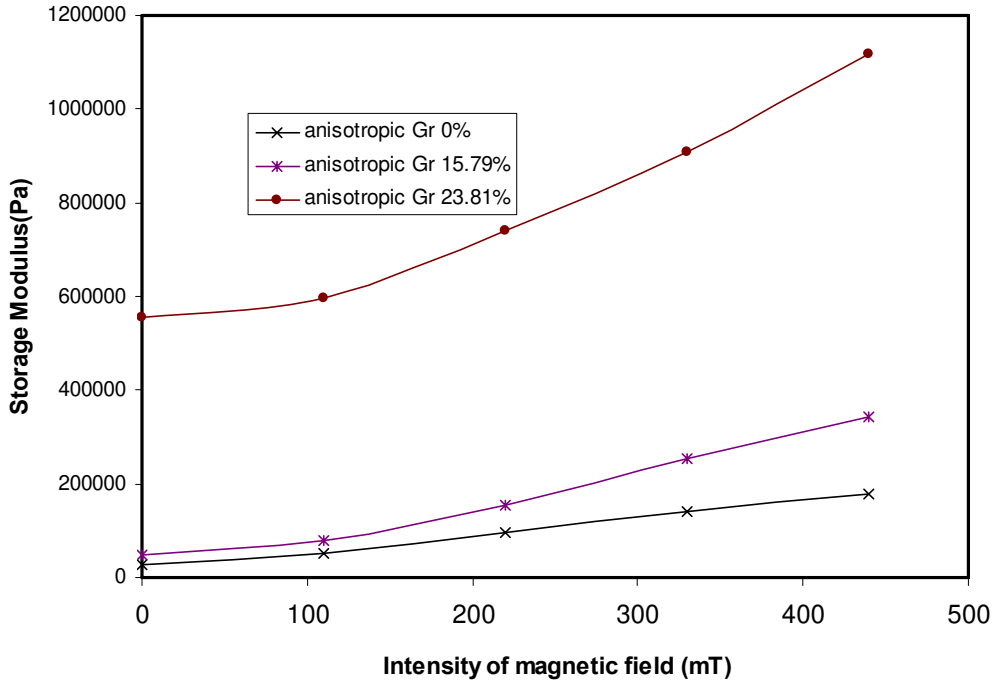

(b)

Fig. 3.27 Storage Modulus versus magnetic field at 10% shear strain (a) isotropic samples (b) anisotropic samples

In Fig. 3.26 & 3.27 we can see that the storage modulus shows an increasing trend with the intensity of magnetic field. The ratio of storage modulus at 440mT to that at 0mT is the MR effect. The MR effect of isotropic MREs with 0% graphite is around 4.5, when the graphite weight fraction increases to 15.79% and 23.81%, the MR effect decreases to around 2.8 and 2.8, respectively, which are all a little bigger than those in the angular frequency sweep. For anisotropic samples, the MR effects of 0%, 20% and 23.81% Gr MREs are 4.8, 3.2 and 2.2, respectively. This proves that again, with the growth of graphite weight fraction, the MR effect decreases.

3.4.3.2 Angular frequency sweep

In this test, the strain is set at 1%. According to the experimental equipments, the angular frequency was varied from 6 to 100 1/s at different magnetic fields as 0, 110, 220, 330 and 440 mT. The Fig. 3.28 to Fig. 3.31 show the storage and loss moduli curves of some MRE samples at frequency sweep.

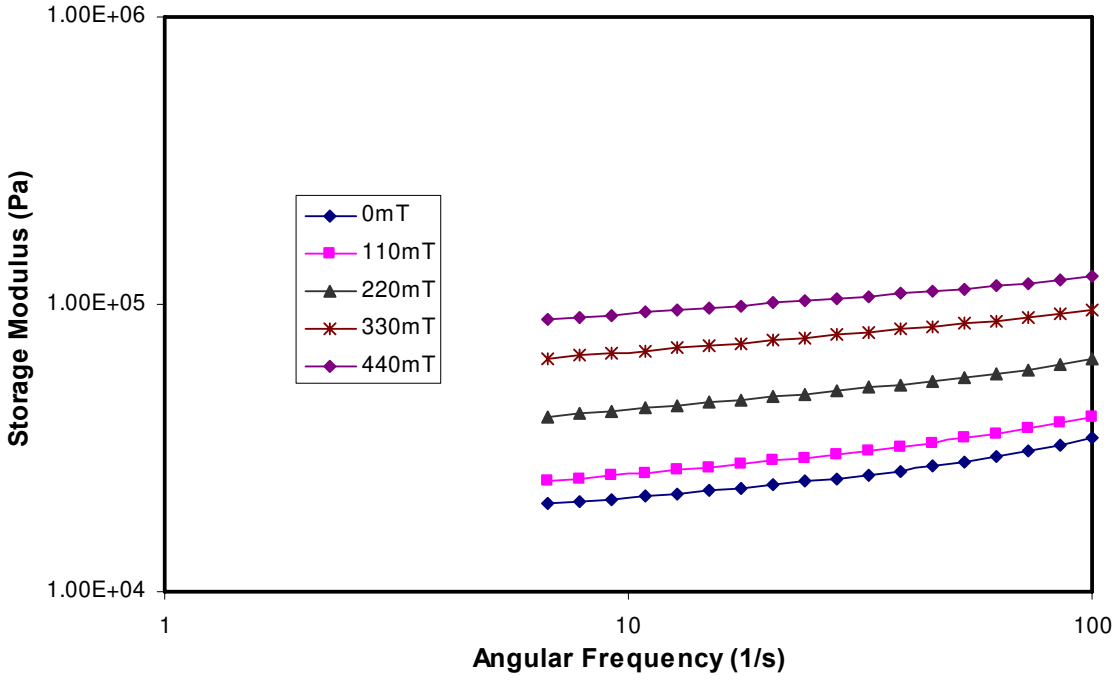

(a)

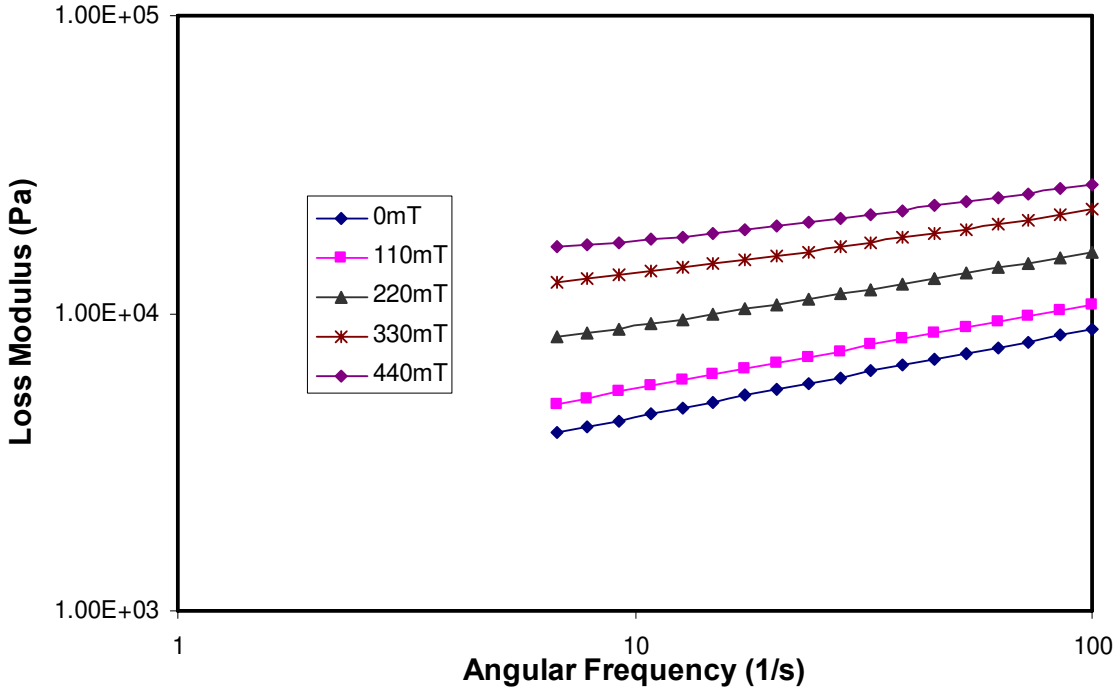

(b)

Fig. 3.28 Storage and Loss Modulus versus angular frequency sweep (isotropic MRE Gr 0%) (a) Storage modulus vs. shear strain (b) Loss modulus vs. shear strain

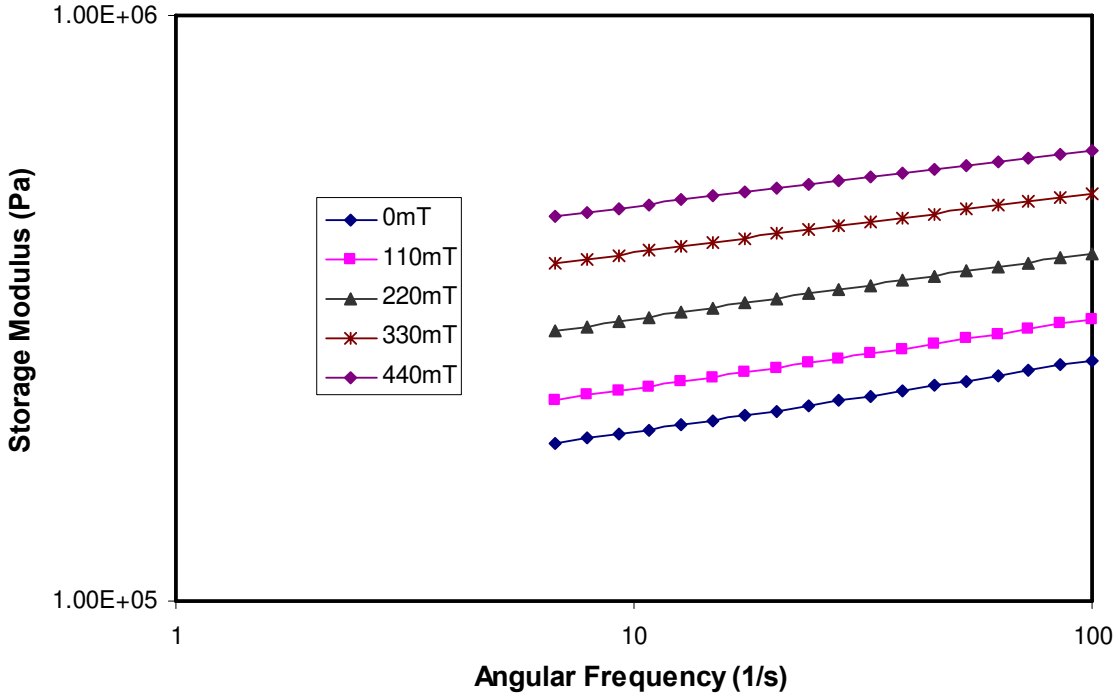

(a)

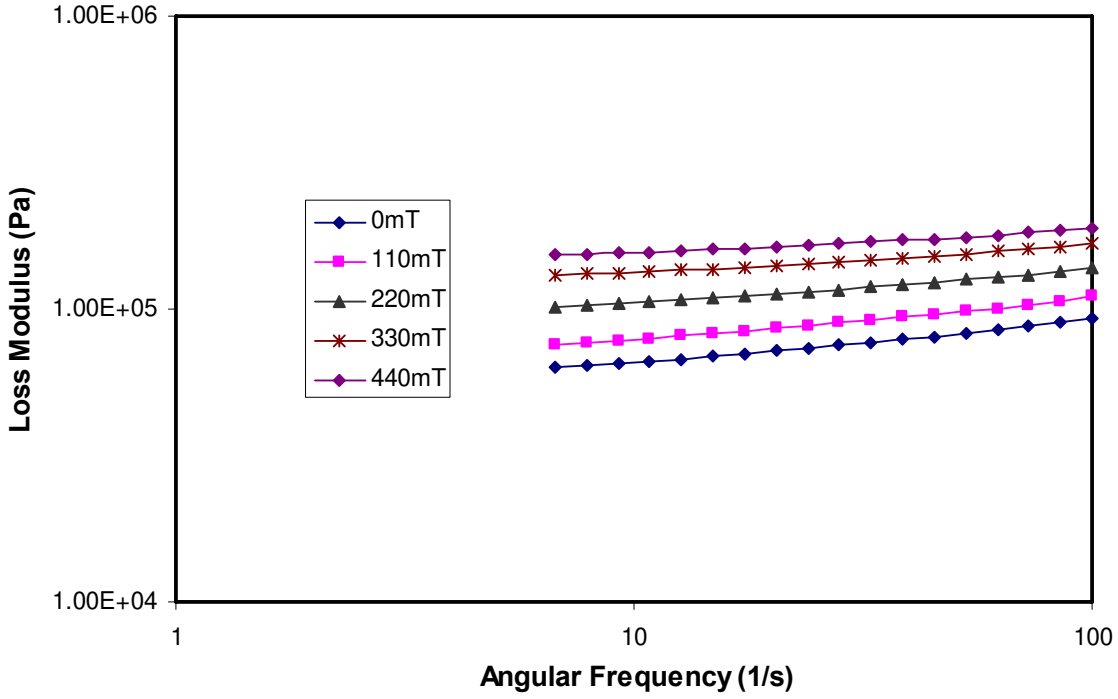

(b)

Fig. 3.29 Storage and Loss Modulus versus angular frequency sweep (isotropic MRE Gr 20%) (a) Storage modulus vs. shear strain (b) Loss modulus vs. shear strain

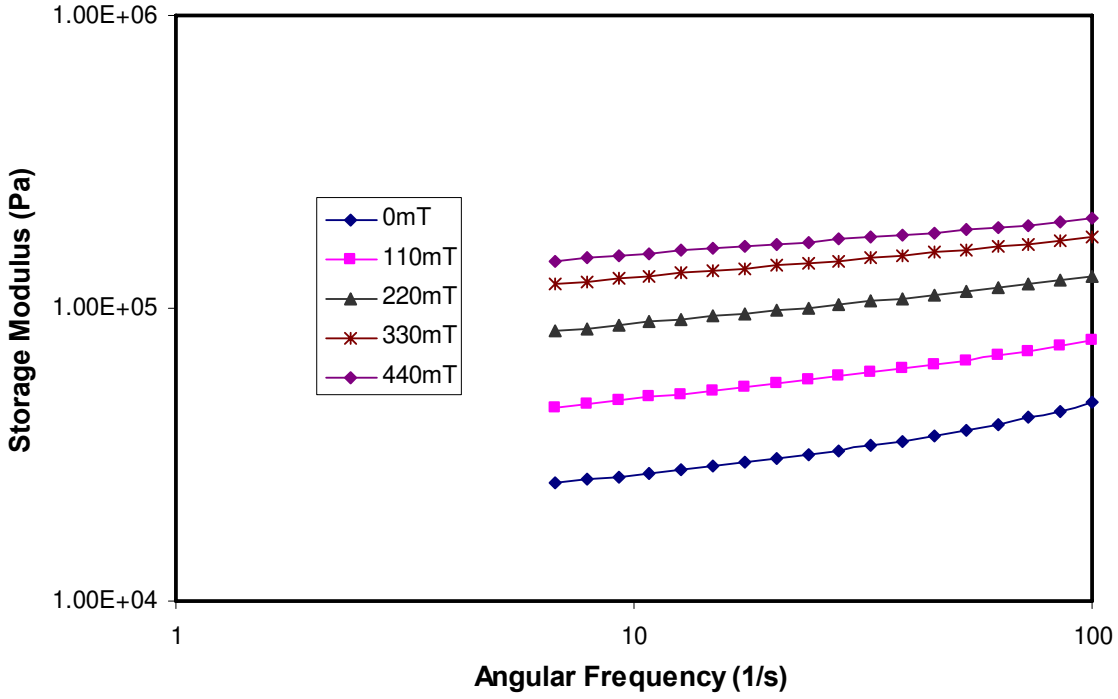

(a)

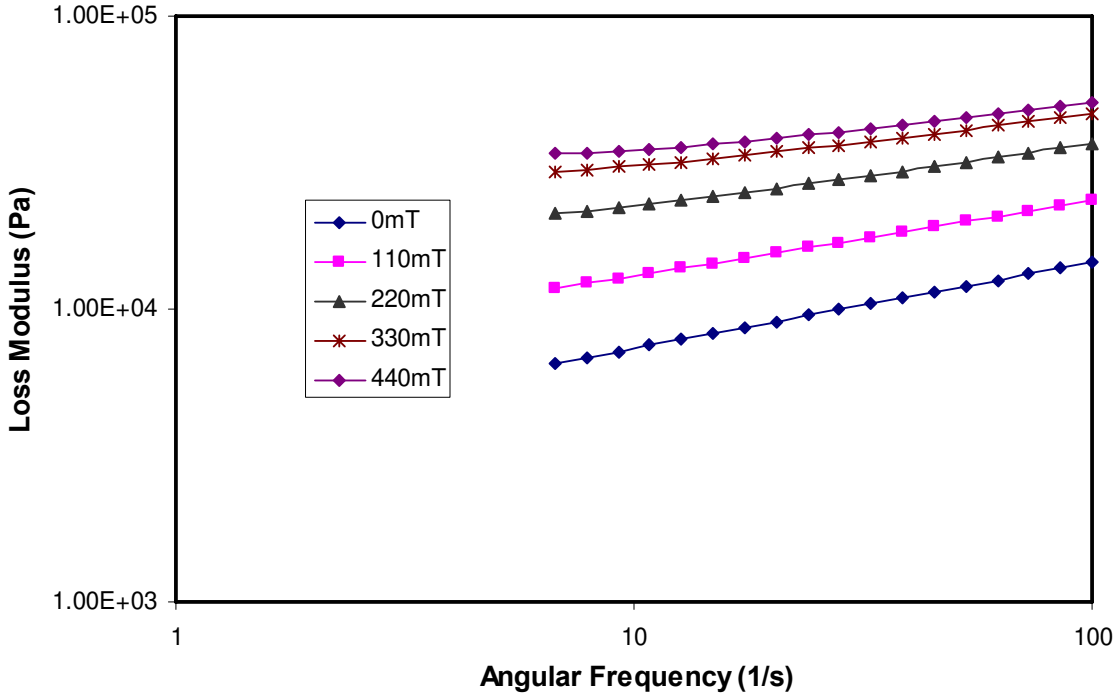

(b)

Fig. 3.30 Storage and Loss Modulus versus angular frequency sweep (anisotropic MRE Gr 0%) (a) Storage modulus vs. shear strain (b) Loss modulus vs. shear strain

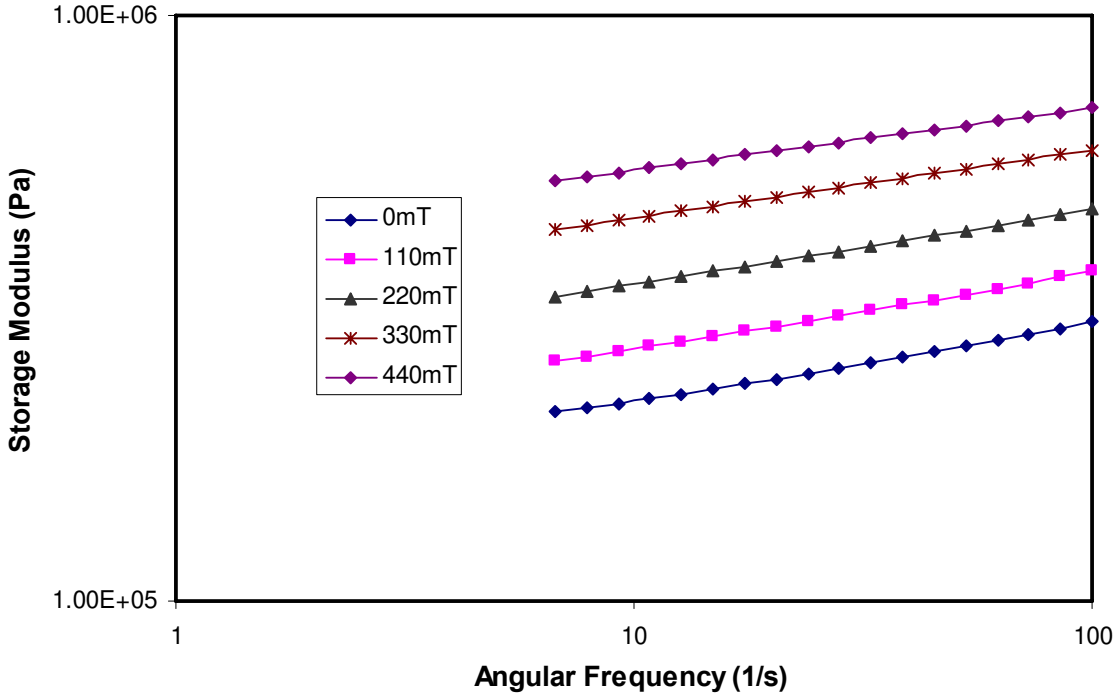

(a)

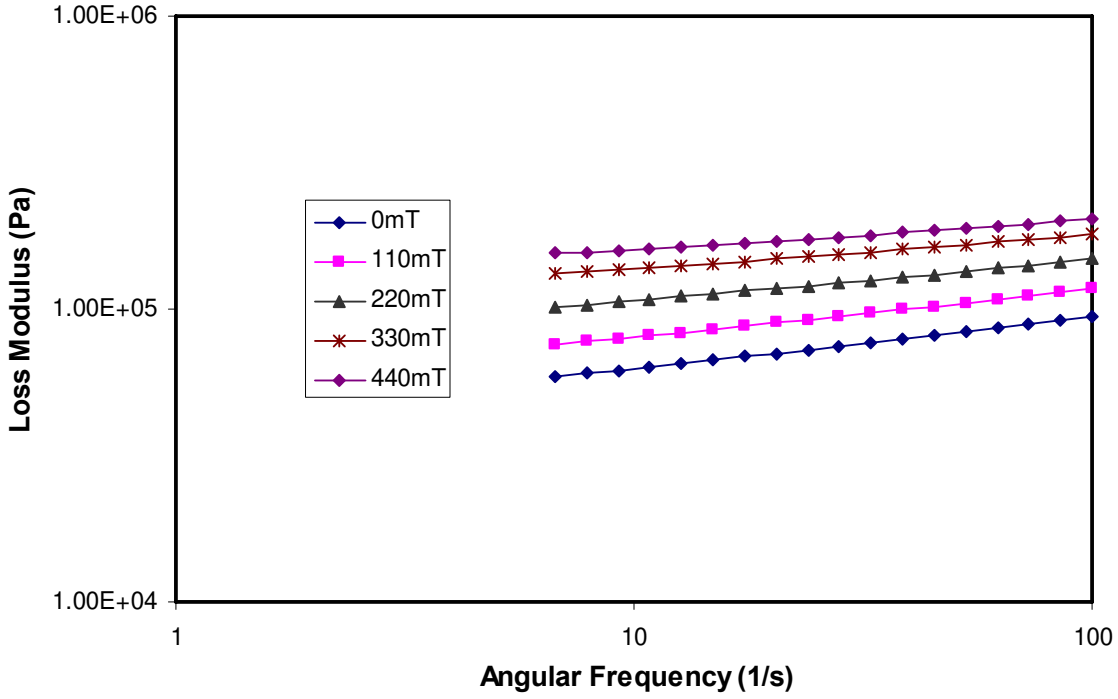

(b)

Fig. 3.31 Storage and Loss Modulus versus angular frequency sweep (anisotropic MRE Gr 20%) (a) Storage modulus vs. shear strain (b) Loss modulus vs. shear strain

From the figures above, we can see that in the log-log curves, the storage and loss moduli of all the samples are both increasing linearly with the growth of angular frequency. This means with at a higher angular frequency, the samples have bigger storage and loss moduli. This linear relationship of the storage and loss moduli to the angular frequency can be used to predict the storage and loss moduli at a certain frequency.

In the Fig. 3.32 to Fig. 3.35, the storage modulus of different samples was compared.

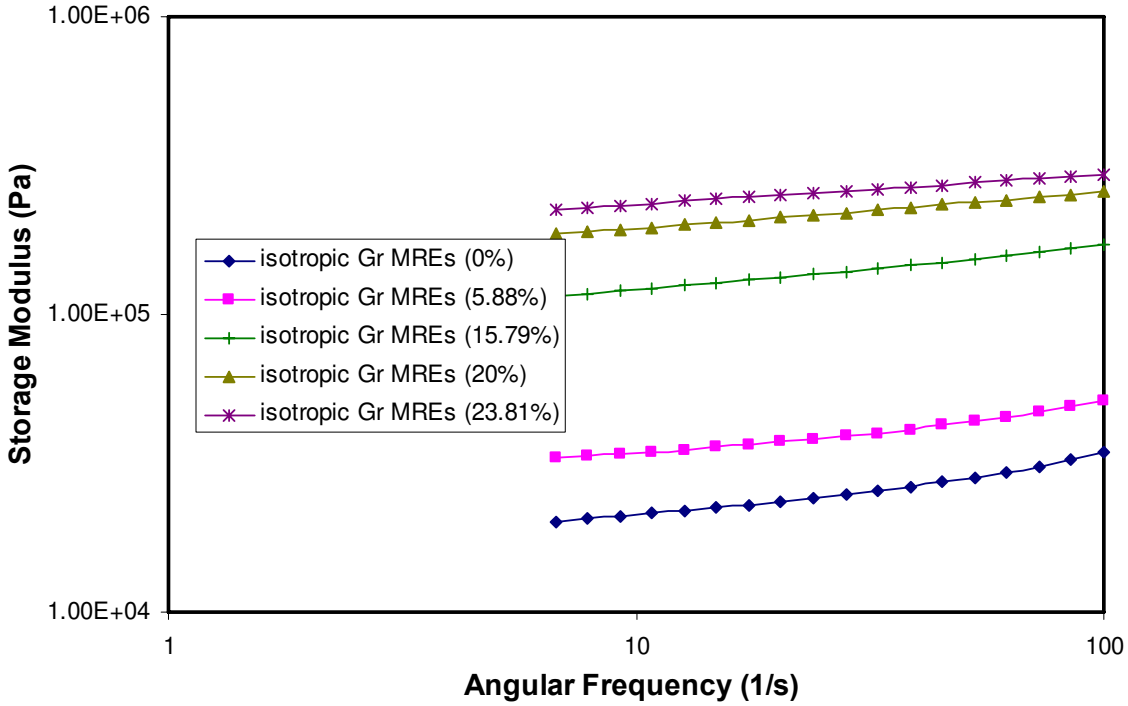

Fig. 3.32 Storage Modulus of isotropic samples versus angular frequency sweep (without magnetic field)

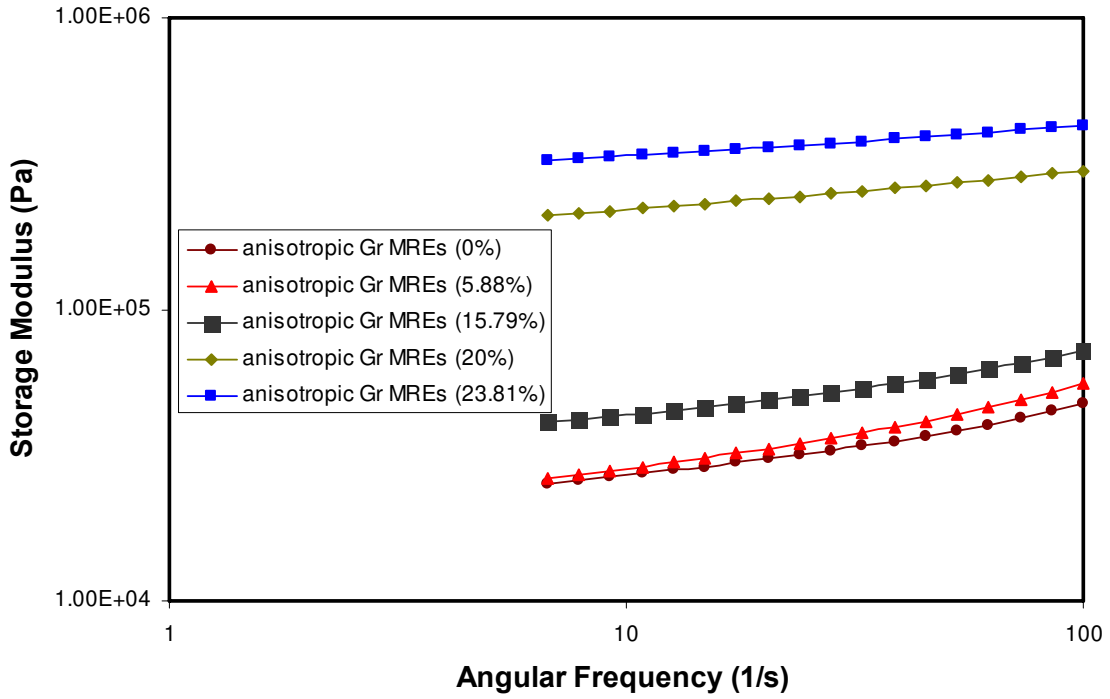

Fig. 3.33 Storage Modulus of anisotropic samples versus angular frequency sweep (without magnetic field)

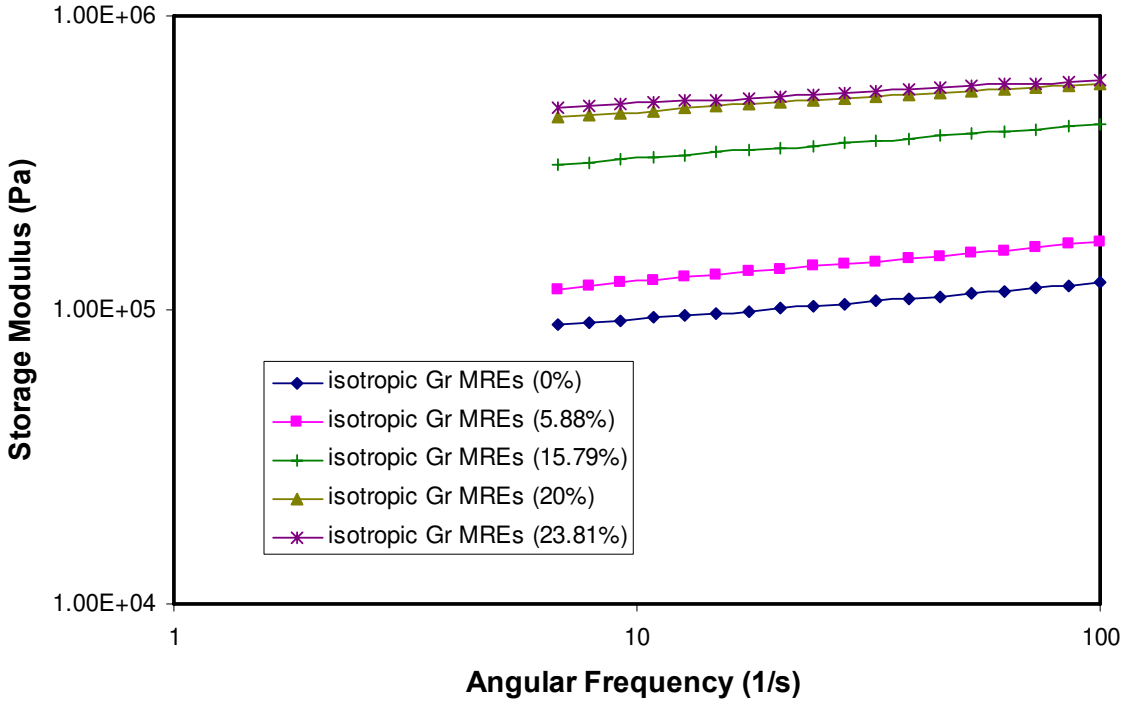

Fig. 3.34 Storage Modulus of isotropic samples versus angular frequency sweep (with 440mT magnetic field)

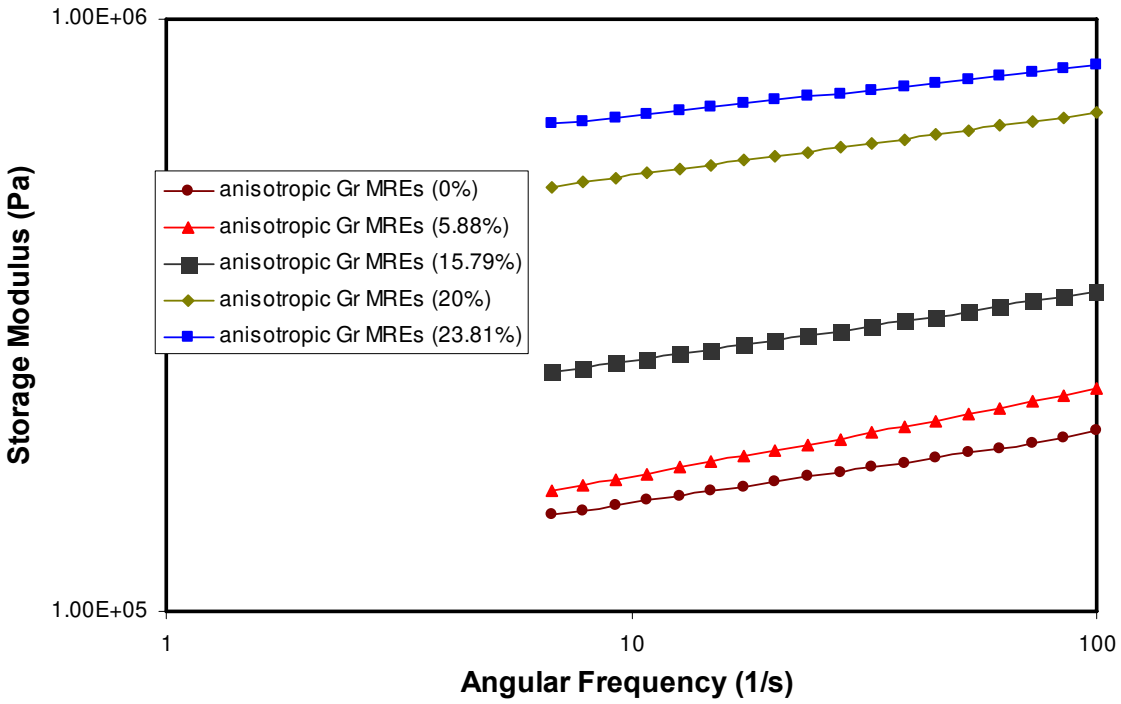

Fig. 3.35 Storage Modulus of anisotropic samples versus angular frequency sweep (with 440mT magnetic field)

The above 4 figures show that with higher graphite weight faction, the samples have a bigger storage modulus. This also proves that the graphite powder contributes to the initial stiffness of MRE samples.

The ratio of storage modulus at 440mT to the storage modulus at 0mT is the MR effect. The ratio of isotropic conventional MREs is around 4, when the graphite weight fraction increases to 15.79% and 23.81%, the MR effect are around 2.6 and 2.1, respectively. For anisotropic samples, the MR effects of conventional MREs, 20% and 23.81% Gr MREs are 5.2, 2.4 and 2.0, respectively. This means with the growth of graphite weight fraction, the MR effect decreases. This phenomenon is cause by the contribution of graphite powder to the samples' stiffness, because of which, the MR effect can only have less effects on the Gr MRE samples than conventional MREs.

3.5 CONCLUSION

In this chapter, the fabrication procedures of both isotropic and anisotropic Gr MREs were introduced. The samples of MREs were shown, too. By the SEM observation, the microstructures of both isotropic and anisotropic conventional MREs and Gr MREs were presented. Also, the steady state and dynamic state characteristics of MRE materials were studied and compared experimentally.

CHANPTER 4
EXPERIMENTAL & MODELING STUDY OF SENSING CAPABILITIES

4.1 INTRODUCTION

This chapter presents both experimental and modeling of MREs.

From the microstructure observation of MREs, we can see that the carbonyl iron particles disperse in the matrix randomly in isotropic samples, which makes the model analysis much more complicated than that of the anisotropic model. In this study, theoretical approach is based on anisotropic MREs. Similarly, in the experiment, only anisotropic MREs were tested.

4.2 EXPERIMENTAL SET UP

4.2.1 Introduction

Fig. 4.1 shows the schematic of the experimental device. In this setup, a long plastic plate is used to hold the weight to apply the load to the Gr MRE samples. A Gaussmeter (HT201, Hengtong magnetoelectricity CO., LTD) is used to test the intensity of magnetic field. A multimeter (Finest 183, Fine Instruments Corporation) measures the Gr MRE samples' resistance.

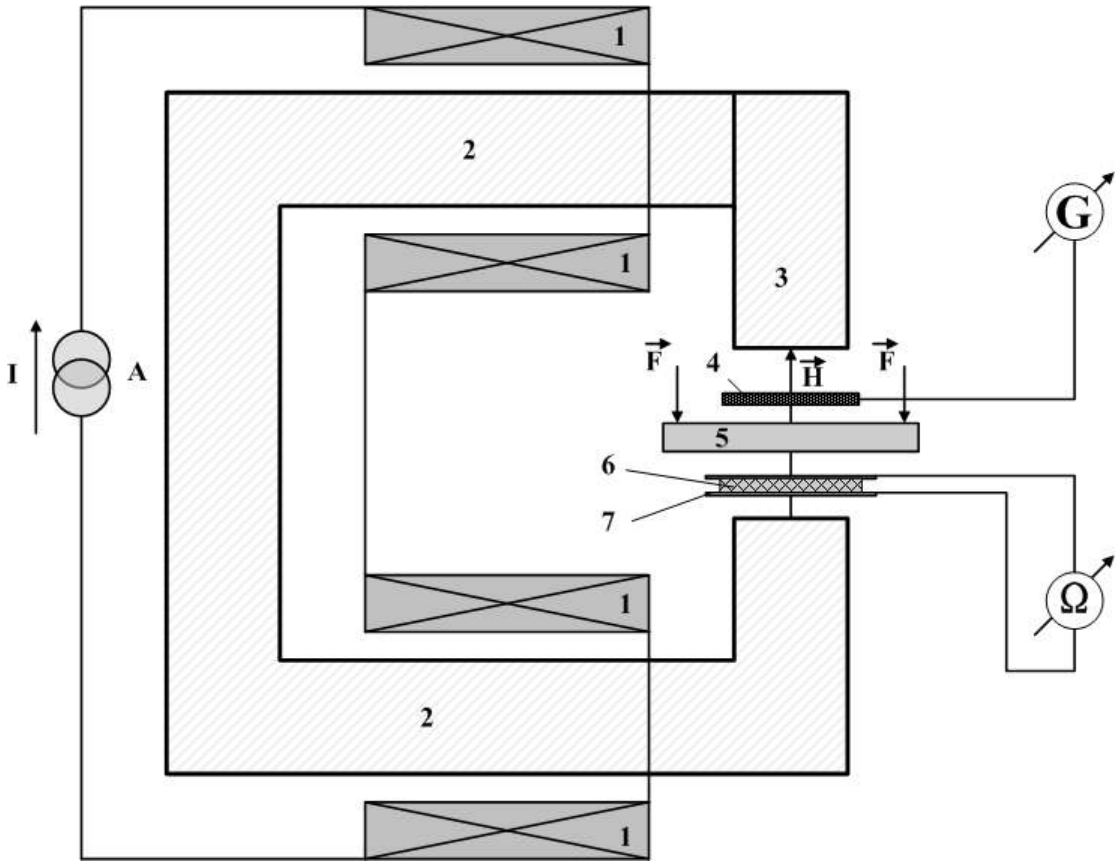

Fig. 4.1 sketch of the experimental device

1- coils; 2- electrical magnetic; 3- moving magnetic pole; 4- Gaussmeter probe; 5- plastic plate; 6- Gr MRE sample; 7- measuring copper plates; G- Gaussmeter; Ω- Multimeter; F- external force applied on Gr MRE samples

As shown in Fig. 4.1, part 3 is a moving magnetic pole. The gap between the upper and lower magnetic poles of the electrical magnet can be controlled by moving it. Because of the Gr MRE samples' thickness varying from 1.1 mm to 1.4 mm, plus the two copper plates which are connected to multimeter to test the samples' resistance and a long plastic plate used to be applied the external force, the initial gap between the upper and lower poles is set at 4 mm for all the tests.

4.2.2 Electrical magnet

At 4 mm gap, the relationship between the current and magnetic field intensity is shown in Table 4.1 and Fig. 4.2. Because of the remanence of the copper coil, there is a weak magnetic field as 13mT when the current is 0A.

Table 4.1 Relationship between current and the magnetic field intensity

Current (A)	0	0.5	1	1.5	2	2.5	3
Magnetic field (mT)	13	34.1	60.5	89.1	117.8	147.3	180.7

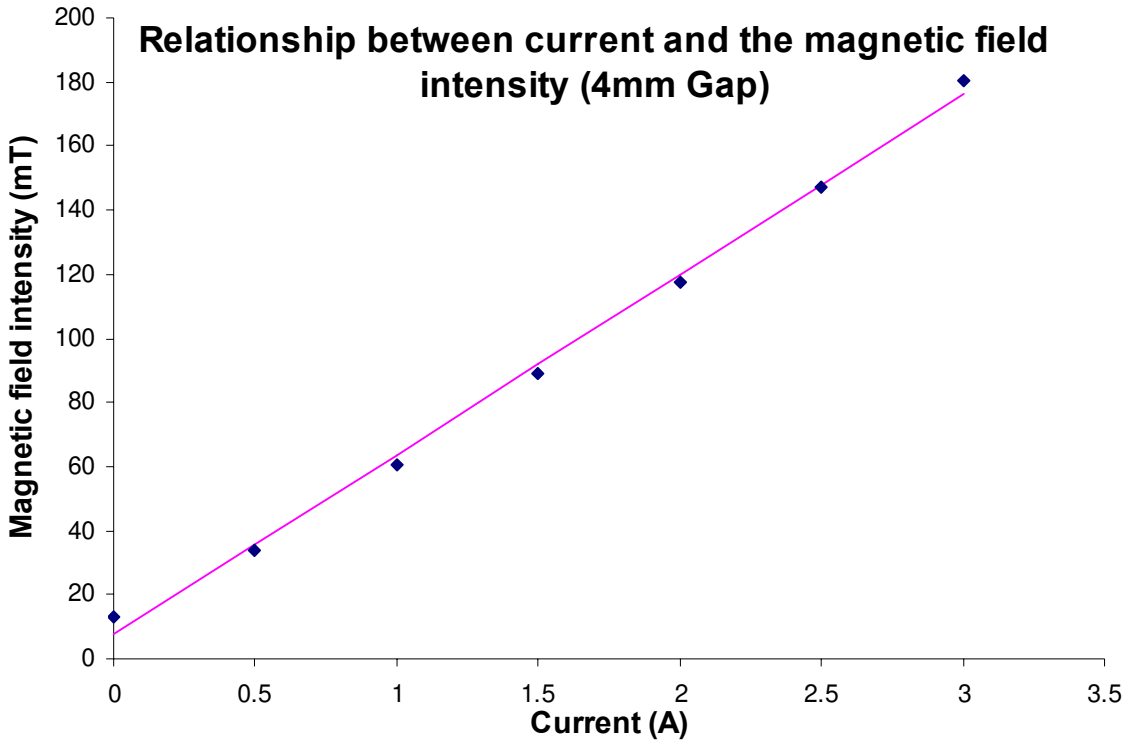

Fig. 4.2 The relationship between current and the magnetic field intensity

The solid line in Fig. 4.2 is the fitting curve for the data, which can be used to predict the magnetic field at other current. The current used in our experiment is from 0 to 3 A with 0.5A increment.

4.3 EXPERIMENTAL RESULT

By testing all the anisotropic MRE samples, only the samples whose graphite weight fraction are no less than 15% are detectable by Finest 183 multimeter. Thus, in all the anisotropic MRE samples, there are only three of them can be detected, whose graphite weight fractions are 20%, 21.95% and 23.81%, respectively.

Through these tests, the following data of anisotropic MRE with graphite weight fraction 20%, 21.95% and 23.81% is shown in Fig. 4.3, Fig. 4.4 and Fig. 4.5, respectively.

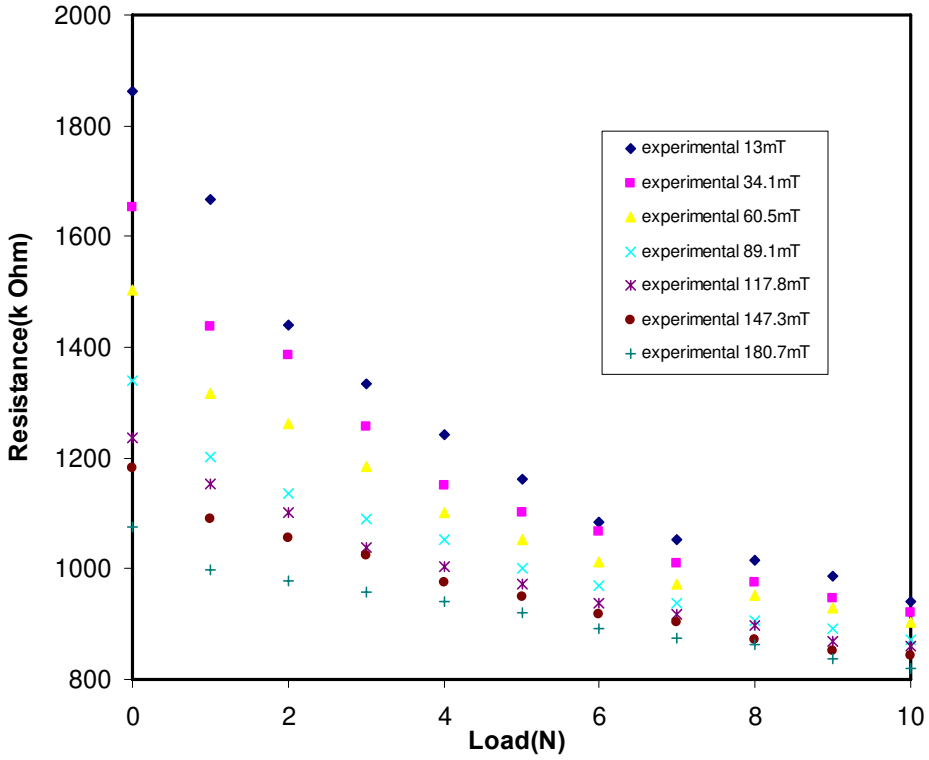

Fig. 4.3 Resistance versus load for anisotropic MRE (Gr 20%)

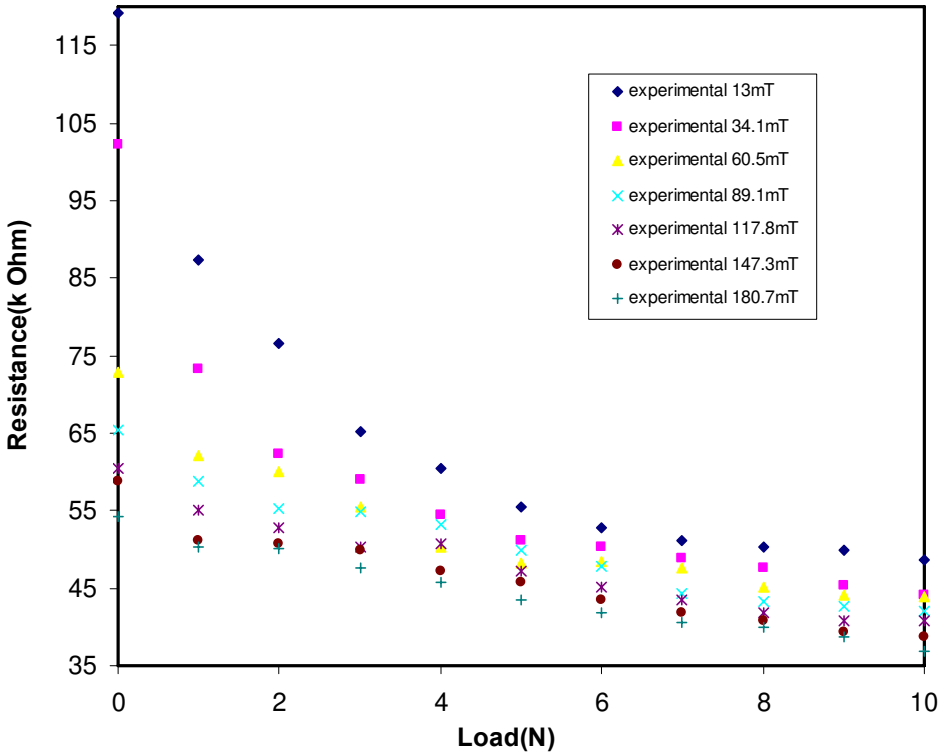

Fig. 4.4 Resistance versus load for anisotropic MRE (Gr 21.95%)

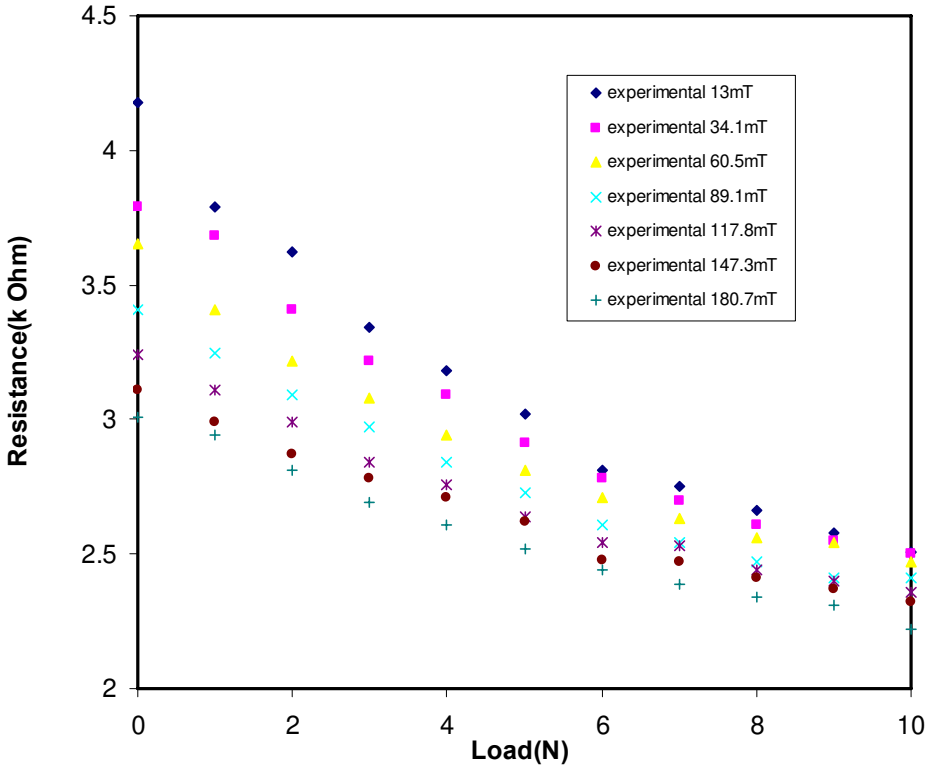

Fig. 4.5 Resistance versus load for anisotropic MRE (Gr 23.81%)

As can be seen in the three figures above, the trends of all three samples are the same. In a fixed magnetic field, when the external load increases from 0 to 10 N, the resistance is in decline for all three samples. With small load, the resistance changes significantly, but it comes decreases slowly when the load is more than 5 N. According to the absolute values, the sample with higher graphite weight fraction shows the higher electrical conductivity and fewer declines of resistance. For instance, the resistance of the sample with graphite weight fraction 20% drops from 1862 kΩ at 0 N to 942 kΩ at 10 N; the decline between 4.18 kΩ to 2.51 kΩ at the 0 N and 10 N is for the sample with graphite weight fraction 23.81%.

Meanwhile, it is clear to see that for each sample, at higher magnetic field intensity, the resistance at a fixed external load comes to lower value. Taking the sample with 21.95% graphite weight fraction as an example, at 5 N external load, the resistance 55.4 kΩ without the magnetic field decreases to 43.5 kΩ at a 440 mT magnetic field. This trend can be see in Fig. 4.6.

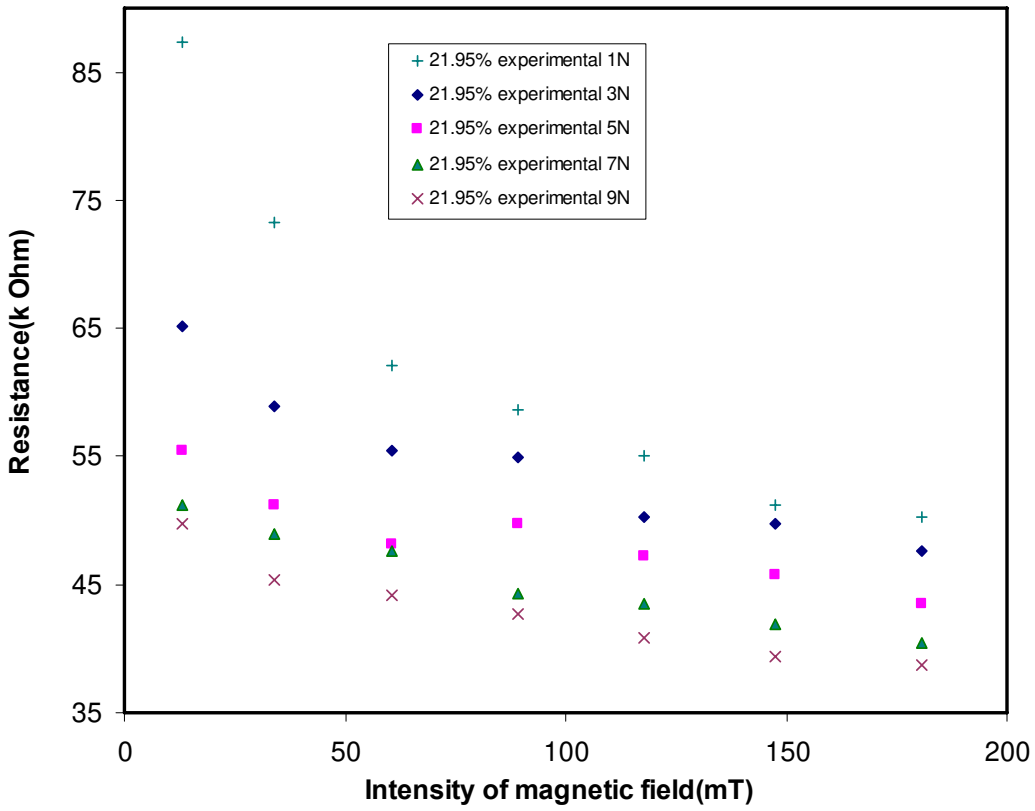

Fig. 4.6 Resistance versus magnetic field (anisotropic MRE Gr 21.95%)

In Fig. 4.6 for the data at 3 N and 5 N external loads, the resistance increases between 60 mT and 90 mT, this change can be ignored as the test error. The total trend is the resistance decline with the magnetic field raising.

4.4 MODELLING ANALYSIS

4.4.1 Introduction

From the Dipole Model, A representative volume unit (RVU) is derived. A RVU consists of two neighboring hemispheres and the surrounding polymer matrix, which can be regarded as the minimum volume element in the conventional MRE. Fig. 4.7 shows the position of RVU in carbonyl iron particle chains, and a longitudinal section of the unit is shown in Fig. 4.8.

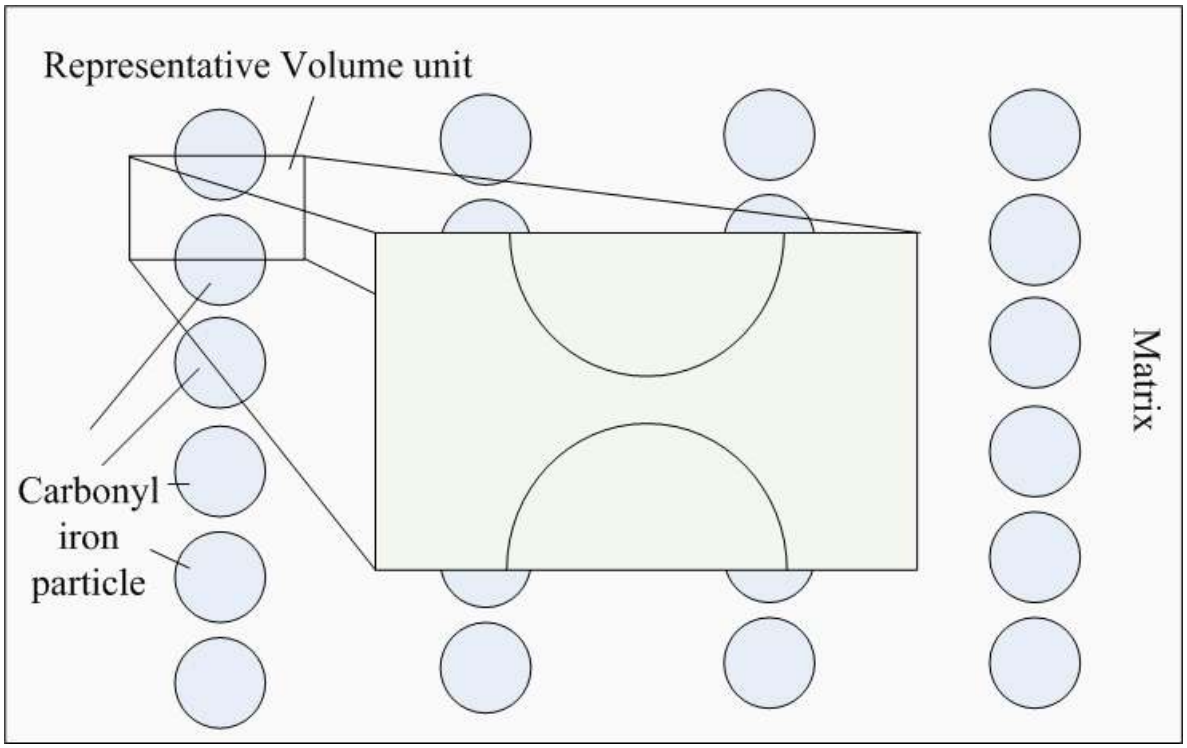

Fig. 4.7 RVU in carbonyl iron chains

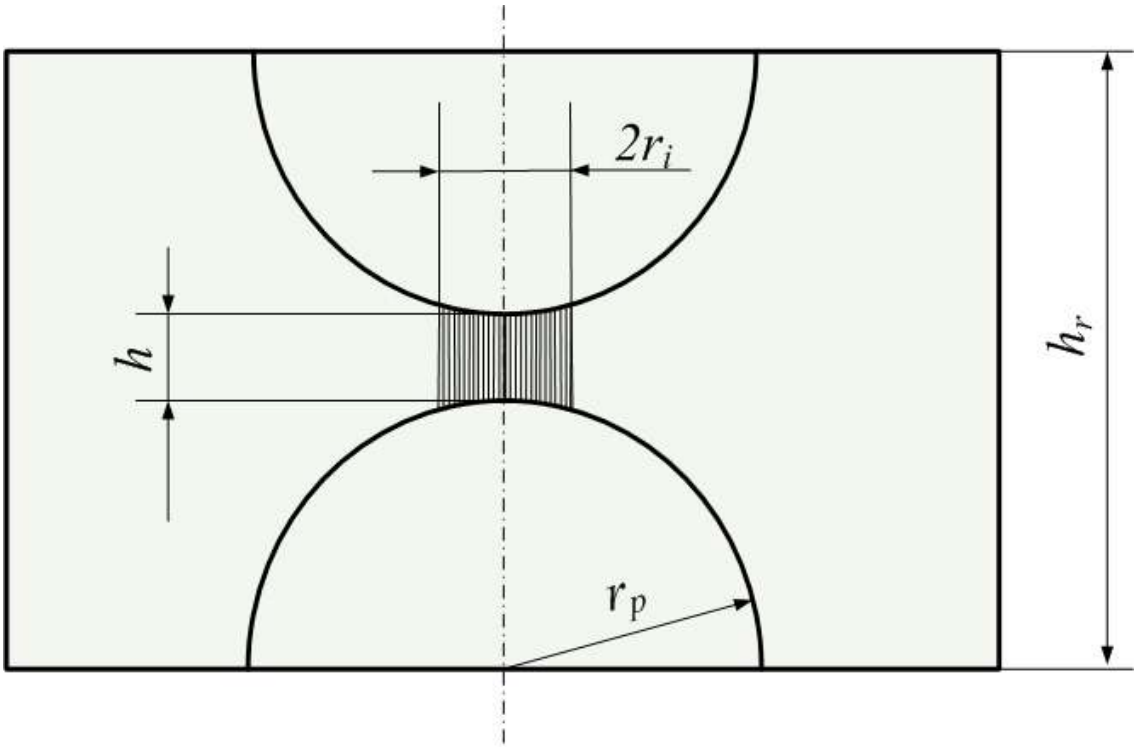

Fig. 4.8 The longitudinal section of RVU

The RVU is a model for ideal anisotropic MREs, which is supposed to have chains structure.

4.4.2 RVU Properties

For this structure, the volume of the two hemispheres is.

$$V_s = 2 * \frac{2}{3}\pi \cdot r_p{}^3 = \frac{4}{3}\pi \cdot r_p{}^3 \tag{4.1}$$

Because the two hemispheres are very close to each other and the radius of the spheres is much bigger than the thickness of the film *h*, the thickness *h* can be negligible.

The thickness of the RVU is

$$h_r = 2r_p + h \approx 2r_p \tag{4.2}$$

Given the iron particle volume fraction ϕ in the RVU, the volume is

$$V_r = \frac{V_s}{\phi} = \frac{4\pi r_p{}^3}{3\phi} \tag{4.3}$$

Thus the area of cross section can be expressed as

$$S_r = \frac{V_r}{h_r} = \frac{4\pi r_p^{\ 3}}{3\phi\left(2r_p + h\right)} \approx \frac{2\pi r_p^{\ 2}}{3\phi} \tag{4.4}$$

Most of the current flowing through the RVU concentrates on the small area between the two adjacent hemispheres. Meanwhile, the conductivity of the iron particles is much higher than that of the polymer. Therefore, the electric potential drops on the particles could be negligible, too. Given the intensity of current flowing through the polymer is *E*, the intensity of the local electric field is

$$E_{loc} = \frac{h_r E}{h} = \frac{(2r_p + h)E}{h} \approx 2r_p \frac{E}{h} \tag{4.5}$$

The insulating polymer film between two neighboring iron particles is very thin because of the magnetic attraction during preparation, across which the electrical field assisted tunnel current can occur. The Fowler-Nordheim equation [43-45] can be used to express the tunnel current. Meanwhile, the iron particles dispersing in the polymer matrix contributes to the conductivity of the polymer. Then the total current density is the sum of the tunnel density j_t and the conduction density j_c

According to the Fowler-Nordheim equation, the relation between the tunnel density j_t and electric field intensity *E* is

$$j_t = \alpha E_{loc}^2 \exp\left(-\frac{\beta}{E_{loc}}\right) \tag{4.6}$$

In which, the α and β are both constants determining the tunnel current.

And $\alpha = \frac{q^3}{8\pi q h \Phi_0}\frac{m_{si}}{m_{ox}}$ $\beta = \frac{8\pi}{3qh}\sqrt{2m_{ox}}\left(q\Phi_0\right)^{\frac{3}{2}}$. α and β depend on the potential barrier height Φ_0 and the ratio of effectives masses (in the oxide conduction band and in the silicone conduction band)

The conduction density j_c is

$$j_c = \sigma_f E_{loc} \tag{4.7}$$

In which σ_f is the conductivity of the polymer film.

So the total current density j is

$$j = j_t + j_c = \alpha E_{loc}^2 \exp\left(-\frac{\beta}{E_{loc}}\right) + \sigma_f E_{loc} \tag{4.8}$$

The total current density j is for the current flowing through the small area between the tips of two adjacent iron particles, however, the density of RVU j_r should be derived from its cross section.

$$j_r = j\frac{\pi \cdot r_i^{\,2}}{S_r} \tag{4.9}$$

In which the r_i is the radius of the area between the two adjacent iron particles.

So from the total density of RVU j_r and the electric field intensity E, the conductivity of typical MRE σ_r can be represented as

$$\begin{aligned}\sigma_r = \frac{j_r}{E} = \frac{\pi \cdot r_i^{\,2} \cdot j}{S_r \cdot E} &= \frac{\pi \cdot r_i^{\,2} \cdot E_{loc} \cdot \left\{\alpha E_{loc} \exp\left(-\frac{\beta}{E_{loc}}\right) + \sigma_f\right\}}{S_r \cdot E} \\ &\approx \frac{\pi \cdot r_i^{\,2} \cdot 2r_p \frac{E}{h} \cdot \left\{2\alpha r_p \frac{E}{h} \exp\left(-\frac{\beta}{2r_p \frac{E}{h}}\right) + \sigma_f\right\}}{\frac{2\pi r_p^{\,2}}{3\phi} \cdot E} \\ &= 3\phi \cdot r_i^{\,2}\left[\frac{2\alpha}{h^2} E \exp\left(-\frac{h\beta}{2r_p E}\right) + \frac{\sigma_f}{r_p h}\right]\end{aligned} \tag{4.10}$$

MRE also has the piezoresistivity. When a MRE sample is compressed, its conductivity increases. To explain this phenomenon there are two factor. One is the increments of the conductive area induced by the deformation of MREs, the other is the reduction of the

thickness of the polymer membrane between the two adjacent iron particles. Because of the high ratio of r_i/h, it's difficult to compress the membrane further. Thus the increment of the conductive area is the significant reason for the conductivity increasing.

When a constant compressive stress σ is applied on MRE, the compressive force F_p between the particles is

$$F_p = \pi \cdot r_p^2 \sigma \tag{4.11}$$

From the Hertz Theory [46-51], the radius r_i of the contact area can be calculated as

$$r_i = \left[\frac{3\pi\sigma\left(1-\nu^2\right)}{2E_p} \right]^{1/3} \cdot r_p \tag{4.12}$$

in which ν is the Poisson's ratio, E_p is the Young's Modulus.

When the initial compressed stress applied on MRE is σ_0, corresponding to which there is an initial contact area radius r_{i0}

$$r_{i0} = \left[\frac{3\pi\sigma_0\left(1-\nu^2\right)}{2E_p} \right]^{1/3} \cdot r_p \tag{4.13}$$

So the radius r_i increases along with the increment of compressed stress

$$r_i = r_{i0} + r_p\left(\left(\sigma_0+\sigma\right)^{1/3} - {\sigma_0}^{1/3}\right)\cdot\left(\frac{3\pi\left(1-\nu^2\right)}{2E_p}\right)^{1/3} \tag{4.14}$$

Meanwhile, the magnetic field also contributes to the resistance of MREs. When the external magnetic field is applied on MREs, the carbonyl iron particles are attracted by the poles of magnetic field. The nearer magnetic pole contributes much more powerful than the other pole. So the attraction from the farther magnetic pole can be negligible.

For the two iron particles in each RVU, the magnetic attraction from the pole applied to the father particle compresses the thin film between the two adjacent iron particles. Similar to

the piezoresistivity, the increment of the conductive area is the main cause for the conductivity increasing.

Thus, the radius r_i can be updated as

$$r_i = r_{i0} + r_p\left(\left(\sigma_0 + \sigma_1 + \sigma_2\right)^{1/3} - \sigma_0{}^{1/3}\right)\cdot\left(\frac{3\pi\left(1-\nu^2\right)}{2E_p}\right)^{1/3} \tag{4.15}$$

in which, σ_1 is the compressive stress , σ_2 is the stress from the magnetic attraction.

The relation is a direct proportion between the magnetic field strength B and the stress σ_2 occurred by magnetic attraction [10, 52-56]. Set the ratio is k_g, so the relation is

$$\sigma_2 = k_g \cdot B \tag{4.16}$$

So the dependence of the conductivity of MREs on electric field intensity and compressive stress is

$$\sigma_m = 3\phi\cdot\left[\frac{2\alpha}{h^2}E\exp\left(-\frac{h\beta}{2r_pE}\right)+\frac{\sigma_f}{r_ph}\right]\cdot\left[r_{i0} + r_p\left(\left(\sigma_0 + \sigma_1 + \sigma_2\right)^{1/3} - \sigma_0{}^{1/3}\right)\cdot\left(\frac{3\pi\left(1-\nu^2\right)}{2E_p}\right)\right]^2 \tag{4.17}$$

When the initial condition σ_0 and r_{i0} are set, except E and σ, the other parameters in this equation are all constants. So the conductivity of MREs σ_m is dependent on the intensity of the electric field E and the compressed stress σ.

From the conductivity, the electrical resistivity of the RVU can be gained

$$\rho = \frac{1}{\sigma_m} \tag{4.18}$$

So the resistance of an ideal iron particle chain is

$$R = \frac{\rho l}{A} = \frac{l}{A\sigma_m} \tag{4.19}$$

In section 3.3, the SEM observation demonstrated that the graphite powders disperse in the polymer randomly. Some graphite powder connects two iron particle chains to make the two chains be parallel connection with each other. Meanwhile, some graphite powder is along with the same direction as the carbonyl iron chains and close to the iron chain, where the graphite powders connect different carbonyl iron chains parallelly. So that when the electrical field is applied on MREs, the current can go through both the graphite powder and the part of iron chain. This is the reason that while the graphite powder is introduced into the conventional MREs, the electrical resistance of graphite based MREs decreases along with the increase of the graphite weight fraction.

According to the effects of graphite and carbonyl iron to the resistance model, two parameter λ_g and λ_i are introduced to show the effects of graphite volume fraction ϕ_g and carbonyl iron volume fraction ϕ_i to the conductivity of new MREs. λ_g and λ_i show the contribution of the carbonyl iron particles and graphite powder to the resistance, respectively. The higher λ_g and λ_i are, the less resistance has the Gr MREs.

The final resistance of Gr MREs is

$$R_g = \lambda_g \lambda_i R = \frac{\lambda_g \lambda_i l}{A\sigma_m}$$

$$= \frac{\lambda_g \lambda_i l}{3A\phi \cdot \left[\frac{2\alpha}{h^2} E \exp\left(-\frac{h\beta}{2r_p E}\right) + \frac{\sigma_f}{r_p h}\right] \cdot \left[r_{i0} + r_p\left(\left(\sigma_0 + \sigma_1 + \sigma_2\right)^{1/3} - \sigma_0{}^{1/3}\right) \cdot \left(\frac{3\pi\left(1-\nu^2\right)}{2E_p}\right)\right]} \tag{4.20}$$

4.5 THEORETICAL RESLUT

According to Equation 4.20, the final resistance of Gr MREs is

$$R_g = \frac{\lambda_g \lambda_i l}{3A\phi \cdot \left[\frac{2\alpha}{h^2} E \exp\left(-\frac{h\beta}{2r_p E}\right) + \frac{\sigma_f}{r_p h}\right] \cdot \left[r_{i0} + r_p\left(\left(\sigma_0 + \sigma_1 + \sigma_2\right)^{1/3} - \sigma_0^{\,1/3}\right) \cdot \left(\frac{3\pi\left(1-\nu^2\right)}{2E_p}\right)\right]}$$

in which, some parameters are constant. Thus the equation can be simplified by substituting these parameters into the equation.

In the RVU, the iron particle volume fraction is set as ϕ = 0.4, which means that the volume of two hemispheres is 40% of the whole volume of RVU.

The shape of Gr MRE samples is fixed. The thickness l is l= 1mm=0.001m, the diameter D is D=0.021m, so the cross section area is $A=\pi \cdot (D/2)^2 = 0.000346\ m^2$.

In the tunneling equation $\left[\frac{2\alpha}{h^2} E \exp\left(-\frac{h\beta}{2r_p E}\right) + \frac{\sigma_f}{r_p h}\right]$, α and β are pre-exponential and exponential terms of the standard Fowler-Nordheim Tunneling which are both constants. In this case, value α is set as 2, value β is set as 1. h is the height of the RVU as two times of iron particle's radius. So h=0.000004 m. The iron particle's radius r_p is 0.000002 m. σ_f is the conductivity of the polymer film namely silicone rubber. Because of the high resistance of silicone rubber, the value of conductivity of silicone rubber σ_f is set as $1*10^{-10}$. The electric field E is from the function file of the multimeter used in the test. The value of E is 9V. So the whole equation can be calculated as $\frac{2\alpha}{h^2} E \exp\left(-\frac{h\beta}{2r_p E}\right) + \frac{\sigma_f}{r_p h} \approx 2.01*10^{12}$.

Therefore, by substituting these parameters into the equation, R_g can be transferred as

$$R_g = \frac{0.001 \times \lambda_g \lambda_i}{6.02\times10^{12} \times 0.000346 \times 0.4 \times \left[r_{i0} + r_p\left(\left(\sigma_0 + \sigma_1 + \sigma_2\right)^{1/3} - \sigma_0^{\,1/3}\right) \cdot \left(\frac{3\pi\left(1-\nu^2\right)}{2E_p}\right)\right]}$$

$$= \frac{4.78*10^{-13} \times \lambda_g \lambda_i}{\left[r_{i0} + r_p\left(\left(\sigma_0 + \sigma_1 + \sigma_2\right)^{1/3} - \sigma_0^{\,1/3}\right) \cdot \left(\frac{3\pi\left(1-\nu^2\right)}{2E_p}\right)\right]} \quad (4.15)$$

In which, E_p is the Young's Modulus and v is the Poisson's ratio of particles. At the normal condition, the MRE samples' Young's Modulus E_p is set as 4000 Pa. The Poisson's ratio of particles v is set as 0.1 [43, 45].

Thus the Equation 4.15 can be changed to

$$R_g = \frac{4.78*10^{-13} \times \lambda_g \lambda_i}{r_{i0} + r_p\left(\left(\sigma_0 + \sigma_1 + \sigma_2\right)^{1/3} - \sigma_0^{\,1/3}\right) \times 0.001166} \tag{4.16}$$

σ_1 is the compressive stress from the external force. The weight of plastic plate is 10 g and the increment of weight is 100 g once. The gravity acceleration is set as 10 m/s^2. So when the external load is from 0 N to 10N, the real load applied on the samples will be an array from 0.1 N to 10.1 N with the increment 1 N. By dividing the Gr MRE samples' cross section A (0.000346 m^2), the compressive stress σ_1 is shown in table 4.2.

Table 4.2 Relation of weight, load and compressive stress

External load(N)	Real load(N)	Compressive stress σ_1 (Pa)
0	0.1	288.7165
1	1.1	3175.881
2	2.1	6063.045
3	3.1	8950.21
4	4.1	11837.37
5	5.1	14724.54
6	6.1	17611.7
7	7.1	20498.87
8	8.1	23386.03
9	9.1	26273.2
10	10.1	29160.36

σ_2 is the compressive stress from the external magnetic field. The magnetic attractive force Fm from the magnetic field to a carbonyl iron particle is in proportion to the intensity of

magnetic field B. Also because the Gr MRE samples' cross section A is very small, the ratio of magnetic attractive force Fm to the intensity of magnetic field B is set as 10000 [10, 53-55].

σ_0 and r_{io} are the initial compressive stress and initial effective cross section for the current to flow through, respectively. Because the initial effective cross section r_{io} is at least 10 times less the iron particles radius r_p, even though the initial pressure is low, the initial compressive stress σ_0 is not at a low value. They are set as $r_{io} = 1*10^{-8}$ m and σ_0=2000 Pa [36, 48, 50].

The anisotropic MRE with graphite weight fraction 21.95% (contains 10g iron particles, 3g silicone rubber, 3g silicone oil and 4.5g graphite powder) can be used as an example. Table 4.3 shows the volume fractions of all the ingredients for this sample.

Table 4.3 Volume fractions of all the ingredients (anisotropic MRE Gr 21.95%)

	Mass(g)	Density(g/cm^3)	volume(cm^3)	Volume fraction
Iron particle	10	7.86	1.272265	16.50%
Silicone rubber	3	3.18	0.943396	12.24%
Silicone oil	3	0.96	3.125	40.54%
Graphite powder	4.5	1.9	2.368421	30.72%

Thus, for all three samples, the volume fractions can be gotten, which are shown in Table 4.4.

Table 4.4 Volume fractions of iron and graphite (anisotropic MRE Gr 20%, 21.95% and 23.81%)

	Gr 20%	Gr 21.95%	Gr 23.81%
Iron particle (ϕ_i)	17.09%	16.5%	15.96%
Graphite powder(ϕ_g)	28.27%	30.7%	33.01%

λ_g and λ_i are the factors showing the efforts of graphite and iron particles to the Gr MREs' resistance, respectively. λ_g and λ_i depend on the graphite volume fraction ϕ_g and iron particles volume fraction ϕ_i. For each sample, there are different λ_g and λ_i. Fig. 4.9 shows the product of λ_g and λ_i versus Gr MREs (Gr 20%, 21.95% and 23.81%). The data is from the ratio of experimental result and theoretical result.

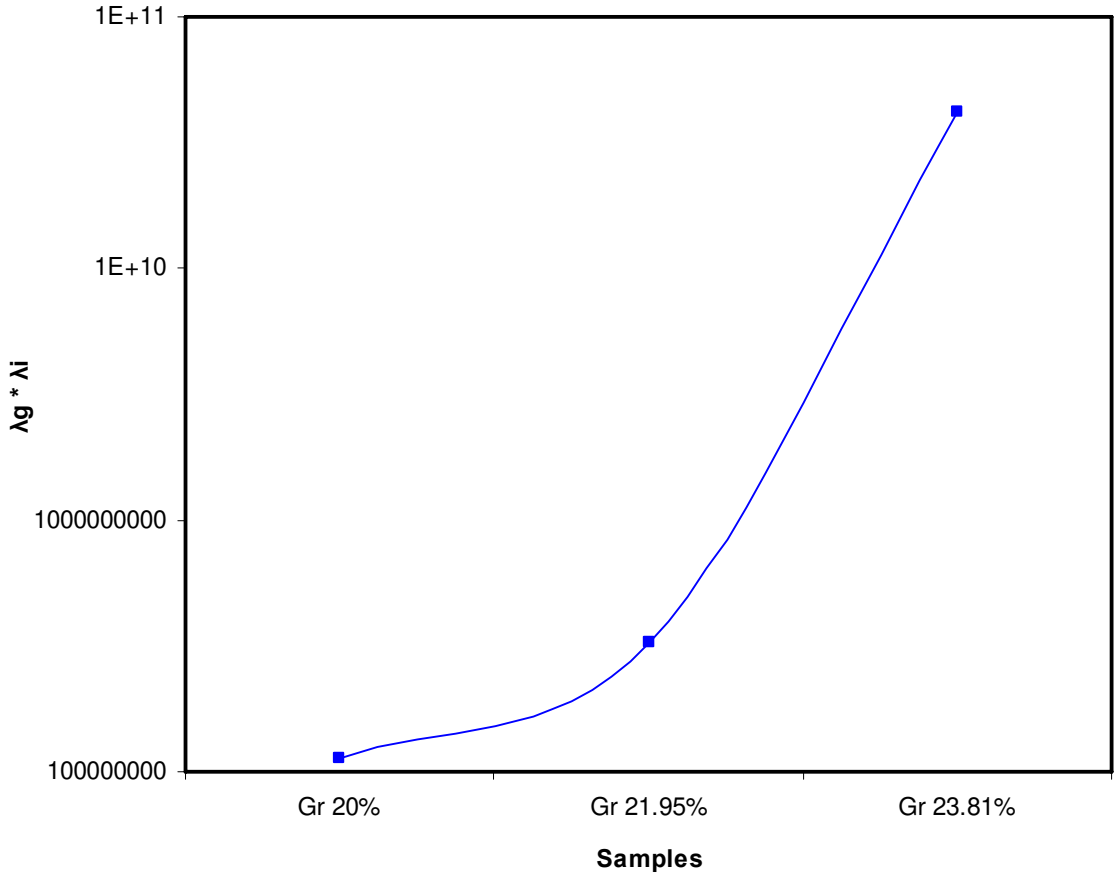

Fig. 4.9 λ_g * λ_i versus graphite weight fraction

Set $\lambda_g = \exp(a \cdot \phi_g)$ and $\lambda_i = \exp(b \cdot \phi_i)$. Substitute the data in Table 4.4 and Fig. 4.9 to λ_g and λ_i, the parameters λ_g and λ_i can be got, so the parameter *a* and *b* can be gotten as -65 and 250. So the relationship of λ_g and λ_i to ϕ_g and ϕ_i are

$\lambda_g = e^{-65*\phi_g}$, $\lambda_i = e^{250\phi_i}$

All the parameters of Equation 4.20 are ready to calculate the final resistance R_g of the anisotropic MRE with graphite weight fraction 20%, which is shown in Table 4.5.

Table 4.5 Theoretical results (anisotropic MRE with graphite weight fraction 20%)

B(T) / load(N)	0.013	0.0341	0.0605	0.0891	0.1178	0.1473	0.1807
0.1	74.7146	67.5736	61.9648	57.8061	54.7071	52.2036	49.9167
1.1	65.6611	61.5454	57.7726	54.6909	52.2515	50.2000	48.2684
2.1	60.3108	57.4724	54.6652	52.2384	50.2399	48.5106	46.8449
3.1	56.5745	54.4338	52.2177	50.2290	48.5446	47.0556	45.5960
4.1	53.7353	52.0309	50.2118	48.5353	47.0852	45.7819	44.4862
5.1	51.4634	50.0560	48.5206	47.0771	45.8080	44.6522	43.4897
6.1	49.5806	48.3876	47.0643	45.8008	44.6754	43.6394	42.5872
7.1	47.9802	46.9487	45.7896	44.6691	43.6603	42.7232	41.7637
8.1	46.5935	45.6876	44.6590	43.6546	42.7422	41.8882	41.0076
9.1	45.3735	44.5680	43.6455	42.7370	41.9056	41.1221	40.3094
10.1	44.2872	43.5635	42.7288	41.9008	41.1381	40.4154	39.6617

4.6 COMPARATION AND ANALYSIS

To show the comparison between experimental results and theoretical results (anisotropic MRE with graphite weight fraction 21.95%) clearly, each four series at both experimental results and theoretical results are picked out to be compared, which is shown in Fig. 4.10

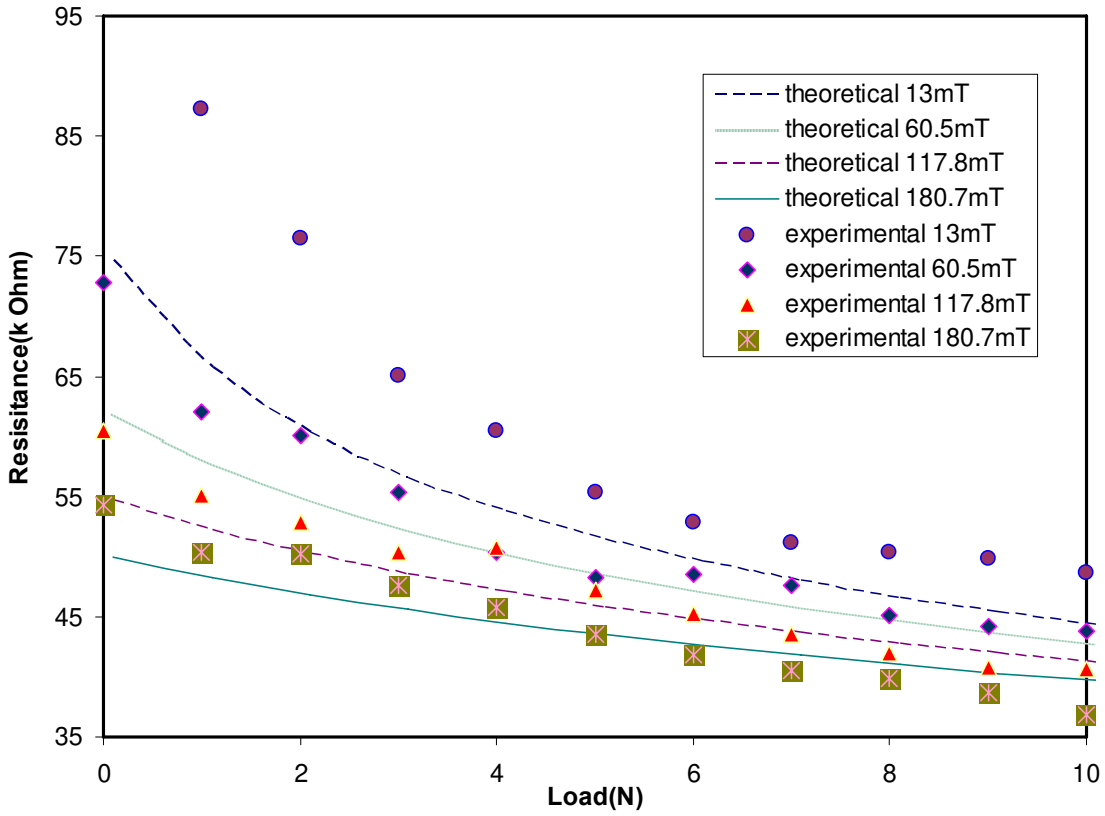

Fig. 4.10 Comparison between experimental results and theoretical results (anisotropic MRE Gr 21.95%)

Fig. 4.10 shows that the experimental results and theoretical results couldn't match each other perfectly. However, the trends of both experimental results and theoretical results are the same. The reason of the fitting will be discussed in the next part of this chapter.

Similarly, from the data, some other comparison can be done. At the fixed external force (which is expressed as load), when the magnetic field intensity increases, the resistance of sample decreases. The data under three external loads such as 1 N, 5 N and 10 N were chosen to compare the experimental and theoretical result in Fig. 4.11.

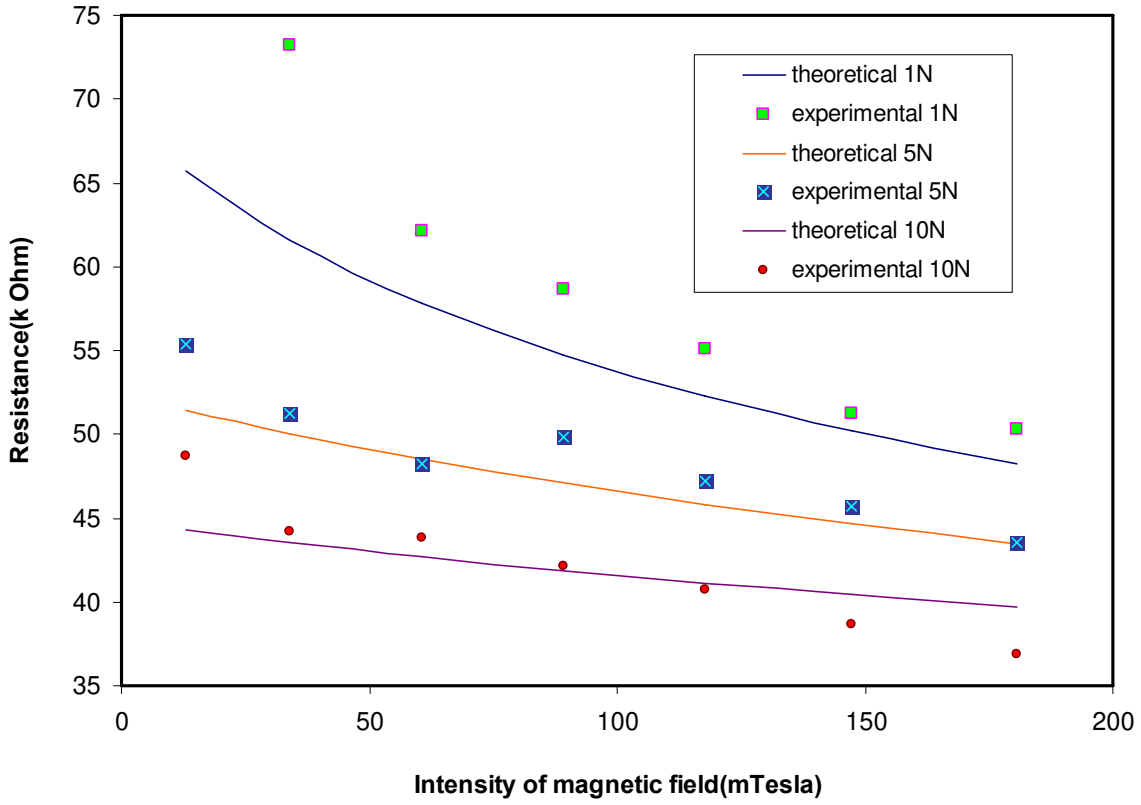

Fig. 4.11 Resistance changing at a fixed load (anisotropic MRE Gr 21.95%)

The Fig. 4.11 shows the changing of the resistance when the external force is fixed. Along with the raising of magnetic field intensity, the sample's resistance decreases. The higher external load applied leads to lower resistance of Gr MREs.

The next two figures Fig. 4.12 and 4.13 show the resistance changing between anisotropic MREs with graphite weight fraction 20%, 21.95% & 23.81%. The magnetic field in fixed in Fig. 4.12 and the external load is fixed in Fig. 4.13.

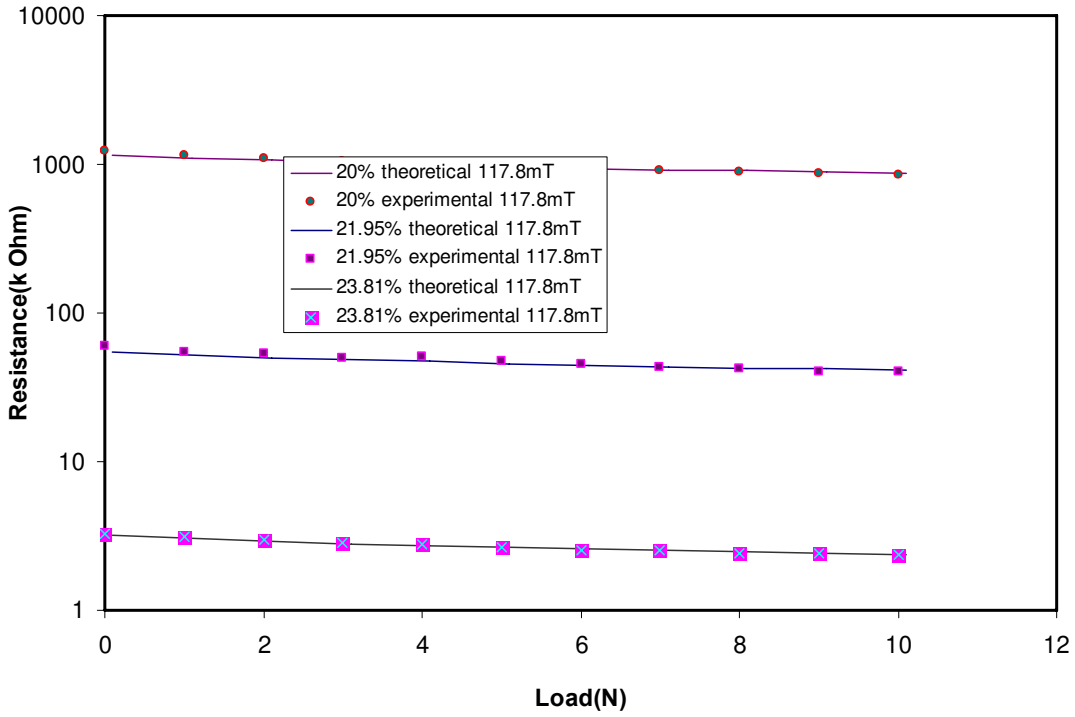

Fig. 4.12 Resistance between different sample at 117.8mT magnetic field (anisotropic MRE with graphite weight fraction 20%, 21.95% & 23.81%

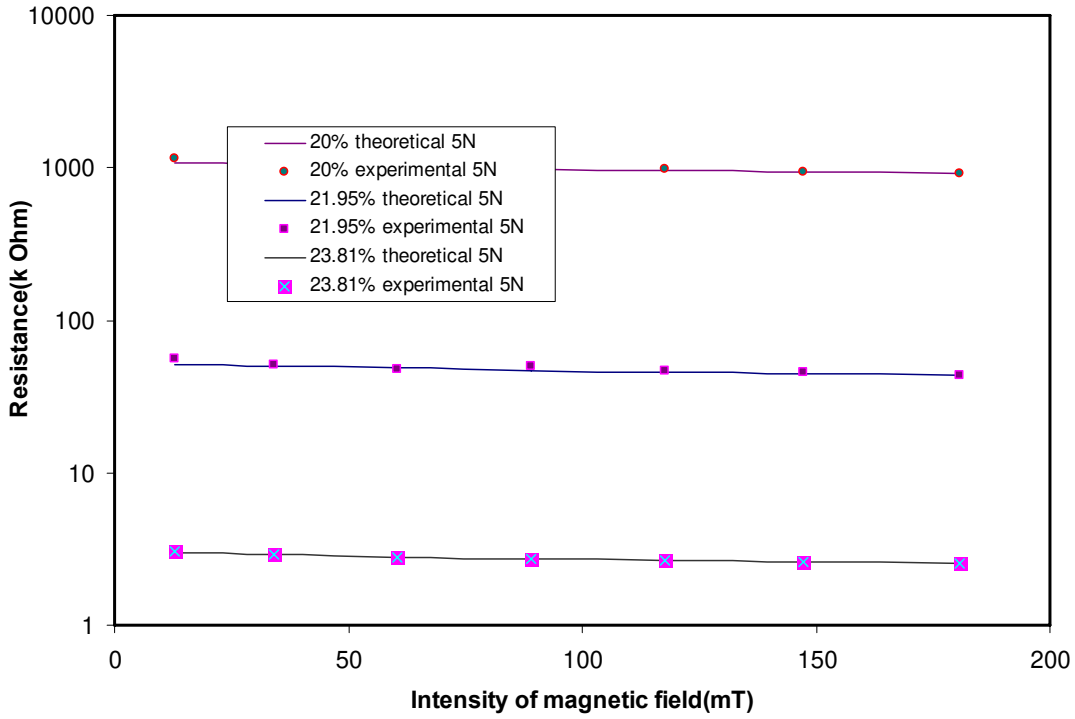

Fig. 4.13 Resistance between different sample at 5.1N external load (anisotropic MRE with graphite weight fraction 20%, 21.95% & 23.81%)

As mentioned, in the tests, only the sample that has graphite weight fraction more than 20% can be detected conductivity by Finest 183 multimeter. The sample with 17.95% graphite weight fraction can be chosen to see if the theoretical result is bigger than the multimeter measuring range 20MΩ. By substituting the weight fraction in to Equation 4.20 the theoretical result is shown in Table 4.6.

Table 4.6 Theoretical resistance of anisotropic MREs with 17.95% graphite weight fraction

B(mT) / load(N)	0.013	0.0605	0.1178	0.1807
0	41626.2462	34522.9	30479.37	27810.45
2	33601.3571	30455.98	27990.52	26099.04
4	29937.9336	27974.83	26232.89	24784.89
6	27623.1735	26221.26	24890.33	23726.91
8	25958.9355	24881.19	23813.27	22846.84
10	24674.0441	23805.79	22919.58	22096.98

In table 4.6, it can be seen clearly that when the maximum load and strongest magnetic field are applied on the sample, the theoretical resistance is 22096.98 MΩ, which is still bigger than multimeter maximum measuring range 20MΩ. This explains why the resistance of the samples that have graphite weight fraction less than 20% is not detectable. More experimental results can be found in Appendix C.

From the Fig. 4.12 & Fig. 4.13, because of the order of values for three samples, it is easy to see that the theoretical result and experimental result can match each other very well. This means that the theory is proved by the test works. Whatever either external load or magnetic field intensity increases, the resistance decrease.

Therefore, when the magnetic field intensity and resistance are got, the Equation 4.20 can be used to calculate the external load. That means the Gr MREs have the potential to work as the key component in a force sensor.

4.7 CONCLUSION

In this chapter, the experimental setup was introduced and the experimental result was shown in figures. And then a representative volume unit model was addressed and the details of theoretical calculation were expressed. Finally, the experimental result and theoretical result were compared. And the data from different samples was compared, too.

CHAPTER 5
CONCLUSION AND FUTURE WORK

The magnetorheological effects and sensing capabilities of MR Elastomers were presented in this thesis. This project attempted to study the magnetorheology of graphite based MREs and to explore the potential of MRE material as smart materials to be used in a force sensor. In the first part of this chapter, the main contributions of this project will be summarized and the characteristics of this system will be outlined. The second part will suggest a direction for further research work.

5.1 SUMMARY

The main contributions of this project can be divided into four parts: 1) MRE fabrication and microstructure observation, 2) The effect of graphite on the MR effect, 3) Study of sensing capabilities, comparison of theoretical result and experimental result.

5.1.1 MRE fabrication and microstructure observation

Both isotropic and anisotropic Gr MREs with various graphite weight fractions were fabricated in this study. LA SEM was used to observe the microstructures of them. The observation shows that the graphite powders effect the forming of carbonyl iron chains. The sample with less graphite shows better aligned carbonyl iron chains, which affects the magnetorheology of MREs. Also by connecting two iron chains parallelly and connecting the disconnected iron chains, the graphite contributes to the conductivity of MREs.

5.1.2 The effect of graphite on the MR effect

The steady state and dynamic tests such as strain amplitude sweep and angular frequency sweep were used to test the magnetorheology of Gr MREs. With the help of graphite in MREs, the storage and loss moduli are both changed. The steady state tests showed that the graphite can diminish the viscoelastic linear range of MREs. The dynamic test proved that the samples with higher graphite weight fraction show higher initial storage and loss moduli and lower MR effects.

5.1.3 Study of sensing capabilities, comparison of theoretical result and experimental result.

Representative volume unit was presented to show the resistance of ideal anisotropic MREs. Experimental result proved the feature of MREs namely the resistance of MREs is dependent on the external force and applied magnetic field. At a certain magnetic field, the the force signal can be converted to a resistance signal. This shows the potentials of using MREs as the key components in a force sensor.

5.2 FUTURE WORK

Future work for this project is divided into three main parts:

(1) In the future, the Impedance Analyzer will be involved to test the impedance of Gr MREs, from which, the impedance might be found at the similar changing trend in those tests. And the theoretical analysis about the impedance should be developed and compared with the tests result.

(2) Also the relaxation of Gr MREs will be considered to affect the resistance. Another model will be addressed to explain the contribution of Gr MREs' relaxation.

(3) The National Instrument LabVIEW software and National Instrument Data Acquisition (DAQ) Board can also be involved the further work. A shaker is controlled by the computer

to generate dynamic sin force on to the Gr MRE samples, meanwhile, the computer controls the DAQ board to generate a electrical current and a electrical potential. The currents is running in the electrical magnet to control the magnetic field intensity and the fixed potential is applied on the Gr MRE samples. The force signal can be selected by a force sensor and the DAQ board selects the MRE circuit current which can be used to calculate the resistances of Gr MRE samples. By this system, the dynamic resistance changing will be measured.

BIBILIOGRAPHY

1. Hovanessian, S.A., *Introduction to sensor systems* 1990, Norwood, MA Dept. of Industry, Technology and Commerce Artech House.

2. Brignell, J. and N. White, *Sensor technology and devices*. Rev ed. 1994, Boston: Artech House Institute of Physics Pub.

3. Liu, S.H., T.S. Huang, and J.Y. Yen. *Sensor fusion in a SMA-based hgxapod bio-mimetic robot*. in *IEEE International Conference on Advanced Robotics and its Social Impacts*. 2008.

4. Hindrichsen, C.G., et al., *Advantages of PZT thick film for MEMS sensors.* Sensors and Actuators A: Physical.

5. Park, J.H., et al., *Effects of the material properties on piezoelectric PZT thick film micro cantilevers as sensors and self actuators.* Journal of Electroceramics. **25**(1): p. 1-10.

6. Gong, X.L., X.Z. Zhang, and P.Q. Zhang, *Fabrication and characterization of isotropic magnetorheological elastomers.* Polymer Testing, 2005. **24**(5): p. 669-676.

7. Song, H.J. and et al., *Field dependent response of magnetorheological elastomers utilizing spherical Fe particles versus Fe nanowires.* Journal of Physics: Conference Series, 2009. **149**(1): p. 012097.

8. Jolly, M.R., J.D. Carlson, and B.C. Munoz, *A model of the behaviour of magnetorheological materials.* Smart Materials & Structures, 1996. **5**(5): p. 607-614.

9. Lokander, M. and B. Stenberg, *Performance of isotropic magnetorheological rubber materials.* Polymer Testing, 2003. **22**(3): p. 245-251.

10. Jiles, D., *Introduction to magnetism and magnetic materials*. 1994: Chapman and Hall.

11. Kchit, N. and G. Bossis, *Electrical resistivity mechanism in magnetorheological elastomer.* Journal of Physics D-Applied Physics, 2009. **42**(10): p. 5505-5505.

12. de Buyl, F., *Silicone sealants and structural adhesives.* International Journal of Adhesion and Adhesives, 2001. **21**(5): p. 411-422.

13. Meunier, L., et al., *Mechanical experimental characterisation and numerical modelling of an unfilled silicone rubber.* Polymer Testing, 2008. **27**(6): p. 765-777.

14. Lokander, M. and B. Stenberg, *Improving the magnetorheological effect in isotropic magnetorheological rubber materials.* Polymer Testing, 2003. **22**(6): p. 677-680.

15. Leblanc, J.L., *Rubber-filler interactions and rheological properties in filled compounds.* Progress in Polymer Science, 2002. **27**(4): p. 627-687.

16. Bica, I., *Influence of the transverse magnetic field intensity upon the electric resistance of the magnetorheological elastomer containing graphite microparticles.* Materials Letters, 2009. **63**(26): p. 2230-2232.

17. Bica, I., *Influence of the magnetic field on the electric conductivity of magnetorheological elastomers.* Journal of Industrial and Engineering Chemistry, 2010. **16**(3): p. 359-363.

18. Zou, H., et al., *Study on the Structure and Properties of Conductive Silicone Rubber Filled with Nickel-Coated Graphite.* Journal of Applied Polymer Science, 2009. **115**(5): p. 2710-2717.

19. Li, W.H., et al., *Development of a Force Sensor Working with MR Elastomers*, in *2009 Ieee/Asme International Conference on Advanced Intelligent Mechatronics, Vols 1-3*. 2009, Ieee: New York. p. 233-238.

20. Chen, L., X.L. Gong, and W.H. Li, *Effect of carbon black on the mechanical performances of magnetorheological elastomers.* Polymer Testing, 2008. **27**(3): p. 340-345.

21. Shen, Y., M.F. Golnaraghi, and G.R. Heppler, *Experimental research and modeling of magnetorheological elastomers.* Journal of Intelligent Material Systems and Structures, 2004. **15**(1): p. 27-35.

22. Ginder, J.M., et al. *Magnetorheological elastomers: properties and applications*. in *Smart Structures and Materials 1999: Smart Materials Technologies*. 1999. Newport Beach, CA, USA: SPIE.

23. Zhou, G.Y., *Shear properties of a magnetorheological elastomer.* Smart Materials and Structures, 2003. **12**(1): p. 139.

24. Ginder, J.M., W.F. Schlotter, and M.E. Nichols. *Magnetorheological elastomers in tunable vibration absorbers*. in *Smart Structures and Materials 2001: Damping and Isolation*. 2001. Newport Beach, CA, USA: SPIE.

25. Ginder, J.M., et al., *Magnetostrictive phenomena in magnetorheological elastomers.* International Journal of Modern Physics B, 2002. **16**(17-18): p. 2412-2418.

26. Davis, L.C., *Model of magnetorheological elastomers.* Journal of Applied Physics, 1999. **85**(6): p. 3348-3351.

27. Shiga, T., A. Okada, and T. Kurauchi, *Magnetroviscoelastic behavior of composite gels.* Journal of Applied Polymer Science, 1995. **58**(4): p. 787-792.

28. Borcea, L. and O. Bruno, *On the magneto-elastic properties of elastomer-ferromagnet composites.* Journal of the Mechanics and Physics of Solids, 2001. **49**(12): p. 2877-2919.

29. Dorfmann, A. and R.W. Ogden, *Magnetoelastic modelling of elastomers.* European Journal of Mechanics - A/Solids. **22**(4): p. 497-507.

30. Farshad, M. and A. Benine, *Magnetoactive elastomer composites.* Polymer Testing, 2004. **23**(3): p. 347-353.

31. Bellan, C. and G. Bossis, *Field dependence of viscoelastic properties of MR elastomers.* International Journal of Modern Physics B, 2002. **16**(17-18): p. 2447-2453.

32. Yalcintas, M. and H.M. Dai, *Vibration suppression capabilities of magnetorheological materials based adaptive structures.* Smart Materials & Structures, 2004. **13**(1): p. 1-11.

33. Zhou, G.Y. and Z.Y. Jiang, *Deformation in magnetorheological elastomer and elastomer–ferromagnet composite driven by a magnetic field.* Smart Materials and Structures, 2004. **13**(2): p. 309.

34. Wang, X.J., et al., *Sensing Behavior of Magnetorheological Elastomers.* Journal of Mechanical Design, 2009. **131**(9): p. 6.

35. Bossis, G., et al., *Electroactive and electrostructured elastomers.* International Journal of Modern Physics B, 2001. **15**(6-7): p. 564-573.

36. Zhao, Y., D.M. Maietta, and L. Chang, *An Asperity Microcontact Model Incorporating the Transition From Elastic Deformation to Fully Plastic Flow.* Journal of Tribology, 2000. **122**(1): p. 86-93.

37. McLachlan, D.S., *Analytical functions for the dc and ac conductivity of conductor-insulator composites.* Journal of Electroceramics, 2000. **5**(2): p. 93-110.

38. Woo, L.Y., et al., *A universal equivalent circuit model for the impedance response of composites.* Journal of Materials Science, 2003. **38**(10): p. 2265-2270.

39. Deng, H.X., X.L. Gong, and L.H. Wang, *Development of an adaptive tuned vibration absorber with magnetorheological elastomer.* Smart Materials & Structures, 2006. **15**(5): p. N111-N116.

40. Hoang, N., N. Zhang, and H. Du, *A dynamic absorber with a soft magnetorheological elastomer for powertrain vibration suppression - art. no. 074009.* Smart Materials & Structures, 2009. **18**(7): p. 74009-74009.

41. Lerner, A.A. and K.A. Cunefare, *Performance of MRE-based vibration absorbers.* Journal of Intelligent Material Systems and Structures, 2008. **19**(5): p. 551-563.

42. Zhou, G.Y. and Q. Wang, *Study on the adjustable rigidity of magnetorheological-elastomer-based sandwich beams.* Smart Materials & Structures, 2006. **15**(1): p. 59-74.

43. Weinberg, Z.A., *On tunneling in metal-oxide-silicon structures.* Journal of Applied Physics, 1982. **53**(7): p. 5052-5056.

44. Serdouk, S., R. Hayn, and J.L. Autran, *Theory of spin-dependent tunneling current in ferromagnetic metal-oxide-silicon structures.* Journal of Applied Physics, 2007. **102**(11): p. 113707-1-113707-5.

45. Dahlke, W.E. and S.M. Sze, *Tunneling in metal-oxide-silicon structures.* Solid State Electronics, 1967. **10**(8): p. 865-873.

46. Mindlin, R.D., *Compliance of elastic bodies in contact.* J. Appl. Mech., 1949. **16**: p. 259-268.

47. Zhupanska, O.I. and A.F. Ulitko, *Contact with friction of a rigid cylinder with an elastic half-space.* Journal of the Mechanics and Physics of Solids, 2005. **53**(5): p. 975-999.

48. Etsion, I., et al., *Experimental investigation of the elastic-plastic contact area and static friction of a sphere on flat.* Journal of Tribology, 2005. **127**(1): p. 47-50.

49. Maouche, N., M.H. Maitournam, and K. Dang Van, *On a new method of evaluation of the inelastic state due to moving contacts.* Wear, 1997. **203-204**: p. 139-147.

50. Chang, W.R., I. Etsion, and D.B. Bogy, *Static Friction Coefficient Model for Metallic Rough Surfaces.* Journal of Tribology, 1988. **110**(1): p. 57-63.

51. Kogut, L. and I. Etsion, *A static friction model for elastic-plastic contacting rough surfaces.* Journal of Tribology, 2004. **126**(1): p. 34-40.

52. Craik, D.J., *Magnetism : principles and applications* 1995, Chichester: New York : Wiley.

53. Jakubovics, J.P., *Magnetism and Magnetic Materials* ed. n. rev.ed. 1994, London: Institute of Materials. 165.

54. Maxwell, J.C., *A treatise on electricity and magnetism*. 3rd ed. 1892, Oxford: Clarendon Press.

55. Nayfeh, M.H. and M.K. Brussel, *Electricity and magnetism* 1985, New York New York : Wiley.

56. Smit, J., *Magnetic properties of materials* Inter-university electronics series. Vol. 13. 1971, New York: McGraw-Hill.

APPENDIX A

The following pictures show the general procedures of the fabrication of conventional isotropic MREs.

(a)

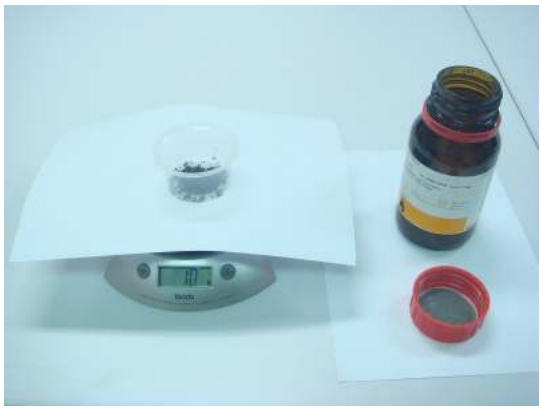

(b)

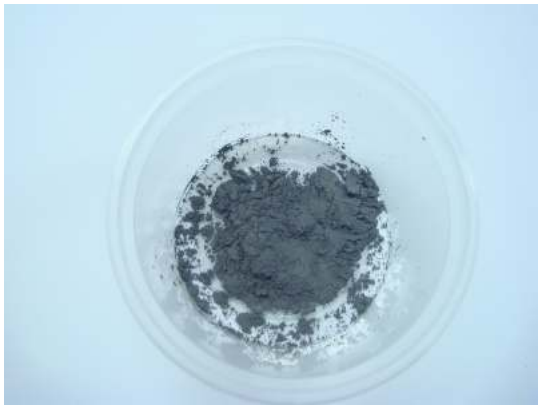

(c)

(d)

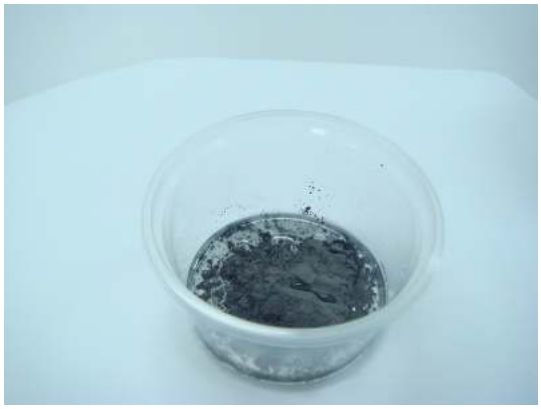

(e)

(f)

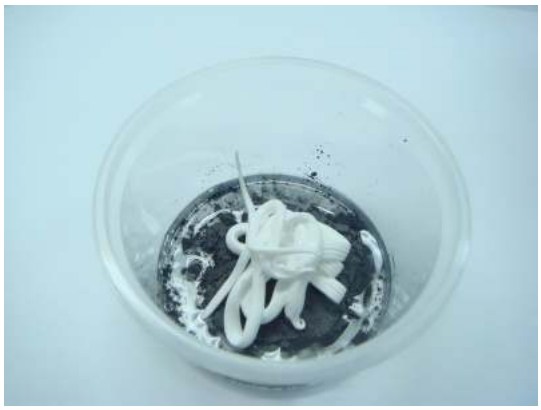

(g)

(h)

(i)

(j)

(k)

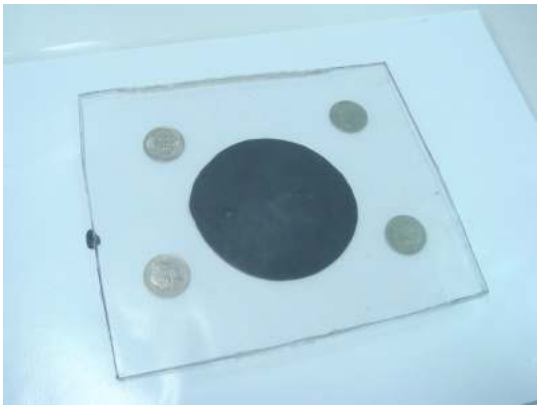

(l)

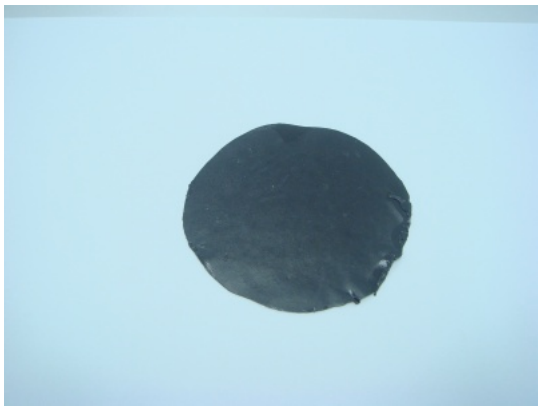

(m)

(a)Materials: carbonyl iron particles, silicone oil and silicone rubber; (b)Measure carbonyl iron particles; (c) Iron particles in container; (d) Add silicone oil to container; (e) Mixture of iron particles and silicone oil; (f) Add silicone rubber to container; (g) Mixture of iron particles, silicone oil & silicone rubber; (h) Use a stirrer to stir the mixture; (i) After sufficient stir, the mixture is mixed evenly; (j) Place the mixture on plastic paper. The coins are used for making the sample at a certain thickness; (k) Cover another piece of plastic paper on the top of mixture; (l) Use a plastic plate to press the mixture at the certain thickness; (m) After 24 hours curing at room temperature, tear off the plastic paper. The isotropic MRE sample is done.

APPENDIX B

Qualitative movements of carbonyl iron particles when the Gr MREs are curing under a magnetic field.

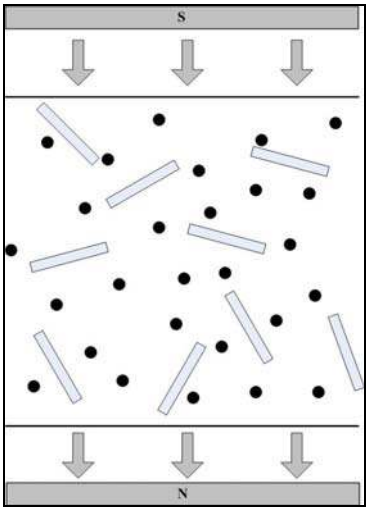

(a) 1st step

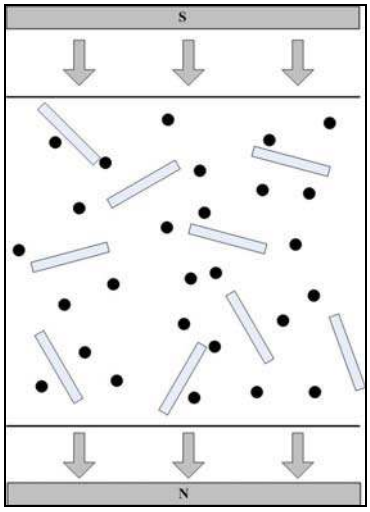

(b) 2nd step

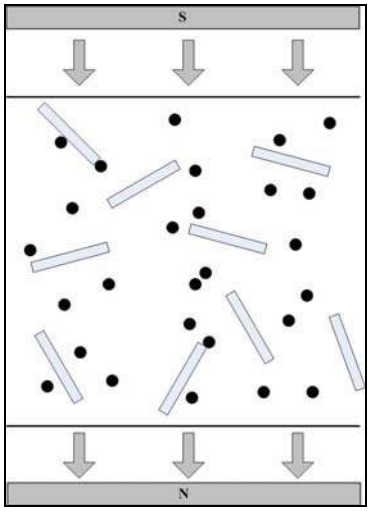

(c) 3rd step

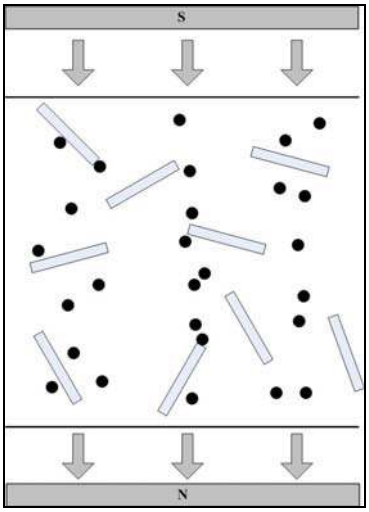

(d) 4th step

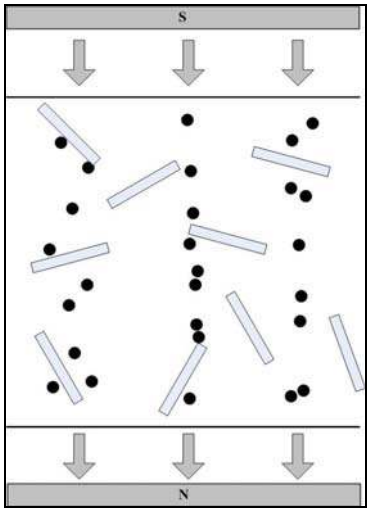

(e) 5th step

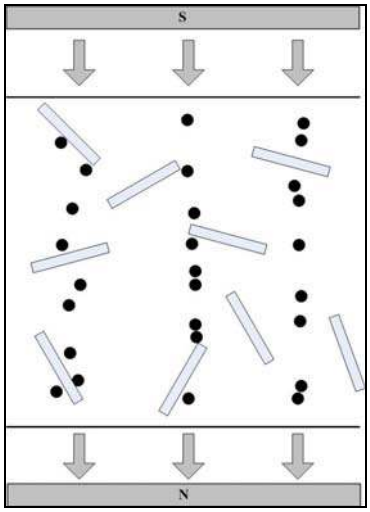

(f) 6th step

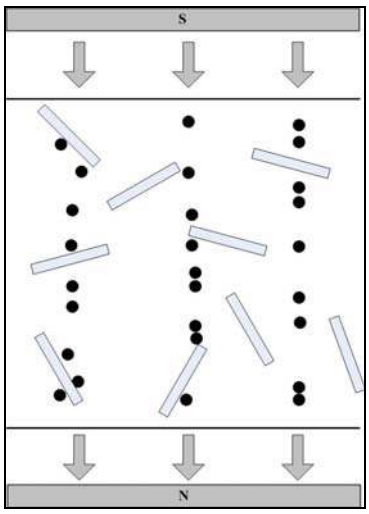

(g) 7th step

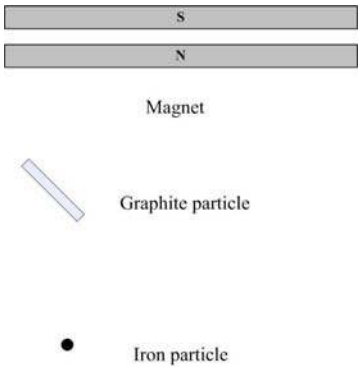

Legend

APPENDIX C

Resistance tests result:

Gr anisotropic MRE (Gr 20%)

B(mT) / Load(N)	13	34.1	60.5	89.1	117.8	147.3	180.7
0	1862	1654	1502	1340	1237	1182	1076
1	1667	1437	1318	1202	1154	1089	999
2	1439	1387	1262	1137	1102	1056	979
3	1334	1256	1184	1089	1037	1024	958
4	1242	1149	1102	1054	1003	975	942
5	1162	1101	1054	1002	972	948	922
6	1083	1067	1012	968	938	918	892
7	1054	1011	972	937	918	904	876
8	1014	976	953	907	897	872	862
9	987	947	928	892	868	851	837
10	942	921	904	872	859	842	821

Unit: kΩ

Gr anisotropic MRE (Gr 21.95%)

B(mT) / Load(N)	13	34.1	60.5	89.1	117.8	147.3	180.7
0	119.2	102.3	72.8	65.4	60.5	58.7	54.3
1	87.3	73.2	62.1	58.7	55.1	51.2	50.3
2	76.5	62.4	60.1	55.3	52.8	50.7	50.2
3	65.1	58.9	55.4	54.9	50.3	49.8	47.6
4	60.5	54.5	50.3	53.2	50.8	47.2	45.8
5	55.4	51.2	48.2	49.8	47.2	45.7	43.5
6	52.8	50.3	48.5	47.8	45.2	43.4	41.8

7	51.2	48.9	47.6	44.3	43.5	41.9	40.5
8	50.4	47.6	45.1	43.2	41.9	40.7	39.9
9	49.8	45.3	44.2	42.7	40.8	39.4	38.7
10	48.7	44.2	43.8	42.1	40.7	38.7	36.9

Unit: kΩ

Gr anisotropic MRE (Gr 23.81%)

B(mT) / Load(N)	13	34.1	60.5	89.1	117.8	147.3	180.7
0	4.18	3.79	3.65	3.41	3.24	3.11	3.01
1	3.79	3.68	3.41	3.25	3.11	2.99	2.94
2	3.62	3.41	3.22	3.09	2.99	2.87	2.81
3	3.34	3.22	3.08	2.97	2.84	2.78	2.69
4	3.18	3.09	2.94	2.84	2.76	2.71	2.61
5	3.02	2.91	2.81	2.73	2.64	2.62	2.52
6	2.81	2.78	2.71	2.61	2.54	2.48	2.44
7	2.75	2.7	2.63	2.54	2.53	2.47	2.39
8	2.66	2.61	2.56	2.47	2.44	2.41	2.34
9	2.58	2.55	2.54	2.41	2.4	2.37	2.31
10	2.51	2.5	2.47	2.41	2.36	2.32	2.22

Unit: k Ω